96

Optimal Control Designs for an Inverted Cart-Pendulum Array

by

John Edwin Shaw

A thesis submitted in partial fulfillment
of the requirements for the degree of

Master of Science in Aeronautics and Astronautics

University of Washington

1991

Approved by _____
(Chairperson of Supervisory Committee)

Program Authorized
to Offer Degree Department of Aeronautics & Astronautics

Date August 22, 1991

REPORT DOCUMENTATION PAGE

Form Approved
OMB No. 0704-0188

1. AGENCY USE ONLY *(Leave blank)*

2. REPORT DATE
August 22, 1991

3. REPORT TYPE AND DATES COVERED
THESIS/~~DISSERTATION~~

4. TITLE AND SUBTITLE
Optimal Control Designs for an Inverted Cart-Pendulum Array

5. FUNDING NUMBERS

6. AUTHOR(S)
John Edwin Shaw, 2d Lt

7. PERFORMING ORGANIZATION NAME(S) AND ADDRESS(ES)
AFIT Student Attending: University of Washington

8. PERFORMING ORGANIZATION REPORT NUMBER
AFIT/CI/CIA- 91-096

9. SPONSORING/MONITORING AGENCY NAME(S) AND ADDRESS(ES)
AFIT/CI
Wright-Patterson AFB OH 45433-6583

10. SPONSORING/MONITORING AGENCY REPORT NUMBER

11. SUPPLEMENTARY NOTES

12a. DISTRIBUTION/AVAILABILITY STATEMENT
Approved for Public Release IAW 190-1
Distributed Unlimited
ERNEST A. HAYGOOD, Captain, USAF
Executive Officer

12b. DISTRIBUTION CODE

13. ABSTRACT *(Maximum 200 words)*

14. SUBJECT TERMS

15. NUMBER OF PAGES
101

16. PRICE CODE

17. SECURITY CLASSIFICATION OF REPORT

18. SECURITY CLASSIFICATION OF THIS PAGE

19. SECURITY CLASSIFICATION OF ABSTRACT

20. LIMITATION OF ABSTRACT

University of Washington

Abstract

Optimal Control Designs for an Inverted Cart-Pendulum Array

by John Edwin Shaw

Chairperson of Supervisory Committee: Prof. Juris Vagners
Dept. of Aeronautics and Astronautics

Optimal control design employing LQG methodology for an inverted cart-pendulum array (a non-minimum phase system) is explored. Motivation for the study is the availability of a laboratory hardware setup for implementation and experimentation, including use of analog computers for controllers. The dynamics of the open-loop plant are developed using Lagrangian techniques. The minimum-time optimization problem involving "pump-up" to an inverted configuration is examined. The optimal regulator problem is solved for several control scenarios, and the use of optional integral states is discussed. Various optimal estimation configurations include optimal estimators as well as simple differentiators. Robustness properties are analyzed for various control configurations. Actual hardware implementation and results are discussed and further study is suggested.

TABLE OF CONTENTS

LIST OF FIGURES

LIST OF TABLES

ACKNOWLEDGMENTS

I would like to express my appreciation to Professor Juris Vagners for guiding me successfully through the thesis maze. Thanks also to Lt. Mike Shepherd, Lt. Marcus Sculthess, and Hamid Montazeri for their assistance in the laboaratory. Special thanks to Professor Robert Clark for the helpful suggestions on motor analysis and testing.

Thanks also to Mom, Dad, and my wife, Tonia, for their support and encouragement during my study here at the University of Washington.

Chapter 1

INTRODUCTION

1.1 Background

The concept of an inverted free-swinging pendulum aboard a movable platform or "cart" provides a variety of interesting control scenarios, the simplest of which is, of course, to maintain a simple pendulum in an upright configuration with as little control as possible. Forces strategically applied on the cart can produce accelerations within the system to keep the pendulum upright.

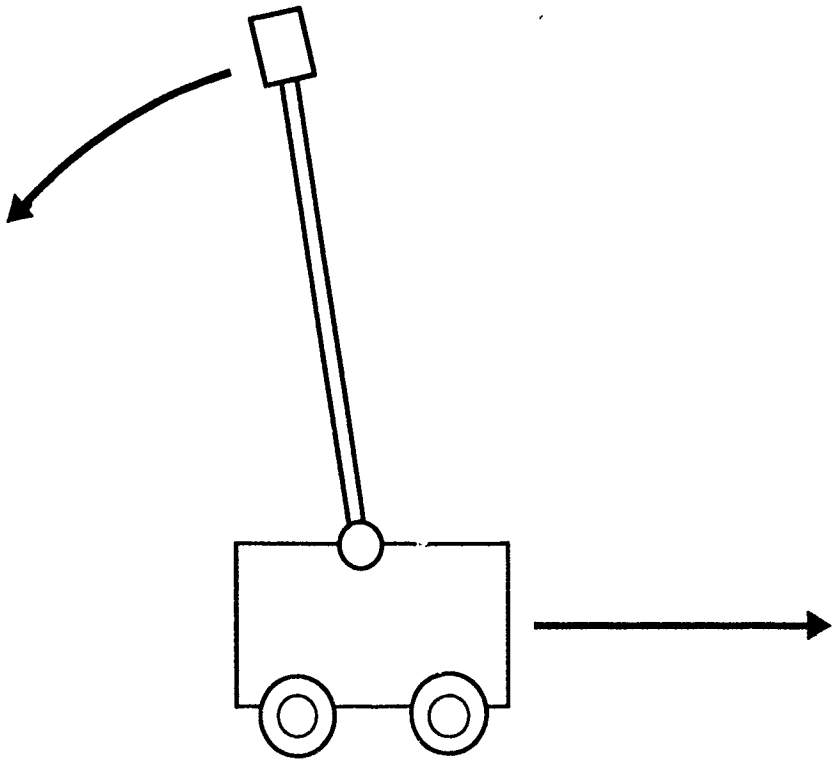

Figure 1.1: A Simple Cart-Pendulum Device

Although the concept of inverted pendulum control has been around for decades, the full nonlinear cart-pendulum problem was first addressed by Mori, Nishihara, and Furuta in the 1975 International Journal of Control. In 1983, Ewald Reekers employed the concepts discussed by Mori et al on an actual hardware arrangement constructed at the University of Duisburg, Germany. Reeker's work involved a digital implementation for the nonlinear "pump-up" phase, and a full-state feedback regulator employing eigenplacement techniques as well as a conventional observer for a linear controller.

In 1990, a duplicate of the Duisburg Cart-Pendulum was delivered to the Controls Laboratory of the Department of Aeronautics and Astronautics at the University of Washington in Seattle. This thesis represents the first attempt to place the U.W. Cart-Pendulum into an operational status. The approach taken here is intended to expand on the work done in Duisburg by applying principles of optimization and linear quadratic regulator (LQR) and estimator (LQE) techniques to optimize performance and maintain robustness. Since the given apparatus represents a fixed system, the control law design approach described is geared towards solving the specific control problem posed by the existing hardware.

Naturally, as we might expect in any control problem, the system has to operate within certain constraints. These include a limit to how far the cart may move along a finite path, and limits on the control mechanism (i.e. motor) used to move the cart and pendulum. Limitations on sensors also play an important role on the control design. As we shall see, the simplest inverted cart pendulum array is at least a fourth-order system. The actual number of states that are directly measurable and the reliability of the outputs can be major drivers in the design of a control system.

1.2 Problem Statement

A variety of control scenarios exist for the inverted Cart-Pendulum array. Clearly, an initially upright pendulum aboard a motionless cart with no outside disturbances is in equilibrium, and, although the equilibrium is unstable, no control is needed. However, usually there exist disturbances, or initial conditions that are not precisely at the equlibrium values, and therefore active control is required to keep the pendulum upright. Thus, the first and simplest control problem would be one involving

nonhomogeneous initial conditions, e.g. a slight "offset" in pendulum angle, or initial motion in the cart that will produce an acceleration in the system when friction comes into play. Another, more complex, scenario might involve a "step" command to the cart to move a linear distance while keeping the pendulum upright. Further scenarios could include periodic commands to the cart, and combinations of commands and nonhomogeneous initial conditions.

But a more "complete" problem would entail a situation in which the pendulum is initially hanging *downward* in its naturally stable equilibrium position, and is subsequently "pumped-up" as quickly as possible into an inverted configuration and then maintained there. This maneuver is best achieved in two distinct phases, involving, respectively: (1) an open-loop control law (or supervisory control logic) utilizing the known nonlinear system dynamics to "pump-up" the pendulum in minimum time, and (2) an optimal linear feedback controller utilizing linearized system dynamics to stabilize the pendulum in its naturally unstable inverted configuration. We will examine this particular "complete" inverted Cart-Pendulum problem, and produce both a "pump-up" control law and linear controller designs that will achieve the desired performance.

The final objective is to actually implement these designs on laboratory hardware, and evaluate performance in light of expectations.

1.3 Hardware Description

1.3.1 Cart-Pendulum Array

A schematic of the actual hardware laboratory setup system used in experimentation is shown in Figure 1.2. The Cart-Pendulum array itself consists of an aluminum "cart" sliding along a lubricated rail, as shown in Figure 1.3. The cart is attached to a belt and pulley arrangement, which is itself attached to the control device, or motor. The complete nonlinear dynamics of the Cart-Pendulum array are developed thoroughly in Chapter 2.

In addition to the physical components, the Cart-Pendulum also has two potentiometers, each of which measures a given quantity in the system. One outputs a voltage (against a reference voltage) proportional to the position of the cart on the track, while the other produces voltage proportional to the angle of the pendulum.

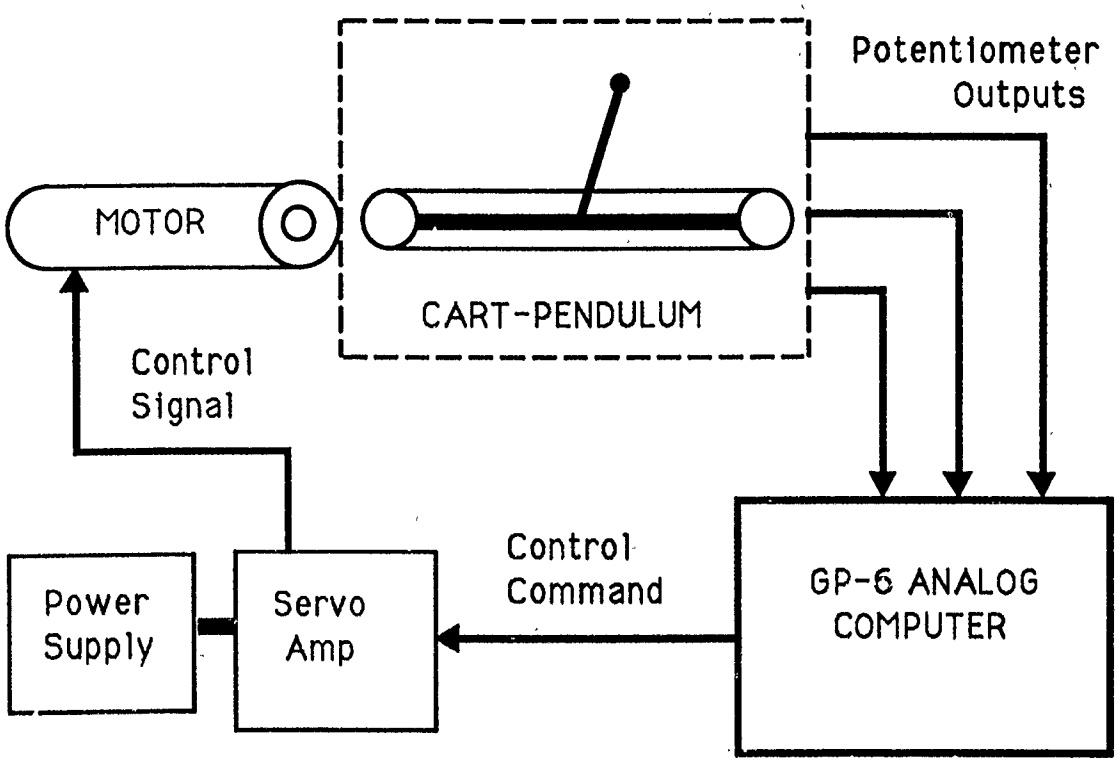

Figure 1.2: Diagram of Hardware Setup in Laboratory

Both of these output signals are directed to the computer controller.

Also of interest are two safety switches, one on each end of the cart track. They are situated such that when the cart passes over either of them, power to the motor is automatically cut, thereby preventing the motor from attempting to drive the cart beyond the confines of the track. One objective of control design is to keep the cart within the track boundaries defined by these switches.

1.3.2 Motor-Actuator Assembly

The motor-actuator assembly consists of (1) the motor itself, which is physically connected to the belt and pulley arrangement, as well as (2) a servo motor amplifier, and (3) a power supply. The "servo amp" serves to convert an input control command signal (usually the output of the controller) into an actual power signal to the motor.

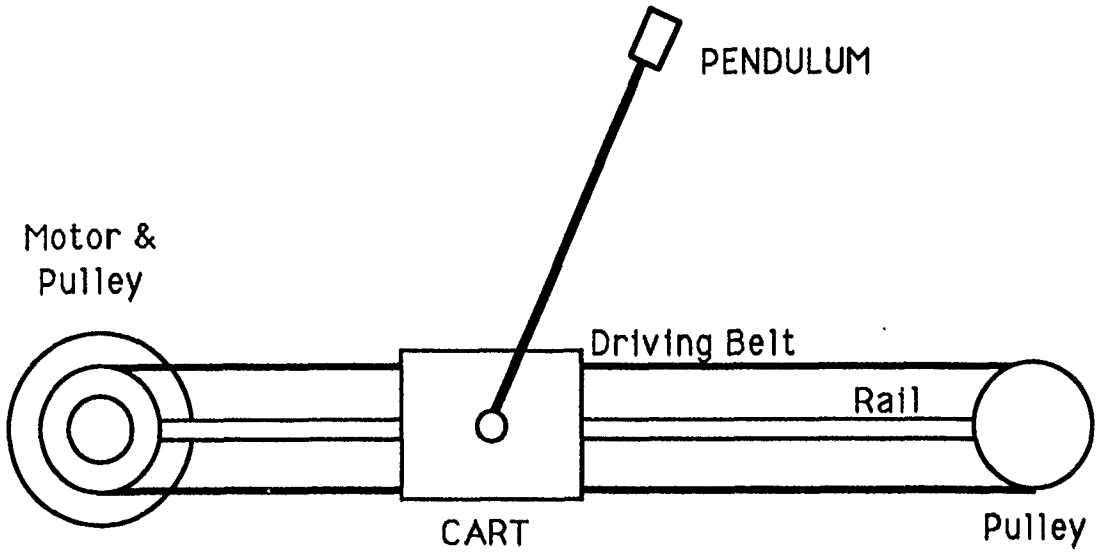

Figure 1.3: Basic Cart-Pendulum Arrangement

It draws on the connected power supply. The motor also has a tachometer attached, which outputs a voltage proportional to the speed of rotation of the motor. Appropriate positive and negative voltages correspond to clockwise or counterclockwise rotation.

Data and results of tests performed on the actual motor used in the laboratory are located in Appendix A.

1.3.3 Analog Computer

The controller for these particular experiments is a Comdyna GP-6 analog computer, which accepts output signals from the potentiometers connected to the Cart-Pendulum and tachometer on the motor, and produces a control command voltage which it sends to the servo amplifier. Its internal structure consists primarily of operational amplifiers and potentiometers, which can be wired and set appropriately to configure the unit as a controller.

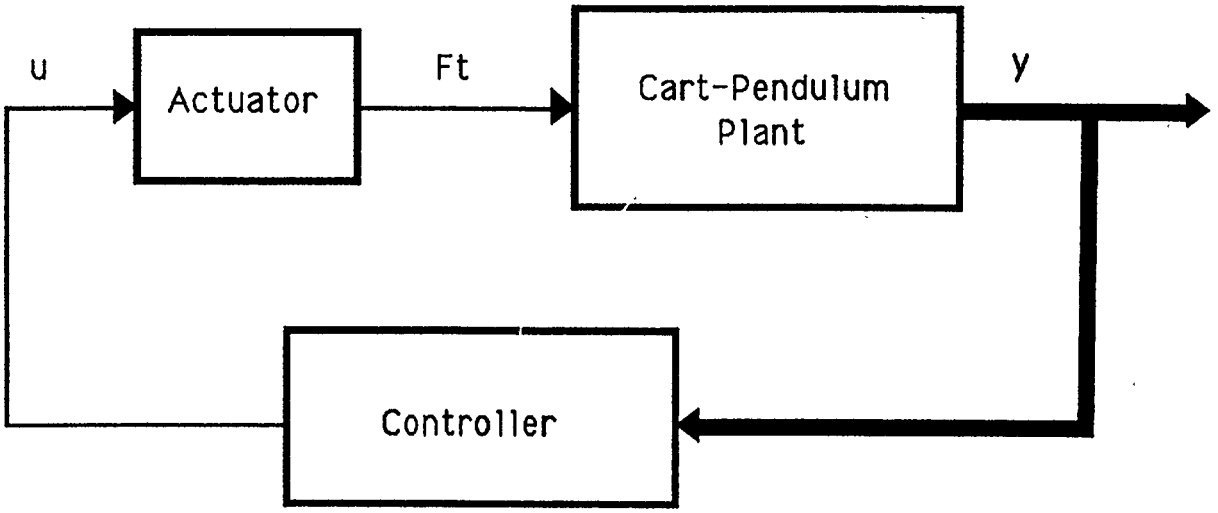

Figure 1.4: Control System Block Diagram

1.3.4 System Inputs and Outputs

The overall control system block diagram is shown in Figure 1.4. Clearly, the system is single-input-multiple-output (SIMO) in nature, with the input being a command signal from the controller and the outputs consisting of voltages from the two potentiometers and tachometer mentioned previously. This is indicated in Figure 1.4, with the thick line representing multiple outputs.

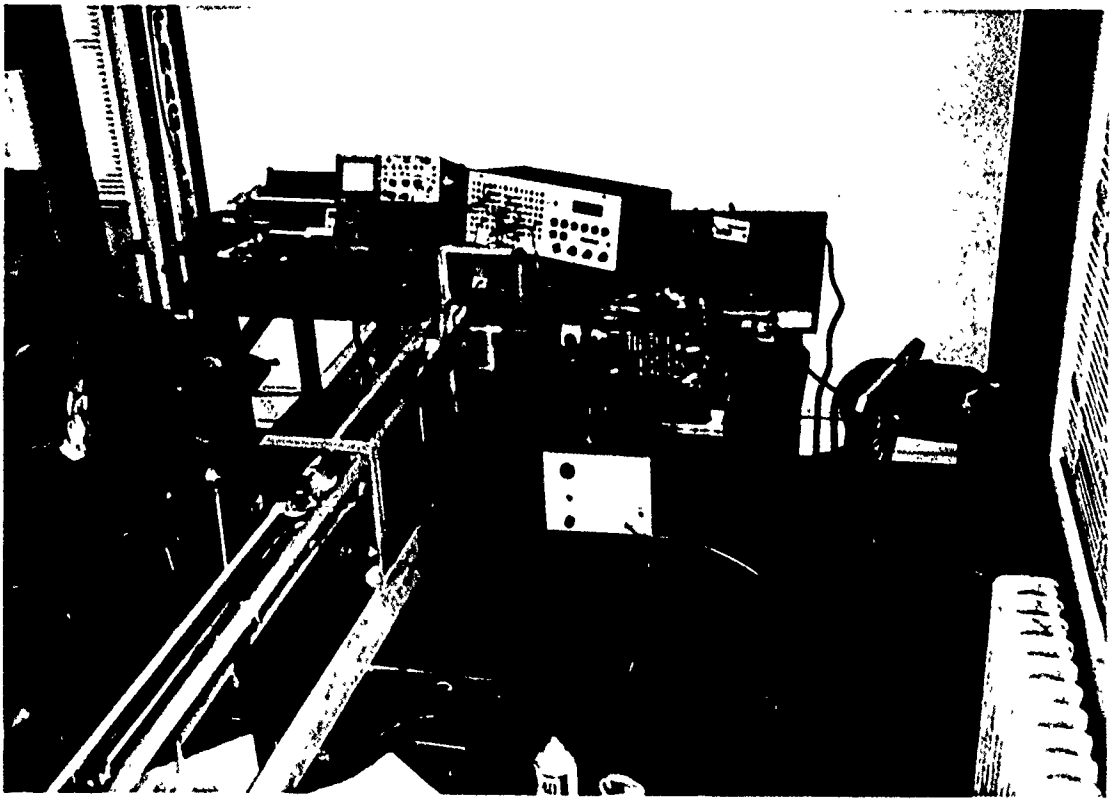

Figure 1.5: Complete Hardware System

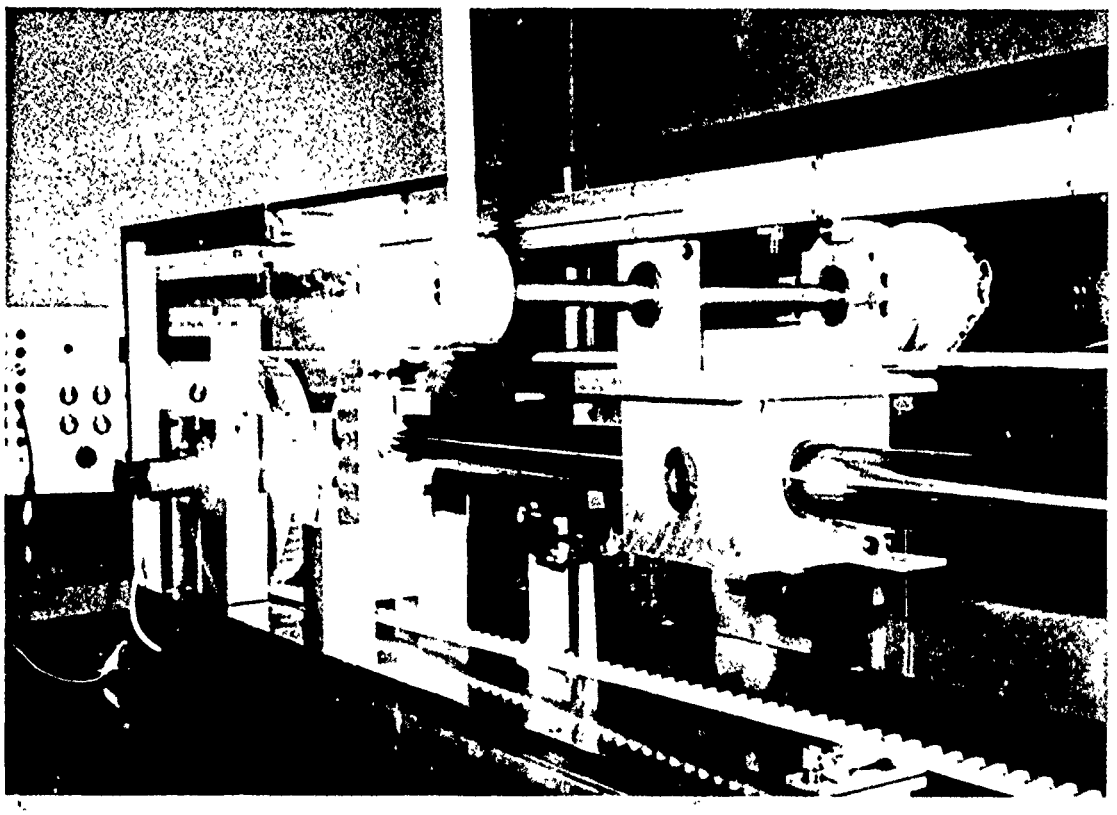

Figure 1.6: Cart, Rail, and Belt-Pulley Arrangement

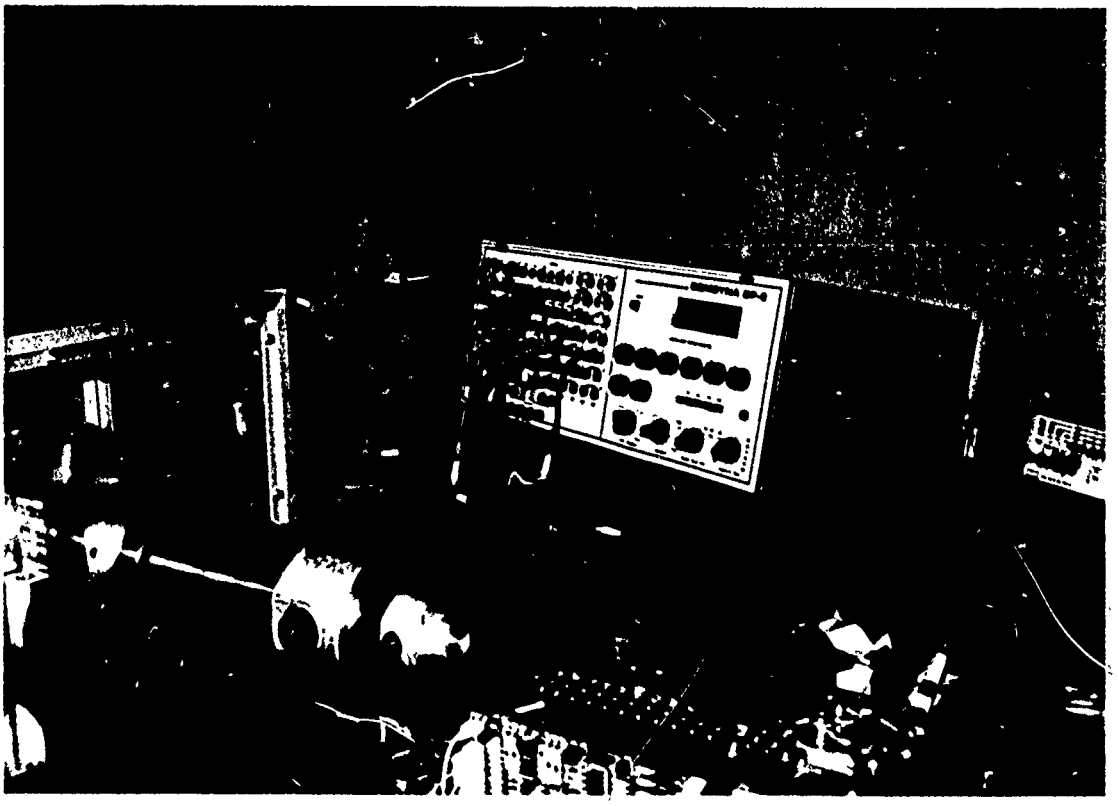

Figure 1.7: Motor, Servo-Amplifier, and Analog Computer

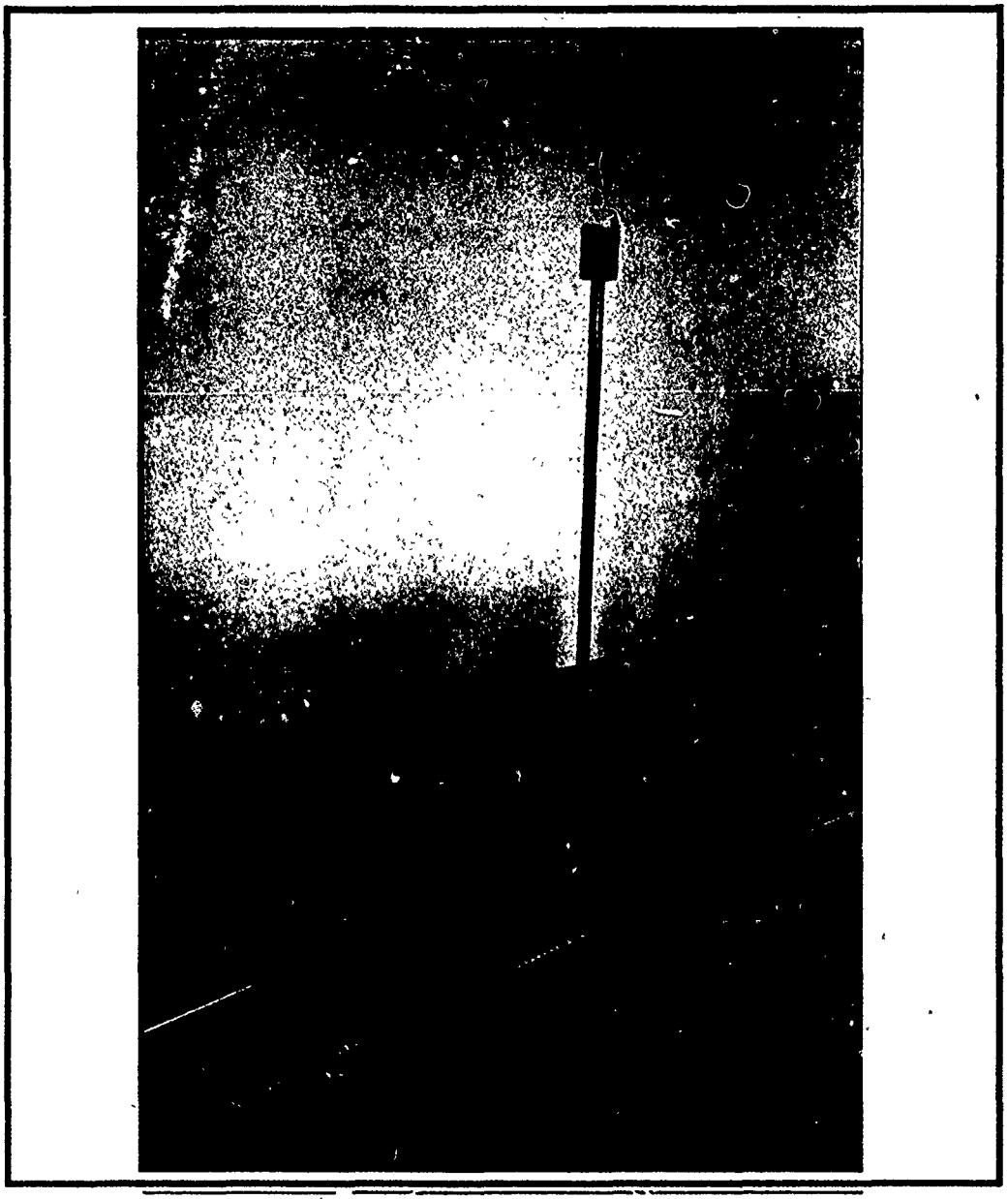

Figure 1.8: Cart-Pendulum in Operation in Laboratory

Chapter 2

SYSTEM MODELING AND DYNAMICS

2.1 Cart-Pendulum Modeling and Dynamics

2.1.1 Basic Cart-Pendulum Model

The Cart-Pendulum array consists simply of a cart moving along a straight track, and a pendulum swinging freely from the mobile cart as shown in Figure 1.3. Before any kind of control analysis can be performed, it is necessary to have an understanding of the natural dynamics of the Cart-Pendulum system. Our approach here is to first develop the full *nonlinear* equations of motion. These will be used to obtain the "pump-up" control law portion (i.e. "Phase 1") of the complete inverted pendulum problem. Then, by making useful assumptions about equlibrium, we can modify the nonlinear equations into a set of more simple *linear* equations of motion. To these we can apply linear control theory to obtain an effective feedback controller to maintain the pendulum in its unstable upright position ("Phase 2").

Figure 2.1 shows the various system parameters (masses, forces, accelerations, etc.) and coordinates used to describe the location of the cart and pendulum in space. Since the cart is restricted to movement in only one dimension (i.e. on the bar only), its position can be described by a single coordinate, s. Similarly, since the pendulum is of fixed length and rotates in a fixed plane, only one coordinate, the angle θ, is required to locate its position relative to the cart. Hence, the system has only two degrees-of-freedom, and only two generalized coordinates are required to completely determine the configuration of the Cart-Pendulum at any instant. These two coordinates (s,θ) plus their respective velocities $(\dot{s},\dot{\theta})$ compose the fourth order dynamics model that will be used to describe the Cart-Pendulum array.

The system parameters (i.e. masses, forces, etc.) may vary with different types of hardware arrangements. Actual values for the parameters for the configuration used for experimentation are given in Appendix B. The parameters and their preferred units are defined as follows:

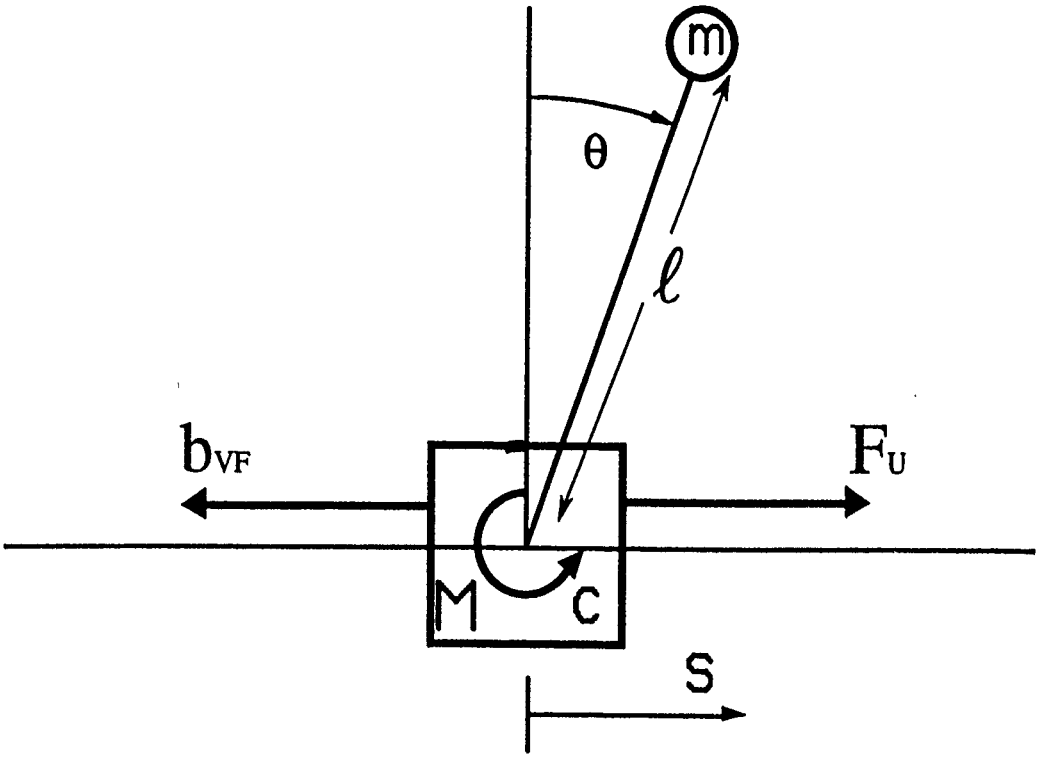

Figure 2.1: Pendulum Diagram

m : pendulum mass (kg)
M : cart mass (kg)
θ : pendulum angle (degrees)
s : cart displacement (meters)
F_U : control input force (Newtons)
b_{VF} : viscous friction constant, proportional to cart velocity (kg/s)
c : rotational friction constant, proportional to angular velocity (kgm^2/s)
ℓ : "effective length" of the pendulum (meters)
g : gravitational acceleration (m/s^2)

Note that the effects of friction are limited to that of the cart sliding on the bar and the pendulum rotating on its hinge, and that both are considered to be *viscous* in

nature, i.e. directly proportional to the cart velocity and pendulum angular velocity, respectively. Thus, we assume constant coulomb friction forces are negligible along the lubricated bar and on the pendulum hinge. Note also the input to the system is a force directed along the direction of cart motion. This model ignores the inertias and frictional forces acting on the belt and pulleys, which are considered to be part of the motor assembly and will be examined later.

2.1.2 Cart-Pendulum Nonlinear Equations of Motion: Lagrangian Techniques

We will develop the system equations of motion using Lagrangian techniques. The approach involves determining the kinetic and potential energies of system components, forming the Lagrangian, and then deriving a motion equation for each generalized coordinate.

The equations for kinetic energy of the system:

$$T = T_{CART} + T_{PENDULUM} \tag{2.1}$$

$$T_{CART} = \frac{1}{2}M(\dot{s})^2 \tag{2.2}$$

$$T_{PENDULUM} = \frac{1}{2}m\left((\dot{s} + \ell\dot{\theta}\cos\theta)^2 + (-\ell\dot{\theta}\sin\theta)^2\right) \tag{2.3}$$

The equations for potential energy of the system:

$$V = V_{CART} + V_{PENDULUM} \tag{2.4}$$

$$V_{CART} = 0 \tag{2.5}$$

$$V_{PENDULUM} = mg\ell(1 + \cos\theta) \tag{2.6}$$

The Lagrangian is given by:

$$\begin{aligned} L &= T - V \\ &= T_{CART} + T_{PENDULUM} - V_{CART} - V_{PENDULUM} \\ &= \frac{1}{2}M(\dot{s})^2 + \frac{1}{2}m\left((\dot{s} + \ell\dot{\theta}\cos\theta)^2 + (-\ell\dot{\theta}\sin\theta)^2\right) - mg\ell(1 + \cos\theta) \end{aligned}$$

The basic Lagrangian equations of motion are given by:

$$\frac{d}{dt}\left(\frac{\partial L}{\partial \dot{s}}\right) - \frac{\partial L}{\partial \dot{s}} = Q_s \tag{2.7}$$

$$\frac{d}{dt}\left(\frac{\partial L}{\partial \dot{\theta}}\right) - \frac{\partial L}{\partial \dot{\theta}} = Q_\theta \tag{2.8}$$

where the generalized forces Q are given by:

$$\begin{aligned} Q_s &= F_U - b_{VF}\dot{s} \\ Q_\theta &= -c\dot{\theta} \end{aligned}$$

Performing the derivatives on L and including the generalized forces produces our final nonlinear Lagrangian equations of motion:

$$(M+m)\ddot{s} + b_{VF}\dot{s} + m\ell(-\dot{\theta}^2\sin\theta + \ddot{\theta}\cos\theta) = F_U \tag{2.9}$$

$$\ddot{\theta} + \frac{c\dot{\theta}}{m\ell^2} - \frac{g\sin\theta}{\ell} + \frac{\ddot{s}\cos\theta}{\ell} = 0 \tag{2.10}$$

The next step is to put these equations into a state space format. A system of two second order equations will contain four states, which we define as follows:

$$\vec{x} = \begin{bmatrix} x_1 \\ x_2 \\ x_3 \\ x_4 \end{bmatrix} = \begin{bmatrix} s \\ \theta \\ \dot{s} \\ \dot{\theta} \end{bmatrix} \tag{2.11}$$

Using the state notation and solving Equations 2.9 and 2.10 for $\ddot{s}$ and $\ddot{\theta}$, we obtain the following nonlinear state equations:

$$\dot{x_1} = x_3 \tag{2.12}$$

$$\dot{x_2} = x_4 \tag{2.13}$$

$$\dot{x_3} = -\frac{b_{VF}}{M+m}x_3 + \frac{m\ell}{M+m}(x_4^2\sin x_2 - \dot{x_4}\cos x_2) + \frac{1}{M+m}F_u \tag{2.14}$$

$$\dot{x_4} = -\frac{cx_4}{m\ell^2} + \frac{g}{\ell}\sin x_2 - \frac{1}{\ell}\dot{x_3}\cos x_2 \tag{2.15}$$

Expression of these equations *explicitly* in terms of the states, for use in computer programs, numerical algorithms, etc. is shown by:

$$\dot{x_1} = x_3 \tag{2.16}$$

$$\dot{x_2} = x_4 \tag{2.17}$$

$$\dot{x_3} = \frac{1}{(M+m) - mcos^2 x_2}[-b_{VF}x_3 + m\ell x_2^2 \sin x_2 + \frac{c}{\ell}x_4 \cos x_2 - mg \sin x_2 \cos x_2 + F_U] \tag{2.18}$$

$$\dot{x_4} = -\frac{c}{m\ell^2}x_4 + \frac{g}{\ell}\sin x_2 - \frac{1}{\ell[(M+m) - mcos^2 x_2]}(-b_{VF}x_3 \cos x_2 + m\ell x_2^2 \sin x_2 \cos x_2 + \frac{c}{\ell}x_4 cos^2 x_2 - mg \sin x_2 \cos^2 x_2 + \cos x_2 F_U) \tag{2.19}$$

2.1.3 Cart-Pendulum Linear Equations of Motion

To linearize the nonlinear equations to form our linear model, we assume the following disturbances from equilibrium, where s_0 and θ_0 denote the equilibrium values:

$$\begin{aligned} \boldsymbol{s} &= \boldsymbol{s_0} + \Delta \boldsymbol{s} \\ \boldsymbol{\theta} &= \boldsymbol{\theta_0} + \Delta \boldsymbol{\theta} \end{aligned}$$

Then, assuming (1) $s_0 = \theta_0 = 0$, and (2) Δs and $\Delta\theta$ are very small, the nonlinear equations 2.9 and 2.10 reduce to the following linearized equations of motion:

$$(M+m)\ddot{s} + b_{VF}\dot{s} + m\ell\ddot{\theta} = F_U \tag{2.20}$$

$$\ddot{\theta} + \frac{c}{m\ell^2}\dot{\theta} - \frac{g}{\ell}\theta + \frac{1}{\ell}\ddot{s} = 0 \tag{2.21}$$

The equations can be rearranged as follows:

$$\ddot{s} + \frac{b_{VF}}{M}\dot{s} - \frac{c}{M\ell}\dot{\theta} + \frac{mg}{M}\theta = \frac{1}{M}F_U \tag{2.22}$$

$$\ddot{\theta} + c[\frac{1}{m\ell^2} + \frac{1}{M\ell^2}]\dot{\theta} - \frac{g}{\ell}[1 + \frac{m}{M}]\theta - \frac{b_{VF}}{M\ell}\dot{s} = -\frac{1}{M\ell}F_U \tag{2.23}$$

From which we define the four linear state equations as follows:

$$\dot{x_1} = x_3 \tag{2.24}$$

$$\dot{x_2} = x_4 \tag{2.25}$$

$$\dot{x_3} = -\frac{mg}{M}x_2 - \frac{b_{VF}}{M}x_3 + \frac{c}{M\ell}x_4 + \frac{1}{M}F_U \tag{2.26}$$

$$\dot{x_4} = -c[\frac{1}{m\ell^2} + \frac{1}{M\ell^2}]x_4 + \frac{g}{\ell}[1 + \frac{m}{M}]x_2 + \frac{b_{VF}}{M\ell}x_3 - \frac{1}{M\ell}F_U \tag{2.27}$$

Therefore, put into a final state space format, we have:

$$\frac{d}{dt}\begin{bmatrix} x_1 \\ x_2 \\ x_3 \\ x_4 \end{bmatrix} = \begin{bmatrix} 0 & 0 & 1 & 0 \\ 0 & 0 & 0 & 1 \\ 0 & -\frac{mg}{M} & -\frac{b_{VF}}{M} & \frac{c}{M\ell} \\ 0 & \frac{(M+m)g}{M\ell} & \frac{b_{VF}}{M\ell} & -\frac{(M+m)c}{Mm\ell^2} \end{bmatrix}\begin{bmatrix} x_1 \\ x_2 \\ x_3 \\ x_4 \end{bmatrix} + \begin{bmatrix} 0 \\ 0 \\ \frac{1}{M} \\ -\frac{1}{M\ell} \end{bmatrix} F_U \tag{2.28}$$

Clearly, this Cart-Pendulum *plant* is a fourth order system. To determine system eigenvalues, we simply compute the determinant of $(\lambda I - A)$ and set it equal to zero:

$$det \begin{bmatrix} \lambda & 0 & -1 & 0 \\ 0 & \lambda & 0 & -1 \\ 0 & \frac{mg}{M} & \lambda + \frac{b_{VF}}{M} & -\frac{c}{M\ell} \\ 0 & -\frac{(M+m)g}{M\ell} & -\frac{b_{VF}}{M\ell} & \lambda + \frac{(M+m)c}{Mm\ell^2} \end{bmatrix} = 0$$

If we let the following variables equal the positive values of their respective expressions in the $-A$ matrix, i.e.:

$$a_{32} = \frac{mg}{M}$$

$$a_{33} = \frac{b_{VF}}{M}$$

$$a_{34} = \frac{c}{M\ell}$$

$$
\begin{aligned}
a_{42} &= \frac{(M+m)g}{M\ell} \\
a_{43} &= \frac{b_{VF}}{M\ell} \\
a_{44} &= \frac{(M+m)c}{Mm\ell^2}
\end{aligned}
$$

then the general form of the characteristic equation is given by:

$$
\begin{aligned}
0 &= \lambda^4 + (a_{33}+a_{44})\lambda^3 + (a_{44}a_{33} - a_{43}a_{34} - a_{42})\lambda^2 + (a_{43}a_{32} - a_{42}a_{33})\lambda \quad (2.29) \\
&= \lambda^4 + C_3\lambda^3 + C_2\lambda^2 + C_1\lambda \quad (2.30)
\end{aligned}
$$

Explicit expressions for the C_i are given below:

$$
\begin{aligned}
C_3 &= \frac{1}{M}(b_{VF} + \frac{(M+m)c}{m\ell^2}) \\
C_2 &= \frac{1}{M\ell}(\frac{(M+m)cb_{VF}}{Mm\ell} - \frac{b_{VF}c}{M\ell} - (M+m)g) \\
C_1 &= \frac{1}{M^2\ell}(mgb_{VF} - (M+m)gb_{VF}) \\
&= -\frac{gb_{VF}}{M\ell}
\end{aligned}
$$

Clearly, one of the system eigenvalues λ_1 will always be at zero, regardless of the values given for system parameters. We can solve for the general location of the other three by using the form for roots of a cubic equation [Eshbach 223]. Let:

$$q = C_3C_1 - C_2^2 \qquad r = \frac{3}{2}C_1C_2C_3 - C_2^3$$

and

$$s_1 = (r + \sqrt{q^3 + r^2})^{\frac{1}{3}} \qquad s_2 = (r - \sqrt{q^3 + r^2})^{\frac{1}{3}}$$

The general form of the roots is then given by:

$$
\begin{aligned}
\lambda_2 &= [(s_1 + s_2) - C_2]/C_3 \\
\lambda_3 &= [-\frac{1}{2}(s_1 + s_2 + \frac{\sqrt{-3}}{2}(s_1 - s_2) - C_2] \,/\, C_3 \\
\lambda_4 &= [-\frac{1}{2}(s_1 + s_2 - \frac{\sqrt{-3}}{2}(s_1 - s_2) - C_2] \,/\, C_3
\end{aligned}
$$

The final expressions for the eigenvalues in terms of the system parameters are rather complex and will not be given here. However, we can see from the explicit expressions for the C_i that C_1 is always negative, and a more careful look at C_2 will show that it, too, will almost always be negative (unless friction constants are absurdly high or pendulum length is zero, etc.). Thus, Equation 2.30 displays only one change in sign. According to Routh's stability analysis, this indicates one of the remaining eigenvalues has a sign opposite the other two [Franklin 113], and, in fact, this one eigenvalue is in the right half-plane, the other two being in the left half-plane. This indicates an unstable system with one unstable mode, which, of course, we expect, since the pendulum is inherently unstable.

Further experimentation with the Routh stability array can reveal instances (if system parameters are at certain values) in which the two stable eigenvalue can actually depart from the real axis and form a conjugate pair of complex poles. However, all four eigenvalues will almost always lie on the real axis for realistic values for system parameters. It is not difficult to show that assuming the system is frictionless will cause the lower right-hand quarter of the state system matrix to disappear, causing C_1 to go to zero, and placing one of the otherwise stable eigenvalues at the origin. This would result in two poles at zero, and two on the real axis, one in each half-plane.

It is also important to note that the Cart-Pendulum plant is typically a *non-minimum phase system*, depending on choice of outputs. As shown in Chapter 4, the transfer functions $\frac{s}{F_U}$ and $\frac{\dot{s}}{F_U}$ each have a finite zero in the right half-plane for typical system parameter values. The implications of this characteristic will be discussed in detail in Chapter 4.

2.2 Motor Assembly Modeling and Dynamics

As discussed in Chapter 1, the entire Cart-Pendulum system consists of three essential components: (1) the Cart-Pendulum itself, (2) the motor assembly, and (3) the controller. The dynamic model for the first component has been thoroughly developed above, and the design of the third component will be the topic of the majority of the following chapters. The task here is to produce a suitable model for the interim

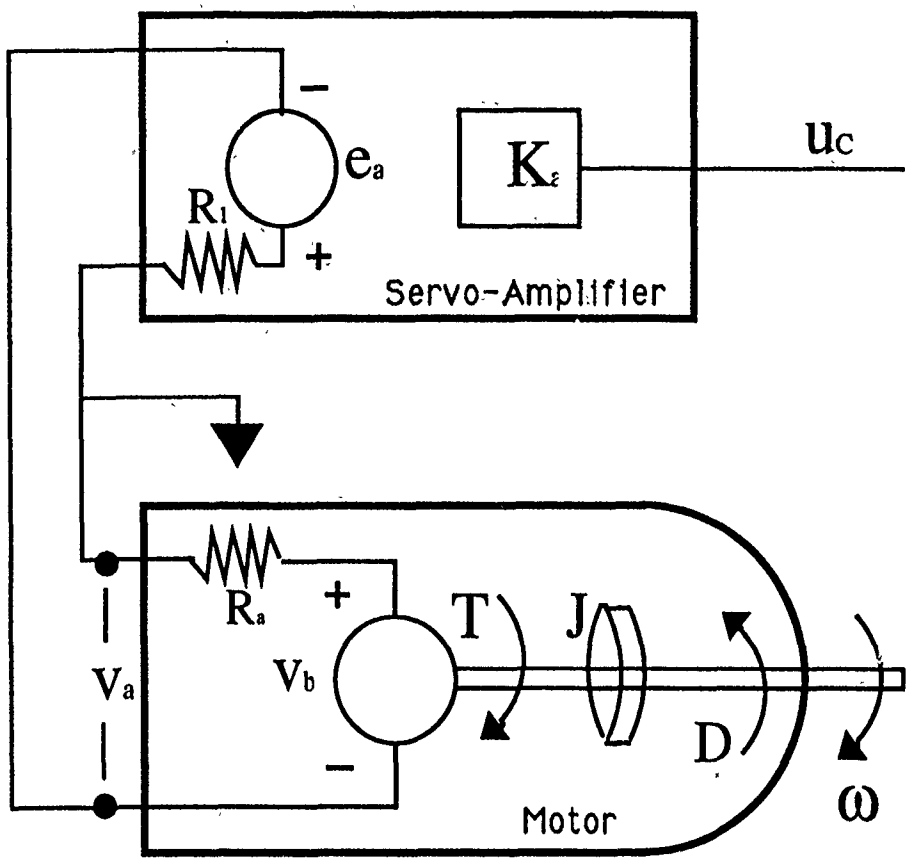

Figure 2.2: Diagram of Servo Amp-Motor Arrangement

component: the motor actuator. As previously mentioned, the "actuator" in this case includes all components that come between the controller output voltage signal, and the force the belt exerts on the cart. Thus, the servo amplifier, motor, pulleys, and belt all contribute to the dynamics of the actuator.

The complete model for the motor actuator is shown in Figure 2.2. As shown, the command signal from the controller enters the servo-amplifier, which is connected to a power supply. The servo-amp then produces a voltage, proportional to the command signal by a constant, K_A. The motor converts the voltage v_a into a net torque on the motor shaft, T_{net}, and, in turn, into a force applied on the cart, F_U. The equations of motion for the motor are given by:

$$v_a = L_a\frac{di}{dt} + R_a i + v_b \tag{2.31}$$

$$v_b = K\omega \tag{2.32}$$

$$J\dot{\omega} = \sum Torques = Ki - D\omega - F_f \tag{2.33}$$

where L_a is motor inductance, K is the motor constant, R_a is resistance within the motor, J is the inertia of the motor *and* of the pulleys and belt attached to the motor, D is viscous damping within the motor, and F contains all forces of friction not contained in viscous friction. Usually motor inductance L_a is small enough that its effects are negligible, and it can be ignored.

Our objective here is to transform the nonlinear motor equations into a linear model that can be employed in linear control design. Substituting Equation 2.32 into Equation 2.31 and assuming inductance is negligible produces:

$$v_a = R_a i + K\omega \tag{2.34}$$

Solving this equation for i and substituting into Equation 2.33 produces:

$$J\dot{\omega} = \frac{K}{R_a}v_a - (\frac{K^2}{R} + D)\omega - F_f \tag{2.35}$$

At this point, to obain a linear model, we must assume the friction term, F_f, is negligible. We can address the friction issue after obtaining the linear model. Eliminating F_f and transforming into the Laplace domain produces the following:

$$Js\omega(s) = \frac{K}{R}v_a(s) - (\frac{K^2}{R} + D)\omega(s) \tag{2.36}$$

which leads to the transfer function:

$$\frac{\omega(s)}{v_a(s)} = \frac{\frac{K}{K^2+DR}}{(\frac{J}{D+K^2/R})s + 1} \tag{2.37}$$

To obtain the transfer function we desire, $\frac{F_U(s)}{v_a(s)}$, we must multiply the above transfer function by the one relating ω to the force applied by the motor to the system,

F_U. This is shown in Figure 2.3, and is expressed by:

$$\begin{aligned}\frac{F_U(s)}{\omega(s)} &= \frac{1}{r}\frac{T_{net}(s)}{\omega(s)} \\ &= \frac{1}{r}Js \\ &= \frac{Js}{r}\end{aligned}$$

where T_{net} is the net torque output of the motor (not including friction) and r is the radius of the pulley, through which we convert output torque to an output force, F. Thus, the complete transfer function is:

$$\frac{F_U(s)}{v_a(s)} = \frac{\frac{JK}{r(K^2+DR)}s}{(\frac{J}{D+K^2/R})s+1} \tag{2.38}$$

Of course, we still have not accounted for the friction force, F_f. Assuming that this force is relatively constant for $\omega \neq 0$, we can express the final force applied to the cart, F_U, as follows:

$$F_U = F - F_f \tag{2.39}$$

where the sign of the friction force is determined by the direction of motor rotation:

$$F_f = sign(\omega)|F_f| \tag{2.40}$$

This relationship is also expressed in Figure 2.3. We are unable to apply this friction term in the linear model, but it will be useful to remember when analyzing system response and results.

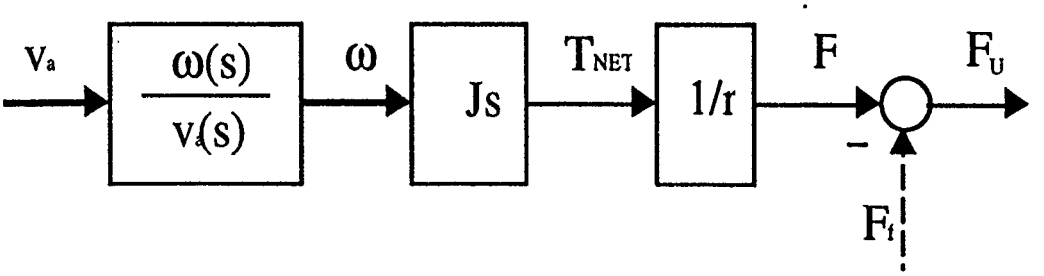

Figure 2.3: Relating Input Voltage to Output Force

Since the tendency of actuators is to introduce a slight delay between given inputs and resultant outputs, they are commonly modeled as first-order systems (a single pole) with an exponential rise or decay, as we have shown with the motor equations. An actuator may or may not have a zero. The transfer function can be expressed in the form:

$$\frac{K_U(s+z)}{\tau s+1} \quad or \quad \frac{K_U}{\tau s+1}$$

where τ is the *time constant* of the actuator, a measure of how quickly it responds to a given input. These forms of actuator models are shown in the bottom of Figure 2.4. In the time domain, the time constant appears as a parameter in a function of exponential decay:

$$x(t) = e^{-\frac{1}{\tau}t}$$

For our motor model,

$$\tau = \frac{J}{D+\frac{K^2}{R}}$$

The addition of a first-order actuator model to our four-state Cart-Pendulum now increases the total order of our system to five, and adds an additional pole to the left half-plane (as well as a zero to the origin for this particular model). Note that this pole will always (for open-loop system) be at the location:

$$\lambda_{ACTUATOR} = -\frac{1}{\tau} + 0i$$

It would appear we are "stuck" with this extra pole in our control system design. *However,* if we discover that the actuator pole is relatively far enough from the imaginary axis (i.e. it has a relatively low time constant) compared to the poles describing the dynamics of the Cart-Pendulum, the behavior of the actuator begins to approximate a simple proportional gain model. In this case, the "connection" between u and F_U is a simple gain, K_U, as shown in the top of Figure 2.4. This gain would provide the appropriate conversion from voltage input to force output. In short, the rate of decay or rise in actuator response is much faster than the response of the natural system, and the effect of the "fast pole" on the system is small [Franklin 54].

Therefore, it may be possible to abandon the first-order model during control system design and replace it with an instantaneous one, thus simplifying design procedure, without suffering in performance. In previous works, this has been common

practice. Mori et al assumed the control command was "directly applied to the cart without any delay" [Mori 674]. Reekers showed that the actuator pole on the servo-motor assembly used in Duisburg was significantly faster than the plant dynamics, and could therefore be approximated by a proportional gain [Reekers 5]. We will examine this possibility more closely during linear control system design. Results of actual analysis performed on the hardware actuator used in the University of Washington laboratory are located in Appendix B.

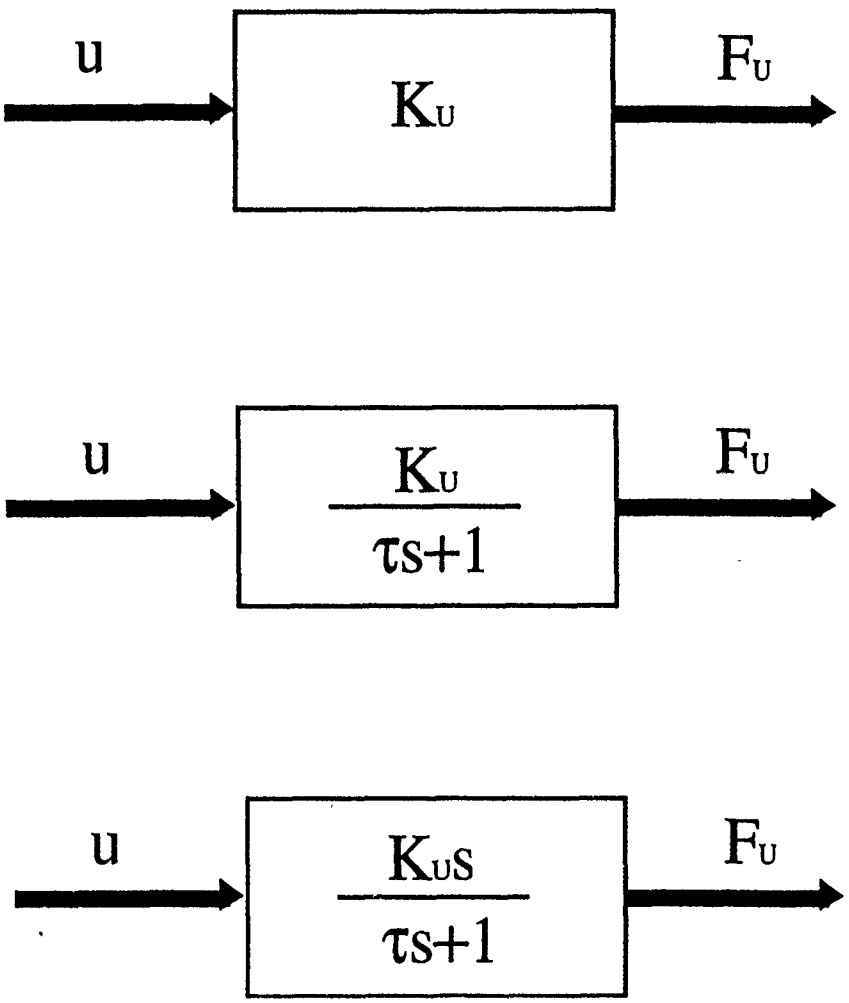

Figure 2.4: Possible Linear Models for Motor Assembly

Chapter 3

PENDULUM "PUMP-UP" CONTROL FROM NON-INVERTED CONFIGURATION

3.1 Introduction

The "complete" inverted pendulum problem, as described in Chapter 1, demands that the pendulum first be "pumped-up" into the inverted configuration ("Phase 1"). The idea of "pump-up" or "swing-up" of the cart-pendulum involves beginning initially in the stable (pendulum hanging downward) position, and subjecting the cart-pendulum to a "schedule" of accelerations in both directions that will eventually cause the pendulum to swing into a nearly upright position. Once there, a linear feedback controller can then be imposed to maintain the pendulum in its otherwise unstable inverted configuration.

The best way to implement the "pump-up" control scenario is through an *open-loop control schedule*; i.e. a preplanned schedule of control inputs that are applied to the system without requiring any continuous feedback (although, we will see that some forms of feedback can be useful in the case of supervisory control). Knowledge of the system parameters and the control available should enable us to analytically determine the optimal pump-up control schedule.

One effective way to pose the pump-up problem is to require that the cart be positioned in the middle of the track ($s = 0$) and the pendulum be upright ($\theta = 0$) at some final time T_F, with little or no cart velocity or pendulum angular velocity. Constraints include requiring the cart to remain within the operating confines of the track, applying only limited control ($u_{min} \leq u \leq u_{max}$), and requiring the terminal time T_F to be *minimized*. What results is a minimum-time optimization problem with terminal constraints on the states (namely, that they be homogeneous). Imposing a path constraint, namely that the cart position not go beyond the track boundaries, could also be added. The nonlinear equations of motion must be used in this pump-up analysis, since the small-angle assumptions made during linearization (i.e. $\sin\theta \approx \theta$

and $\cos\theta \approx 1$) are no longer valid.

3.2 Formulation of the Optimization Problem

Note that our non-linear state equations (2.16, 2.17, 2.18, and 2.19) can be separated into terms containing functions of the states x and control u by themselves. So let our n non-linear state equations of motion take the following form:

$$\dot{x} = f(x,u) = f_0(x) + f_1(x,u) \tag{3.1}$$

Our objective is to minimize the amount of time required to pass from an initial state (described at $t = 0$) to a final state (described at $t = T_F$), determined when specified conditions are met. Thus, as a minimum-time problem, the general form of the non-constrained cost function takes the form:

$$J = \int_0^{T_F} 1\, dt \tag{3.2}$$

The final time T_F is characterized by specified terminal constraints on the states. The number of constraints for our problem may vary from 1 (where we demand only that $\theta = 0$ at T_F) to 4 (where we demand all states, positions and velocities, return to zero). Clearly, the more constraints, the more complex the problem and the more likely T_F will be greater. These terminal constraints on the states ($x(T_F) = 0$) can be expressed as a vector function ψ of length v, where $1 \leq v \leq n$:

$$\psi(x(T_F), T_F) = 0 \tag{3.3}$$

Of course, in addition to specified terminal constraints, the states must adhere to natural constraints within the interval $0 \leq t \leq T_F$; namely, the equations of motion themselves. Adjoining these constraints on the states produces a Hamiltonian function in the following form:

$$H(x,u,\lambda) = 1 + \lambda^T f(x,u) \tag{3.4}$$

which can be broken down using Equation 3.1 to form the following, where λ^T is the transpose of the n-dimensional adjoint (or co-state) vector λ:

$$H(x,u,\lambda) = 1 + \lambda^T f_0(x) + \lambda^T f_1(x,u) \tag{3.5}$$

A rigorous pursuit of the optimal minimum-time solution requires the solution of a system of equations which define the necessary conditions. The necessary conditions for optimality [Bryson 89] are as follows:

$$\dot{x} = f(x,u) = (\frac{\partial H}{\partial \lambda})^T \tag{3.6}$$

$$x(t_0) = x_0 \tag{3.7}$$

$$\dot{\lambda} = -(\frac{\partial H}{\partial x})^T = -(\frac{\partial f}{\partial x})^T \lambda \tag{3.8}$$

$$\lambda^T(T_F) = (\nu^T \frac{\partial \psi}{\partial x})^T_{t=T_F} \tag{3.9}$$

$$\psi(x(T_F), T_F) = 0 \tag{3.10}$$

and finally, to determine the final time,

$$\Omega = [\nu^T \frac{d\psi}{dt} + L]_{t=T_f} = 0 \tag{3.11}$$

The control is defined from:

$$0 = -(\frac{\partial H}{\partial u})^T = -(\frac{\partial f_1}{\partial u})^T \lambda \tag{3.12}$$

if u is not bounded, or simply from

$$min_u \; H$$

if u is bounded.

These equations (3.6 through 3.12) provide enough conditions to find all unknown quantities. This results in a rather complex two-point boundary value problem [Bryson 89], and is a complete project in itself. But we can obtain a simple and practical optimal pump-up theory by simply looking at Equation 3.5 more closely and deriving the form that the control must take. Rewrite 3.5 to read:

$$H(x, u, \lambda) = H_1(x, \lambda^T) + H_2(x, \lambda^T)u \tag{3.13}$$

which is legitimate, since u is linear in all terms of the non-linear equations of motion (Equations 2.9 and 2.10). Since our goal is to minimize H and our only means of doing so is our control u, the form (and sign) of H_1 is irrelevant. To minimize the term $H_2(x, \lambda^T)u$, we employ the following for u:

$$H_2 < 0 \quad \Rightarrow \quad u = u_{MAX} \tag{3.14}$$

$$H_2 > 0 \quad \Rightarrow \quad u = u_{MIN} \tag{3.15}$$

The conclusion is that the optimal control for the pump-up scenario must be of the "bang-bang" variety, where only the minimum (greatest negative) and maximum (greatest positive) possible control inputs are used [Mori 93]. There is a possible exception: note that if $H_2 = 0$, the value of u with regard to minimization of H *cannot be determined* since the Hamiltonian itself gives no information concerning explicit minimization with respect to u. In this case, the optimal control is hidden within the dynamics of the system which determine H_2, and the control solution is a singular arc [Bryson 252]. For purposes of simplicity, we will assume an optimal pump-up control law can be found that demands only three possible values for u:

$$u = u_{MAX}$$

$$u = u_{MIN}$$

$$u = 0$$

The $u = 0$ instance may be necessary to restrict the cart from moving beyond the track limits.

3.3 *Open Loop Bang-Bang Control Scheduling*

Given that bang-bang control should produce a near-minimum-time pump-up, a strategy for designing a control schedule can be devised. The idea is to accelerate the pendulum forcefully enough to swing it up quickly, yet keep the cart within its operating limits on the cart, and return all velocities to near zero and the cart to the center position when the pendulum has reached a nearly upright configuration. The cart should be moving slowly or not at all and in the center of the track ($s = 0$) so that when the linear controller takes over, it has plenty of room in which to operate. Similarly, we want the pendulum angular velocity near zero at the terminal time so that there is no danger the pendulum will continue to swing around out of the "zone of linearity" before the linear controller has time to engage and become effective.

Keeping these "constraints" in mind, we can proceed with the control schedule philosophy. Accelerations on the cart produce the most effective accelerations on the swinging pendulum when the pendulum is in a *vertical* state. Thus, it is desirable to coordinate the reversals in control (i.e. the"bangs") with crossings of the pendulum with the vertical. Thus, a clever strategy to employ is one used by Reekers [Reekers 100], whereby each pendulum crossing of the $\theta = 180°$ point is followed by three control phases: (1) an acceleration to pump up the pendulum, (2) a deceleration to return the velocity of the cart to zero (and keep it within the track boundaries), and (3) a "waiting period," where $u = 0$ until the pendulum again crosses the $\theta = 180°$ point. Once another crossing takes place, the sequence is repeated, with the control directions reversed.

The optimal control profile using this strategy will vary as system parameters vary. Changes in masses, friction terms, pendulum length, and especially available control will affect the control schedule. But, for a given set of masses, pendulum length, frictional forces, and maximum available control force, there will be one optimal control schedule. Figure 3.1 shows the time histories of the four system states, given a control schedule described by Figure 3.2 for the basic cart-pendulum system parameters given in Table B.1 in Appendix B. The maximum control available was assumed to be 15 Newtons. Note that the velocities approach zero as the pendulum angle approaches 0° (that being upright), and the cart returns to the middle of the track.

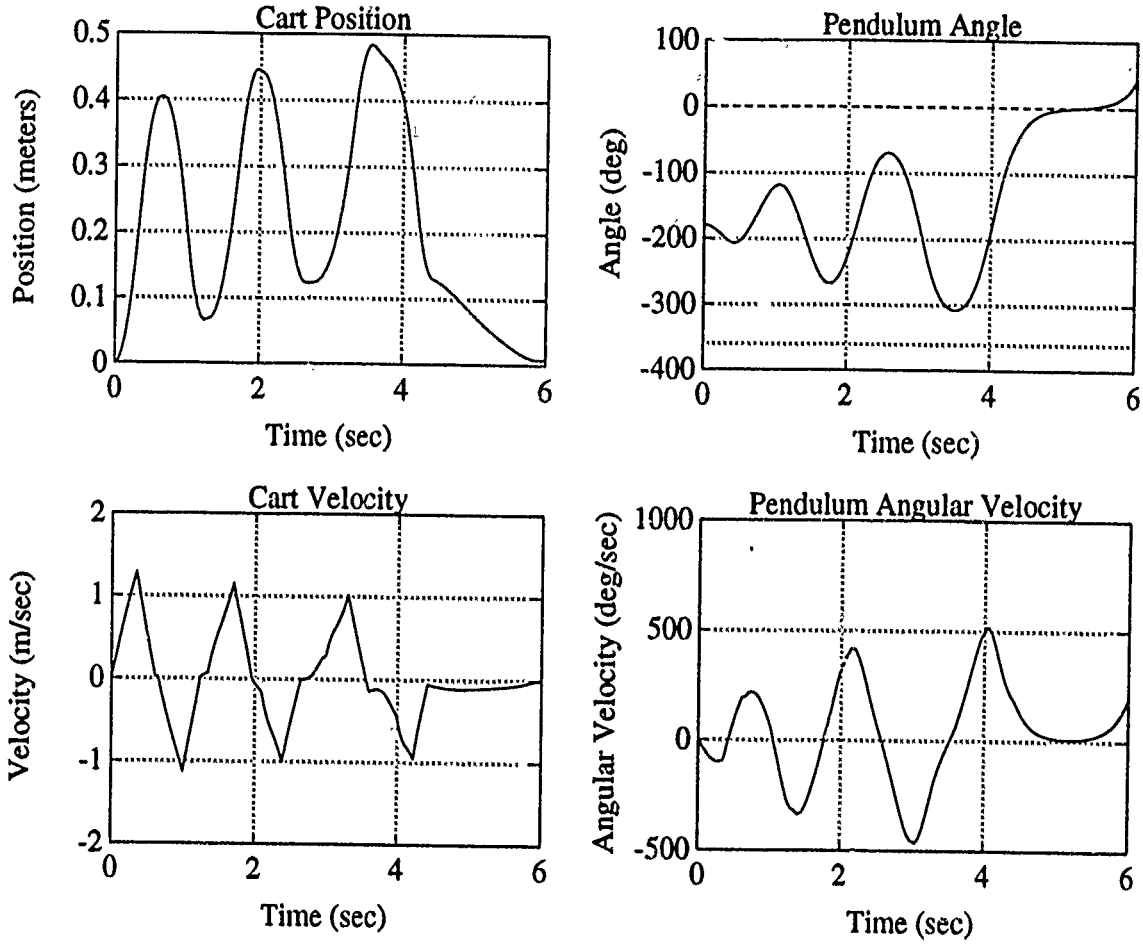

Figure 3.1: State Time Histories with Typical Bang-Bang Control Schedule

The actual switching times employed are listed in Table 3.1. These were obtained through computer analysis by simulating the nonlinear dynamics of the cart-pendulum. The pump-up maneuver was initiated by applying the first "bang" to the cart (pendulum resting at $\theta = 180°$), then monitoring the simulated pendulum angular velocity to detect when the pendulum reached the highest point of its first upswing. When pendulum velocity had decayed to zero, the first reverse "bang" was be applied. Then cart velocity was monitored; when it returned to zero, the third phase–zero control input–began. The control sequence began again, in the form of another "series" of phases, when the pendulum crossed the 180° position. In sum-

mary:

$$\begin{aligned} \theta = 180^{\circ} &\Rightarrow \textit{Positive Control Input (Phase 1)} \\ \dot{\theta} = 0 &\Rightarrow \textit{Negative Control Input (Phase 2)} \\ \dot{s} = 0 &\Rightarrow \textit{Zero Control Input (Phase 3)} \\ \theta = 180^{\circ} &\Rightarrow \textit{Negative Control Input (Phase 1)} \end{aligned}$$

and so on.

The pump-up problem could theoretically be optimized even further by timing series changes to coincide not only with crossings of the 180^0 point, but also with crossings of the 90° and -90° points. It is easy to show that such accelerations on the pendulum while above the horizontal would help to drive it upwards even quicker.

3.4 "Pump-up" Feedback Possibilities

Up to this point we have assumed that the pump-up maneuver would be strictly open-loop. However, it may actually be possible to use a form of supervisory control strategy using observations of the system states to schedule the timing of the "three-phase" control strategy, and therefore abandon a pre-programmed control schedule.

The control logic used in computer simulation to obtain the open-loop control schedule could also be employed *actively* to command the actuator bang-bang control switches. As before, the pump-up maneuver would be started with a positive command to the actuator. Then, by monitoring pendulum angle, pendulum angular velocity, and cart velocity, the successive switches could be directed by a supervisory controller at the appropriate times to perform the optimal pump-up schedule. It may also be possible, even necessary, to monitor cart position feedback as a safeguard against tendencies to exceed the limits of the track.

3.5 "Hand-off" to Linear Controller

The ultimate goal of the pump-up control law, regardless of whether it is open-loop or employs a supervisory control scheme, is to bring the pendulum as close to

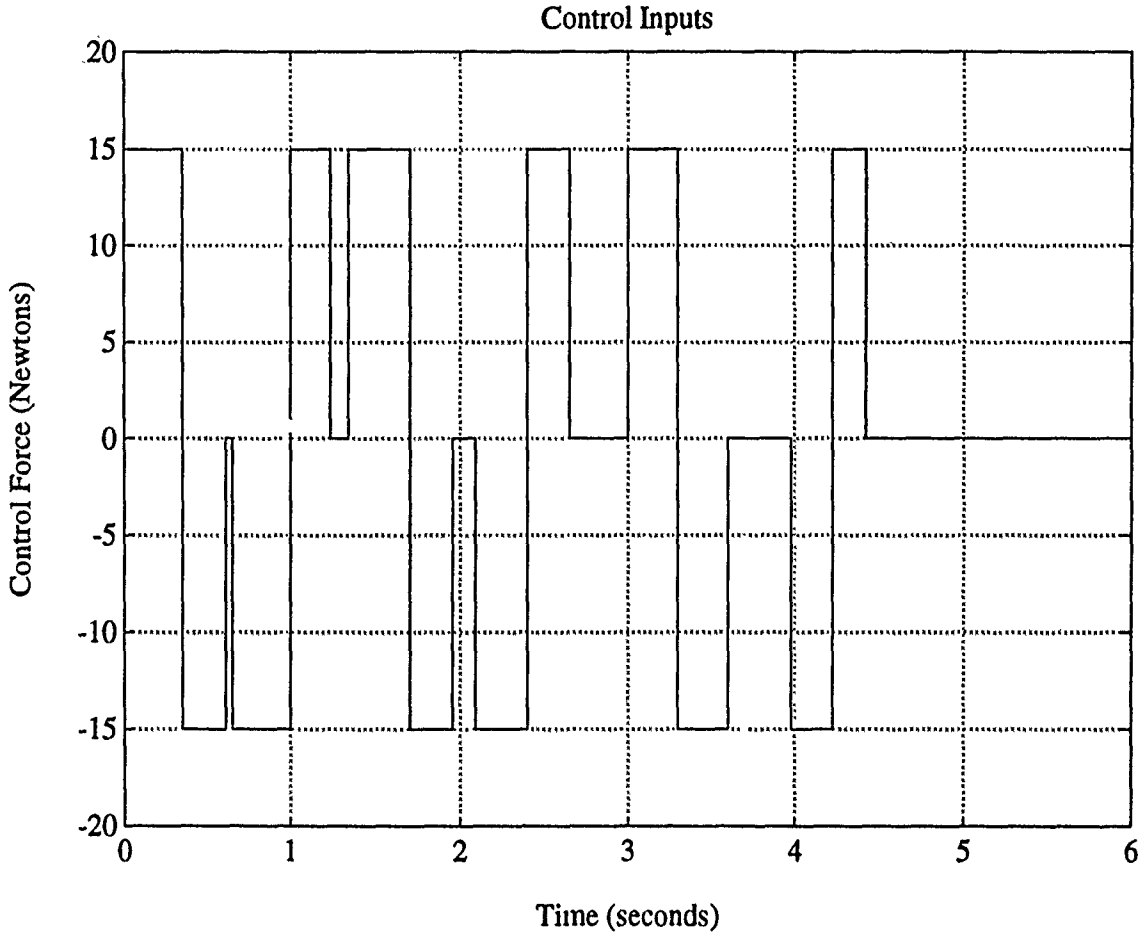

Figure 3.2: Bang-Bang Control Schedule

its unstable equilibrium position as possible, allowing a linear feedback controller to "assume control" of the system and maintain the pendulum there. This "hand-off" point needs to be chosen carefully, and will involve evaluation of not only the pendulum's position, but also its velocity, as well as cart position and velocity. Even if the pendulum is nearly upright and moving slowly, linear control may not yet be possible if the cart is at the end of the track (and therefore has no room to maneuver), or is moving quickly enough that it will reach the end before linear control can take effect.

The ideal situation is the one already shown in Figure 3.1, where not only is the

pendulum essentially upright and motionless, but the cart is hardly moving and near the center of the track ($s = 0$). We would expect any reasonably effective feedback controller to be able to control the system at this point. Indeed, the plots indicate a period of "relative stability" of .5 seconds or more (from approximately 5.0 to 5.5 seconds) in which a hand-off could take place. Table 3.1 indicates 5.20 seconds as a good time to initiate linear control.

Hand-off difficulties arise when the states are not as close to their ideal homogeneous values as we would like. What is necessary, then, is a determination of a "zone of control" within which the linear controller is effective. This enters into the realm of "fuzzy" control logic, in which penalty weightings on nonhomogeneous values for the states can produce a related cost function. Linear control would be initiated when this cost falls below a certain value.

3.6 Experimental Observations

Experience with the pump-up problem in Duisburg [Reekers 68] and at the University of Washington has revealed that experimentation with the actual system, employing the same strategy of three-phase pumping and using theoretical performance (like that shown in Figures 3.1 and 3.2) as a guide, is a reliable method for determining a useful bang-bang pump-up control law. Unmodeled and/or unpredictable frictional forces within the system, plant model inaccuracies, and a variety of other possible factors make physical experimentation a necessary part of determining the final control sequence.

Implementation of supervisory control logic would hopefully eliminate the problems posed by unexpected forces in the system. However, it would tend to make the timing of transition to linear control a bit more unpredictable, and makes the need for effective hand-off logic greater.

SERIES 1	Phase 1	F_{Umax}	0.00	sec
	Phase 2	F_{Umin}	0.35	sec
	Phase 3	0	0.61	sec
SERIES 2	Phase 1	F_{Umin}	0.65	sec
	Phase 2	F_{Umax}	1.00	sec
	Phase 3	0	1.235	sec
SERIES 3	Phase 1	F_{Umax}	1.34	sec
	Phase 2	F_{Umin}	1.70	sec
	Phase 3	0	1.955	sec
SERIES 4	Phase 1	F_{Umin}	2.09	sec
	Phase 2	F_{Umax}	2.40	sec
	Phase 3	0	2.65	sec
SERIES 5	Phase 1	F_{Umax}	3.00	sec
	Phase 2	F_{Umin}	3.30	sec
	Phase 3	0	3.60	sec
SERIES 6	Phase 1	F_{Umin}	3.98	sec
	Phase 2	F_{Umax}	4.22	sec
	Phase 3	0	4.42	sec
HANDOFF TO LINEAR CONTROLLER			5.20	sec

Table 3.1: Table of Bang-Bang Switching Times

Chapter 4

OPTIMAL LINEAR QUADRATIC CONTROL AND ESTIMATION

4.1 Introduction

We assume that the "pump-up" control sequence has successfully raised the pendulum to a near vertical position, brought the cart near the middle of the track, and reduced both velocities to nearly zero. Phase 1 is complete, and responsibility for pendulum control is now "handed off" to a linear controller (Phase 2). Such a controller may take many forms, but our approach here will be to develop an *optimal full-state feedback* control system. Such a controller is certainly more complex than a classical first or second order control system, but, if properly implemented, is capable of being far more effective, while hopefully maintaining similar levels of robustness.

As shown in linear dynamics in Chapter 2, the Cart-Pendulum is either a fourth or fifth-order system, depending upon whether or not an actuator state is included. If we assume the actuator acts with very little delay, the system has four states, and employs the state system matrix given in Equation 2.28 and shown again below:

$$\frac{d}{dt}\begin{bmatrix} x_1 \\ x_2 \\ x_3 \\ x_4 \end{bmatrix} = \begin{bmatrix} 0 & 0 & 1 & 0 \\ 0 & 0 & 0 & 1 \\ 0 & -\frac{mg}{M} & -\frac{b\nu_F}{M} & \frac{c}{M\ell} \\ 0 & \frac{(M+m)g}{M\ell} & \frac{b\nu_F}{M\ell} & -\frac{(M+m)c}{Mm\ell^2} \end{bmatrix}\begin{bmatrix} x_1 \\ x_2 \\ x_3 \\ x_4 \end{bmatrix} + \begin{bmatrix} 0 \\ 0 \\ \frac{1}{M} \\ -\frac{1}{M\ell} \end{bmatrix} F_U \quad (4.1)$$

Our full-state feedback controller, then, will require feedback values for the quantities s, θ, $\dot{s}$, and $\dot{\theta}$ (x_1, x_2, x_3, and x_4). As already noted, the system hardware provides for the direct output measurements of the first two quantities through potentiometers attached to the Cart-Pendulum, as well a measurement for the third

quantity in the form of the motor tachometer output. However, no direct measurement of the fourth quantity, $\dot{\theta}$, is available. Thus, in order for the full-state feedback controller to be effective, this value must somehow be *estimated* continuously. This provides an additional challenge to the optimal linear control design.

The complete system (aside from the controller itself) has a minimum order of four, and can be successfully modeled as such. However, a fourth-order model assumes control commands and the subsequent control inputs are nearly instantaneous, and that the motor produces no delay. But, as pointed out in Section 2.2, if we decide the dynamics of the motor assembly are slow enough compared to the dynamics of the plant, it may be necessary to include an additional fifth state in our design: an actuator state. This state, too, must be estimated in some way to make full-state feedback feasible. We will examine both system models, fourth and fifth order, in the control design.

The optimal control and estimation problem can be approached in a variety of ways, but almost always boils down to three essential tasks: (1) synthesis of an optimal control law, (2) synthesis of an optimal estimator, and (3) integration of both estimator and control law into an optimal controller [Maciejowski 224].

The approach here will be to first develop the optimal LQ regulator and control law. This is done, of course, assuming all states are available through measurement. The next task is to develop the optimal estimator, which, for this particular problem, can be done several ways. Finally, the two can be integrated, and the performance and robustness of the control design can be examined.

4.2 LQ Regulator Design

4.2.1 Basic LQR Design for Fourth-Order System

As shown in Figure 4.1, all four states x are employed using full-state feedback through the gain matrix G to obtain the control u. Under conventional eigenplacement approach, G is found by determining what gains are necessary to place the closed loop poles at designated locations [Franklin 419]. While effective, this method lacks the versatility and efficiency of an optimization approach.

In its simplest form, the optimization problem involves minimizing the following cost function:

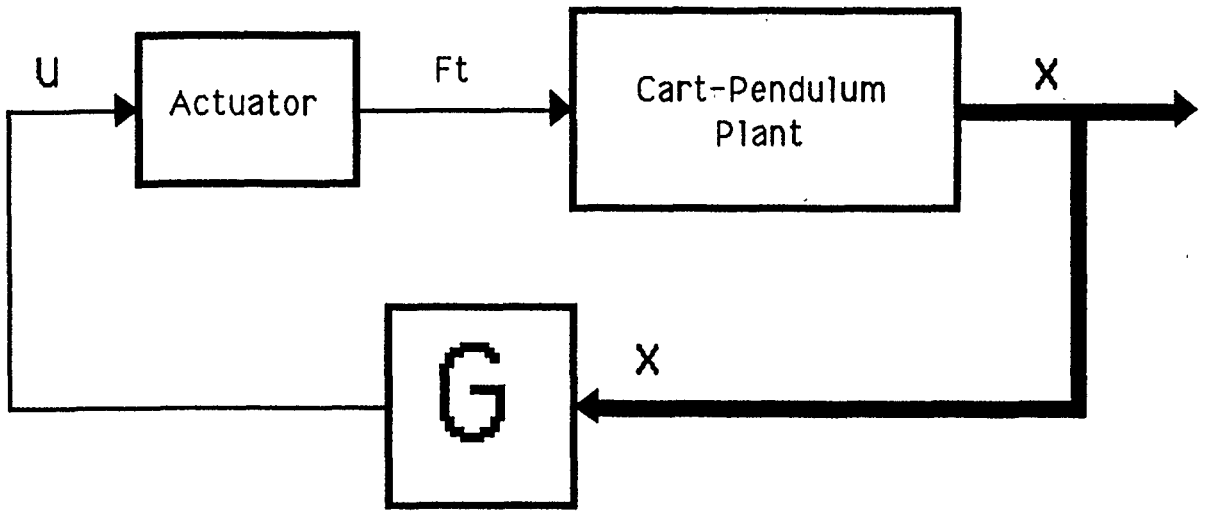

Figure 4.1: LQ Regulator Controller Block Diagram

$$J = \frac{1}{2}\int_{t_0}^{\infty} x^T Q x + u^T R u \, dt \tag{4.2}$$

where Q is a positive semi-definite weighting matrix on states x and R is a positive definite weighting matrix on controls u [Bryson 158]. The optimal control law u(t) for the regulator problem is given by:

$$u(t) = -R^{-1} B^T S_0 x(t) \tag{4.3}$$

where S_0 is the symmetric positive semi-definite solution to the following steady-state Ricatti equation:

$$-A^T S_0 - S_0 A + S_0 B R^{-1} B^T S_0 - Q = 0 \tag{4.4}$$

The optimal full-state feedback gain matrix G is, of course, given simply by:

$$G = -R^{-1} B^T S_0 \tag{4.5}$$

and has dimensions $p \times n$, with p the number of inputs (1 for this SIMO system), and n the number of states incorporated in the full-state feedback design. This second number may vary, depending on how actuators are modeled, whether we include additional states within our controller, etc. The final simplified optimal control law

takes the form:

$$u(t) = Gx(t) \tag{4.6}$$

The closed loop system, as shown in Figure 4.1, is guaranteed to be asymptotically stable as long as the following conditions hold:

(1) The pair (A,B) is stabilizable, i.e. all unstable modes are controllable.

(2) The pair (A,H) is detectable, i.e. all unstable modes are observable.

The matrix H is defined as the square root of the weighting matrix Q, such that $H^T H = Q$.

Clearly, the most important part in the optimal design process is selection of the weights within the weighting matrices Q and R. In the simplest arrangement, both matrices are diagonal with diagonal elements corresponding to weights on the states x and controls u, respectively. The inverted Cart-Pendulum array provides, at a minimum, four states, and generally one control. Thus, the Q and R matrices might take the following form:

$$Q = \begin{bmatrix} q_1 & 0 & 0 & 0 \\ 0 & q_2 & 0 & 0 \\ 0 & 0 & q_3 & 0 \\ 0 & 0 & 0 & q_4 \end{bmatrix} \tag{4.7}$$

$$R = [r_1] \tag{4.8}$$

where the weights q_i and r_i are to be determined.

Selection of these weights can be dependent upon the type of performance desired from the system for any particular control scenario or maneuver. Variation in the weights will result in changes to the gain matrix G and will ultimately affect the type of control imposed on the system. [For example, in a scenario that would emphasize minimizing the pendulum angle and angular velocity but puts little or no restriction on cart position or velocity, we would expect q_2 and q_4 (the weights on θ and $\dot{\theta}$, respectively) to be large relative to q_1 and q_3 (weights on s and $\dot{s}$.] The end result is that we will have a variety of "gain schedules" G corresponding to various control scenarios and weighting schemes.

For practical applications, the weights may be fine-tuned to specific values after observation and trial-and-error. However, for initial selection of weights to set up a

"general" control scenario, it is helpful to employ a rule of thumb first suggested by Bryson:

$$q_i = \frac{1}{\sigma_i^2} \tag{4.9}$$

$$r_i = \frac{1}{\gamma_i^2} \tag{4.10}$$

where σ_i and γ_i are the maximum allowable values for the respective states/controls.

4.2.2 Addition of Integral States

We might find it useful to include more states in our system than just the four that are the natural dynamics of the Cart-Pendulum. Use of integral states and proper weights upon them may help to eliminate any steady-state or residual error that may linger in the system. The weights placed upon these states in the Q matrix will dictate how quickly we would like our control system to respond to error that has accumulated. The addition of two integral states expands our state vector and Q matrix as shown:

$$\vec{x} = \begin{bmatrix} x_1 \\ x_2 \\ x_3 \\ x_4 \\ x_5 \\ x_6 \end{bmatrix} = \begin{bmatrix} s \\ \theta \\ \dot{s} \\ \dot{\theta} \\ \int s \\ \int \theta \end{bmatrix} \tag{4.11}$$

$$Q = \begin{bmatrix} q_1 & 0 & 0 & 0 & 0 & 0 \\ 0 & q_2 & 0 & 0 & 0 & 0 \\ 0 & 0 & q_3 & 0 & 0 & 0 \\ 0 & 0 & 0 & q_4 & 0 & 0 \\ 0 & 0 & 0 & 0 & q_5 & 0 \\ 0 & 0 & 0 & 0 & 0 & q_6 \end{bmatrix} \tag{4.12}$$

The addition of integral states increases the order of the controller by one or two (we could use either or both integrators), but allows an added dimension of control design. Note that by setting $q_5, q_6 = 0$ we effectively cut the connection of the

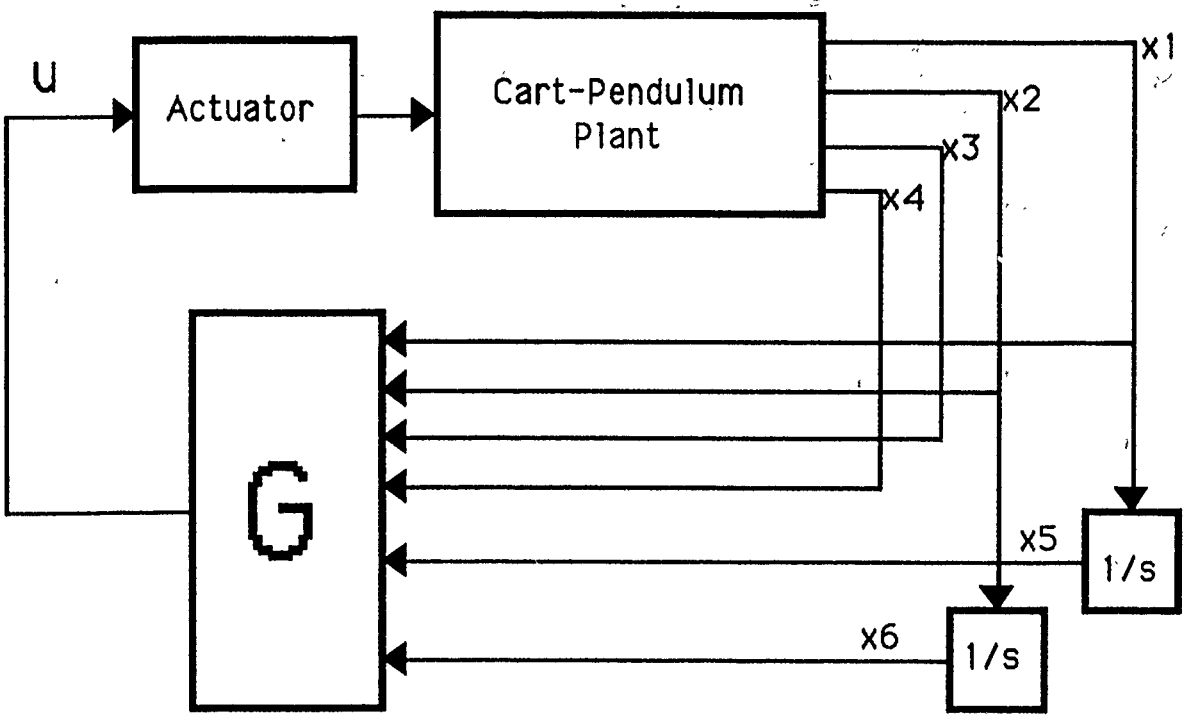

Figure 4.2: LQ Regulator with Integral States

integrators to the system and regain the original fourth-order model. Figure 4.2 shows how the addition of integrators to the system produces two additional states. It should be noted that the addition of integral states, though it may aid in error reduction, often adversely affects system performance. Careful consideration must be given (through experimenatation, etc) to the assigned weights on these states to be certain they do not dominate the regulator control law.

4.2.3 Addition of Actuator State

Thus far we have assumed the actuator could be modeled with simply a proportional gain. However, as pointed out in Section 2.2, the actuator lag or delay may be significant compared to the dynamics of the Cart-Pendulum, and an additional state modeling the first-order lag may be necessary. Such a model may take the following

form within the control loop:

$$\frac{F_U}{u_{command}} = \frac{K_U}{\tau s + 1}$$

If the actuator transfer function can be determined explicitly from simple motor dynamics, it may include the zero at the origin described in Chapter 2:

$$\frac{F_U}{u_{command}} = \frac{K_U s}{\tau s + 1}$$

In either case, the LQR design expands to a possible seventh-order system, producing a feedback gain for the actuator state as well. The addition of this state increases the complexity of the system and can affect performance (especially if the actuator pole is close to the poles of the plant), but may be necessary to accurately model the actual system dynamics. The weighting placed on this state is best determined by experimentation, but should be somewhat low compared to that of the others. Figure 4.3 shows the feedback path of the actuator state to the gain matrix G.

Analysis of theoretical performance should indicate how much the addition of an actuator state *does* affect the system. If little difference is noticed, then the initial assumption that the actuator dynamics are relatively fast compared to the system dynamics may indeed be accurate, and the actuator state can be ignored.

4.2.4 LQR Performance Capabilities

Now we have essentially completed the LQ regulator design. It is a matter of proof to show that a stable LQR design guarantees certain robustness characteristics. In terms of Bode analysis, the following margins are guaranteed at our control input:

Gain Margin GM: $6\,db \leq GM \leq \infty$
Phase Margin ϕ: $60^\circ \leq \phi$

As briefly mentioned in Chapter 2, the Cart-Pendulum system is *non-minimum phase* in nature; i.e. the system transfer matrix has zeros located in the right-hand plane. This characteristic prevents us from achieving perfect regulation as the weighting on the control term in our cost function goes to zero, in contrast to perfect regu-

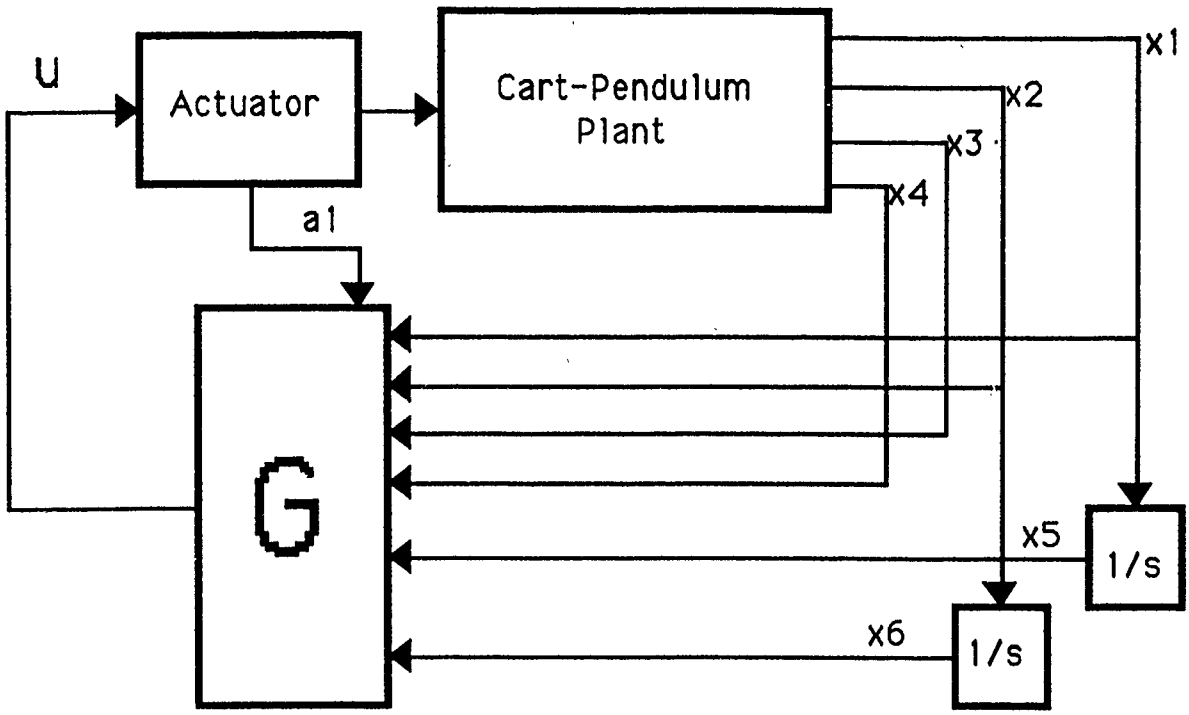

Figure 4.3: 7th-Order Regulator with Actuator State

lation that could be achieved if the system were minimum phase:

$$\text{Minimum Phase:} \quad R \to 0 \implies J = 0$$
$$\text{Non-Minimum Phase:} \quad R \to 0 \implies J \neq 0$$

Thus, regardless of the amount of control available, our cost J will always have some nonzero minimum value. This minimum cost can be calculated, and is a function of the Riccati solution matrix S_0:

$$J = \frac{1}{2} x_0^T S_0 x_0 \tag{4.13}$$

where x_0 is the initial condition vector for the states. Note that if all states are initially at their nominal values, we have $J = 0$, the only instance in which this is possible for our system.

This concludes the optimal LQ regulator design. In a later section, we will examine the theoretical performance of a Cart-Pendulum system in a basic configuration employing several variations of the LQR design outlined above.

4.3 LQ Estimator Design

It is not always the case, unfortunately, that all states are available from measurements. And it is also not realistic to assume that all measurements of states are in fact the actual values of the states without any error. Having solved the LQ regulator problem and obtained an optimal control law, the next task is to assure it can be implemented as efficiently as possible. This requires providing the part of the controller that includes the gain matrix G with values for the states that are as accurate as possible. In our particular hardware configuration described in Chapter 1, only three of the four plant states are measurable as system outputs: s (x_1), θ (x_2), and $\dot{s}$ (x_3). Additional states may involve one or two integral states, as well as an actuator state. Somehow, the three measured states must supply the one to four other states needed by the appropriate LQR gain matrix.

To simplify the design procedure, we will assume that we have available "black box" integrator devices that are capable of producing near perfect integral signals of input quantities (these devices are simply part of the controller, and are physically located within the analog computer in the laboratory) Thus, by simply sending the cart and pendulum position outputs through these integrators, suitable values for the integral states are obtained. This constitutes a crude form of "optimal estimation," but is fairly reliable (it should also be noted that the integral states themselves are "optional" in nature, and are a fabrication of the controller used to provide an extra dimension in control possibilities).

The primary task remaining, then, is to provide suitable estimates for the pendulum angular velocity $\dot{\theta}$ (x_4), and, if necessary, the actuator state a_1.

4.3.1 Employment of a Simple Diferentiator

To begin, we will assume we have a high-performance motor (i.e. fast actuator dynamics), so only a value for $\dot{\theta}$ is required. Since this one required estimated state is simply the derivative of another measurable state, the first logical step is to simply

employ a "black-box" differentiator to approximate its value. In theory, this is no different from using integrators to obtain integral states, and is indeed a practical first step towards implementing a practical control system. The appearance of such a control system is shown in Figure 4.4.

However, in practice, simple differentiators tend to introduce significant amounts of noise into output signals. Also, use of a simple differentiator assumes the input signal is reliable, and does not provide the capability to use the information available in other states to provide a truly accurate estimate of the desired state. Thus, insertion of an output-feedback estimator into the loop, even to obtain an estimate for $\dot{\theta}$ alone, may produce the best results.

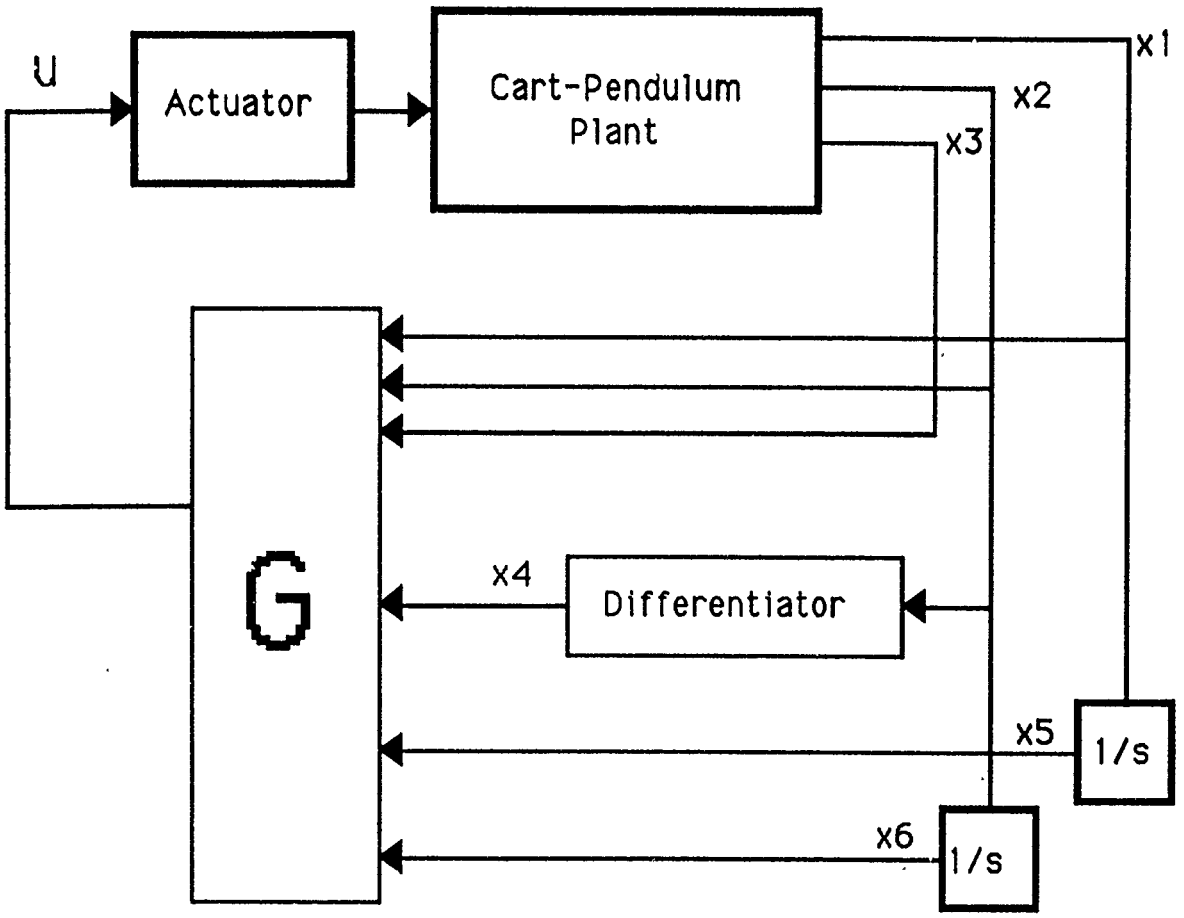

Figure 4.4: Control System with Simple Differentiator

4.3.2 Optimal Estimator Design

The conventional method for determining the poles of the estimator (or observer) is not too different from the eigenplacement approach used to obtain a full-state feedback gain matrix: an estimator gain matrix K is slected such that the poles of the estimator system matrix (A-KC) are placed at designated stable locations. However, as before, an optimal approach to the synthesis of this gain matrix is more versatile and efficient.

If we approximate the actuator with a proportional gain (no added state(s)) and include integrators in the design, our system takes the shape shown in Figure 4.5. Note that some kind of estimator is required to obtain an estimate for $\dot{\theta}$ (the x_4 state).

In a manner very similar to the LQ regulator design, we employ weighting matrices and a steady-state Ricatti equation to obtain an optimal LQ estimator. The optimal estimation problem involves finding the best estimate for the states, $\hat{x}$ [Maciejowski 241] that minimizes the cost function:

$$J = \lim_{t \to \inf} E[(x - \hat{x})(x - \hat{x}] \tag{4.14}$$

To introduce noise into our system, we consider our plant model to have the form:

$$\dot{x} = Ax + Bu + \Gamma w$$

$$y = Cx + v$$

where w and v are white noises with covariances given by [Maciejowski 223]:

$$E[ww^T] = W \qquad E[vv^T] = V$$

The optimal estimation Kalman-filter gain matrix K is obtained from:

$$K = PC^T V^{-1} \tag{4.15}$$

where P is the solution to the following steady-state Riccati equation:

$$PA^T + AP - PC^T V^{-1} CP + \Gamma W \Gamma^T = 0 \tag{4.16}$$

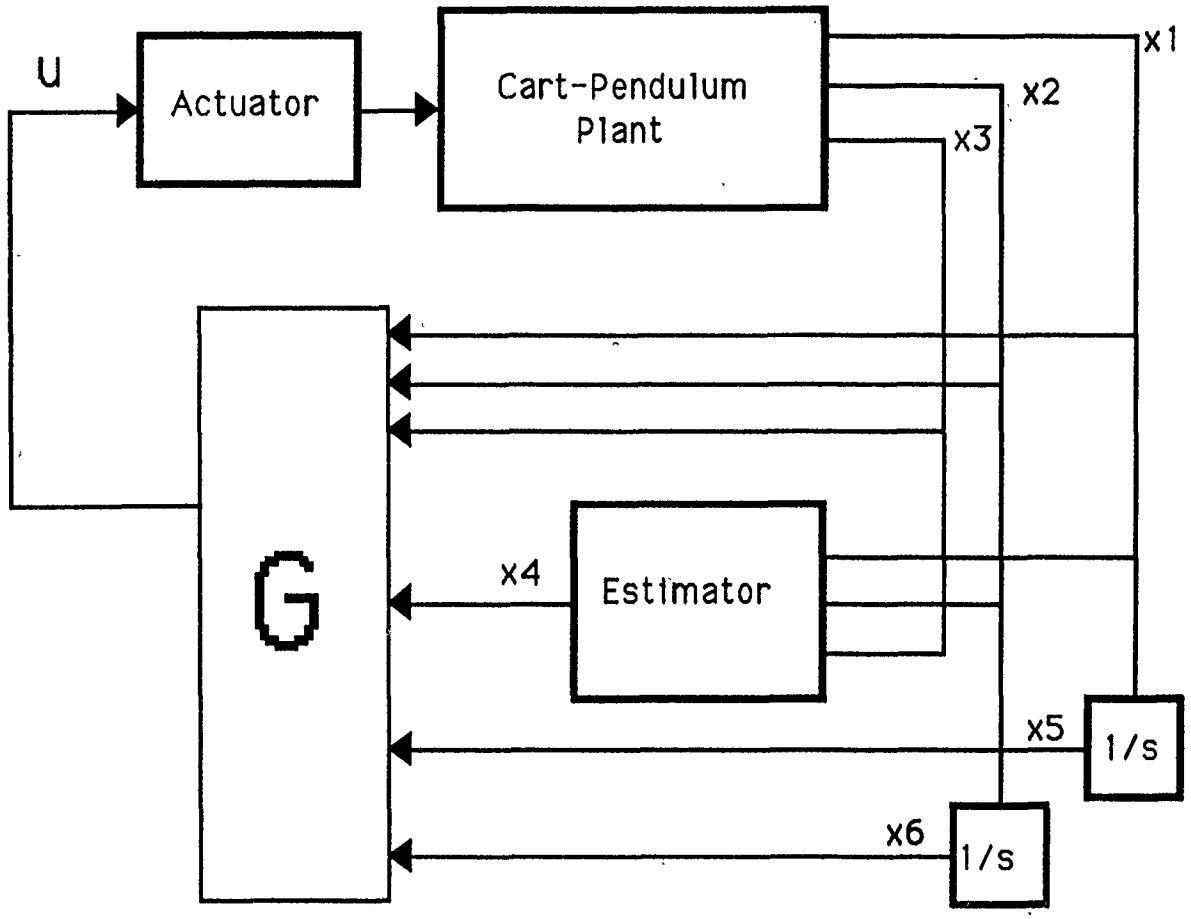

Figure 4.5: LQG System with Integrators

Equation 4.16 is "dual" to Equation 4.4 [Maciejowski 224]. The gain matrix K is $n \times m$, with n the number of states and m the number of outputs y from the actual plant. The estimator dynamics then take the form:

$$\dot{\hat{x}} = A\hat{x} + Bu + K(y - \hat{y}) \tag{4.17}$$

$$\hat{y} = C\hat{x} \tag{4.18}$$

which can be rewritten:

$$\dot{\hat{x}} = (A - KC)\hat{x} + Bu + Ky \tag{4.19}$$

$$\hat{y} = C\hat{x} \tag{4.20}$$

Clearly, the estimator gain matrix K "optimizes" placement of the estimator state matrix poles, i.e. the eigenvalues of $(A - KC)$. The values within K are determined primarily by the noise weighting matrices, W and V. Both are square matrices, with W having dimensions equal to the number of input disturbances modeled in the system, and V having dimensions $m \times m$, the number of outputs of the plant. Choosing the weights for these matrices is similar to choosing the weights for their "dual" counterparts, Q and R. Typically, the weights within W will reflect root-mean-square disturbance levels of the respective process noises, while weights within V will indicate the error statistics associated with respective sensors (i.e. unreliable measurements will have smaller weights).

The final objective of the optimal estimator is to produce estimates for those states which we are unable to measure directly. In our case, input of the three plant outputs s, θ, and $\dot{s}$ into the estimator produces a reliable estimate for the fourth state, $\dot{\theta}$.

4.4 Regulator-Estimator Integration, Loop Transfer Recovery

The third essential step in the LQG design is to *integrate* the LQR and LQE designs into the single multi-variable feedback control loop. This is done by simply aligning the appropriate outputs of the plant itself, the additional outputs provided by the estimator (or differentiator), and the outputs of the integrators (if included) with the inputs to the optimal full-state feedback gain matrix G. This is essentially the arrangement already shown in Figure 4.5.

There are problems which arise as a result of this connection. As shown by Maciejowski, the remarkably high stability margins guaranteed by LQR design alone have a tendency to become very poor once the LQE design is incorporated into the loop. The suggested method for solving this problem involves modifying the estimator dynamics (i.e. the poles of $[A - KC]$) by causing them to either (1) cancel plant dynamics, especially zeroes, or (2) become much *faster* than the plant dynamics [Maciejowski 231].

The procedure is called "Loop Transfer Recovery" (LTR), and involves introducing more weight on the process noise matrix W by multiplying it by a scalar constant ρ. As ρ is increased, to quote Maciejowski, "the Kalman filter is being 'told' that an increasing proportion of the variance in the plant output is due to state variations,

and a decreasing proportion to measurement errors" [233].

The advantage is this: as ρ is increased, the usually poor stability margins resulting from the integration of the LQE design with the LQR design grow, and approach the original LQR robustness as $\rho \rightarrow \infty$. Thus, we can effectively "recover" the robustness properties lost through LQR-LQE integration.

But there are two problems with this. First, as ρ is increased, the ability of the system to respond effectively to disturbances in the system is decreased. And more importantly, as Maciejowski again makes clear, LTR is *not guaranteed to work for non-minimum phase systems.* The reason goes back to the original idea that some of the estimator dynamics should try to cancel plant zeroes. Since some zeros are in the right half-plane for our system, LTR cannot necessarily achieve all of its objectives. So what should be done? According to Maciejowski: "the strategy to use with non-minimum phase plants is to follow the usual LTR procedure and hope for the best" [259]. By experimentation and analysis, we can determine whether LTR will help us recover LQR stability margins without detrimental effect on the rest of the system.

Thus, to properly apply LTR, we first connect the LQR gain matrix with its appropriate inputs, and check stability margins and compare them to those of the original LQR design. Then, test increasing values for the scalar constant ρ:

$$W = \rho \times W_0$$

until acceptable stability margins are regained.

4.5 *Theoretical Performance of Basic Configuration*

Having discussed the methodology employed in the design of an optimal LQG control system for the inverted Cart-Pendulum, we now apply it to the system in a particular configuration and examine numerical computer simulation results. The integrators can be incorporated into the plant itself (since the gain matrix "sees" a sixth order system) by placing poles very close to the origin (placing them directly on the origin can present numerical difficulties).

4.5.1 CASE 1: No Actuator State

Using system parameters defined in Table B.1 (see Appendix B), assuming all three measurements are available, we obtain the following state space model for the Cart-Pendulum plant:

$$A = \begin{bmatrix} 0 & 0 & 1 & 0 & 0 & 0 \\ 0 & 0 & 0 & 1 & 0 & 0 \\ 0 & -0.8946 & -0.7256 & 0.0007 & 0 & 0 \\ 0 & 24.9454 & 1.6915 & -0.0183 & 0 & 0 \\ 1 & 0 & 0 & 0 & -.00002 & 0 \\ 0 & 1 & 0 & 0 & 0 & -.00001 \end{bmatrix}$$

$$B = \begin{bmatrix} 0 & 0 & 0.2815 & -.6563 & 0 & 0 \end{bmatrix}^T$$

$$C = \begin{bmatrix} 1 & 0 & 0 & 0 \\ 0 & 1 & 0 & 0 \\ 0 & 0 & 1 & 0 \end{bmatrix} \qquad D = \begin{bmatrix} 0 \\ 0 \\ 0 \end{bmatrix}$$

This configuration gives us open-loop plant poles at:

$$\begin{aligned} \lambda_1 &= 0.0 \\ \lambda_2 &= 4.9588 \\ \lambda_3 &= -5.0388 \\ \lambda_4 &= -0.6639 \\ \lambda_5 &= -.00002 \\ \lambda_6 &= -.00001 \end{aligned}$$

Incidentally, finite zeros are located at the following points for the listed transfer functions:

$$\frac{s}{F_U}: \qquad z_1 = -4.7896 \quad z_2 = 4.7729$$

$$\frac{\dot{s}}{F_U}: \qquad z_1 = -4.7896 \quad z_2 = 4.7729 \quad z_3 = 0$$

The zeros of the transfer functions $\frac{\theta}{F_U}$ and $\frac{\dot{\theta}}{F_U}$, as well as the remaining zeros of the other two transfer functions are either infinite or very close to the origin. Note the two zeros in the right half-plane: these make the system non-minimum phase, and also have a frequency close to that of the poles of the system. This characteristic becomes important during Loop Transfer Recovery.

To form the LQR weighting matrices Q and R, let the "maximum allowable excursions" be as follows:

$$\begin{aligned} s &: \sigma_1 = 0.2\ meters \\ \theta &: \sigma_2 = 0.1\ radians \\ \dot{s} &: \sigma_3 = 0.2\ meters/second \\ \dot{\theta} &: \sigma_4 = 0.1\ radians/second \\ \int s &: \sigma_5 = .2 \\ \int \theta &: \sigma_6 = .1 \\ F_T &: \gamma_1 = 3.1623\ Newtons \end{aligned}$$

producing:

$$Q = \begin{bmatrix} 25.0 & 0 & 0 & 0 & 0 & 0 \\ 0 & 100.0 & 0 & 0 & 0 & 0 \\ 0 & 0 & 25.0 & 0 & 0 & 0 \\ 0 & 0 & 0 & 100.0 & 0 & 0 \\ 0 & 0 & 0 & 0 & 25.0 & 0 \\ 0 & 0 & 0 & 0 & 0 & 100.0 \end{bmatrix} \qquad R = \begin{bmatrix} 0.100 \end{bmatrix}$$

Solution of the related Ricatti equation (Equation 4.4) produces the following 1×6 LQR gain matrix G:

$$G = [\ -39.8530 \quad -249.4119 \quad -44.8988 \quad -60.0125 \quad -15.8106 \quad -3.2014e-9\ ]$$

When this LQ regulator is "hooked up" to create the closed loop system shown in Figure 4.1, the control loop Bode plot shown in Figure 4.6 is obtained, and the

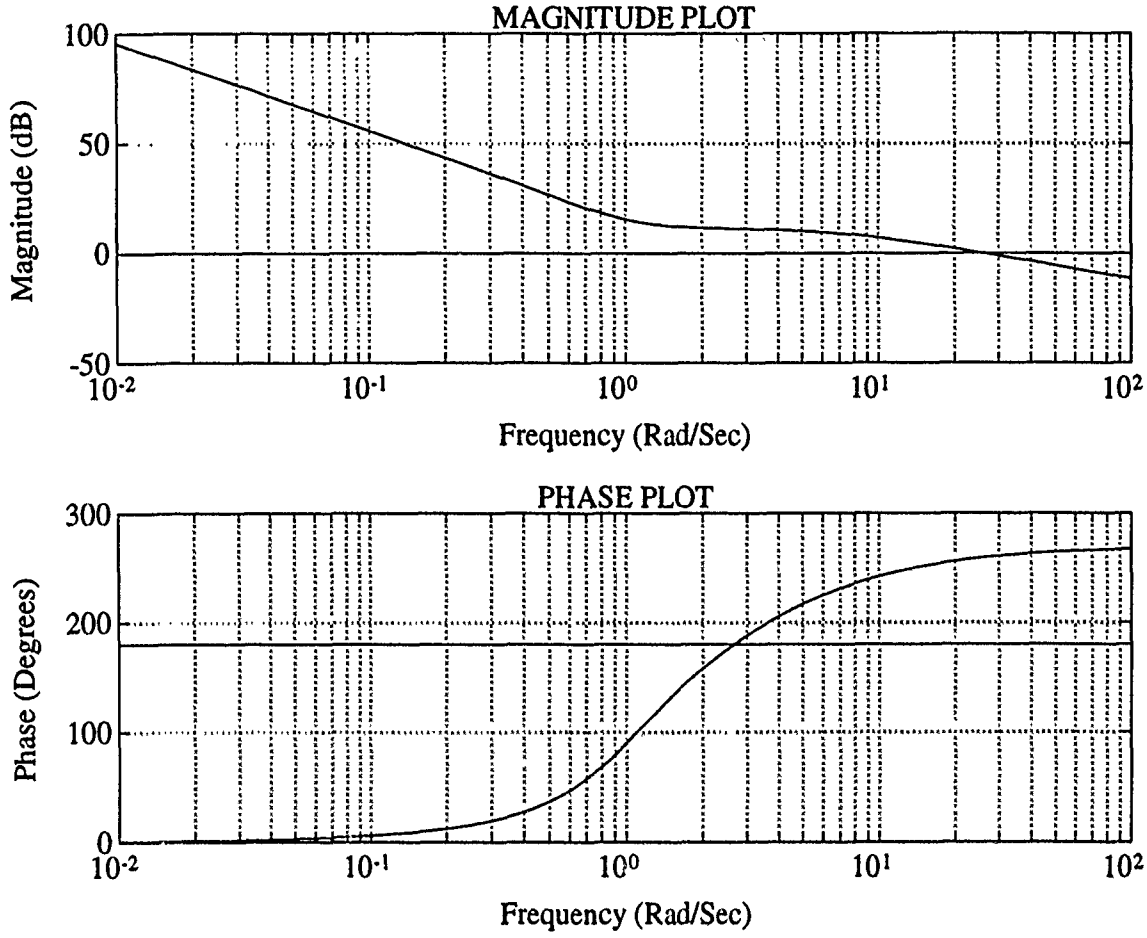

Figure 4.6: Control Loop Bode Plot for Case 1: LQR Only

following control loop robustness properties are recovered:

$$\begin{aligned} Gain\ Margin\ GM &= 11.19\ db \\ Phase\ Margin\ \phi &= 79.12^{o} \end{aligned}$$

The closed loop poles, or the eigenvalues of $(A - BG)$, are located at:

$$\begin{aligned} \lambda_1 &= -22.2917 \\ \lambda_2 &= -1.7309 + 1.2205i \\ \lambda_3 &= -1.7309 - 1.2205i \end{aligned}$$

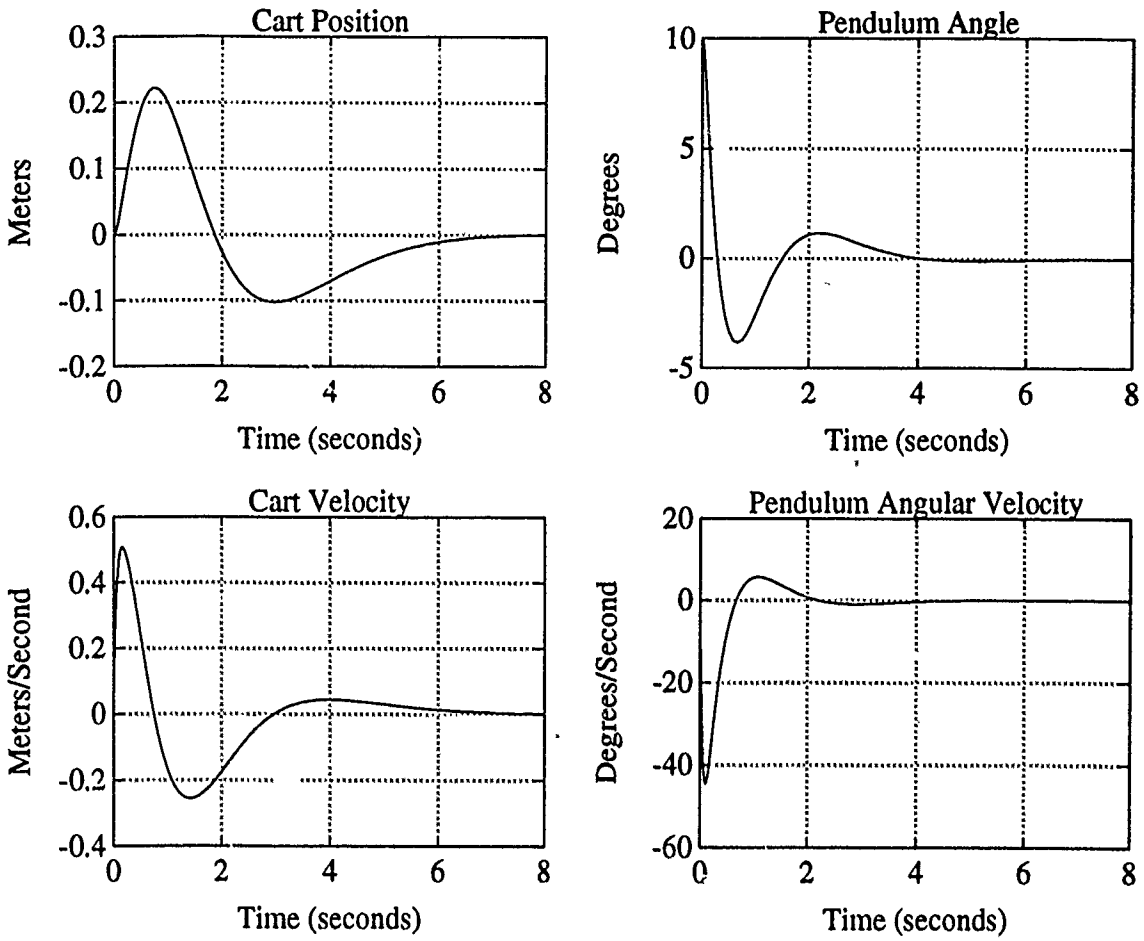

Figure 4.7: State Time Histories for Case 1: LQR Only

$$\begin{aligned} \lambda_4 &= -.8667 + .5163i \\ \lambda_5 &= -.8667 - .5163i \\ \lambda_6 &= -.00001 \end{aligned}$$

For purposes of comparison, if the integrators are removed from the system (i.e. $\sigma_5 = \sigma_6 = 0$), we obtain a slightly different gain matrix G:

$$G = [\ -15.8114 \quad -209.0301 \quad -31.0045 \quad -52.9470 \quad 0 \quad 0\ ]$$

Also, without integrators, the following control loop robustness properties are

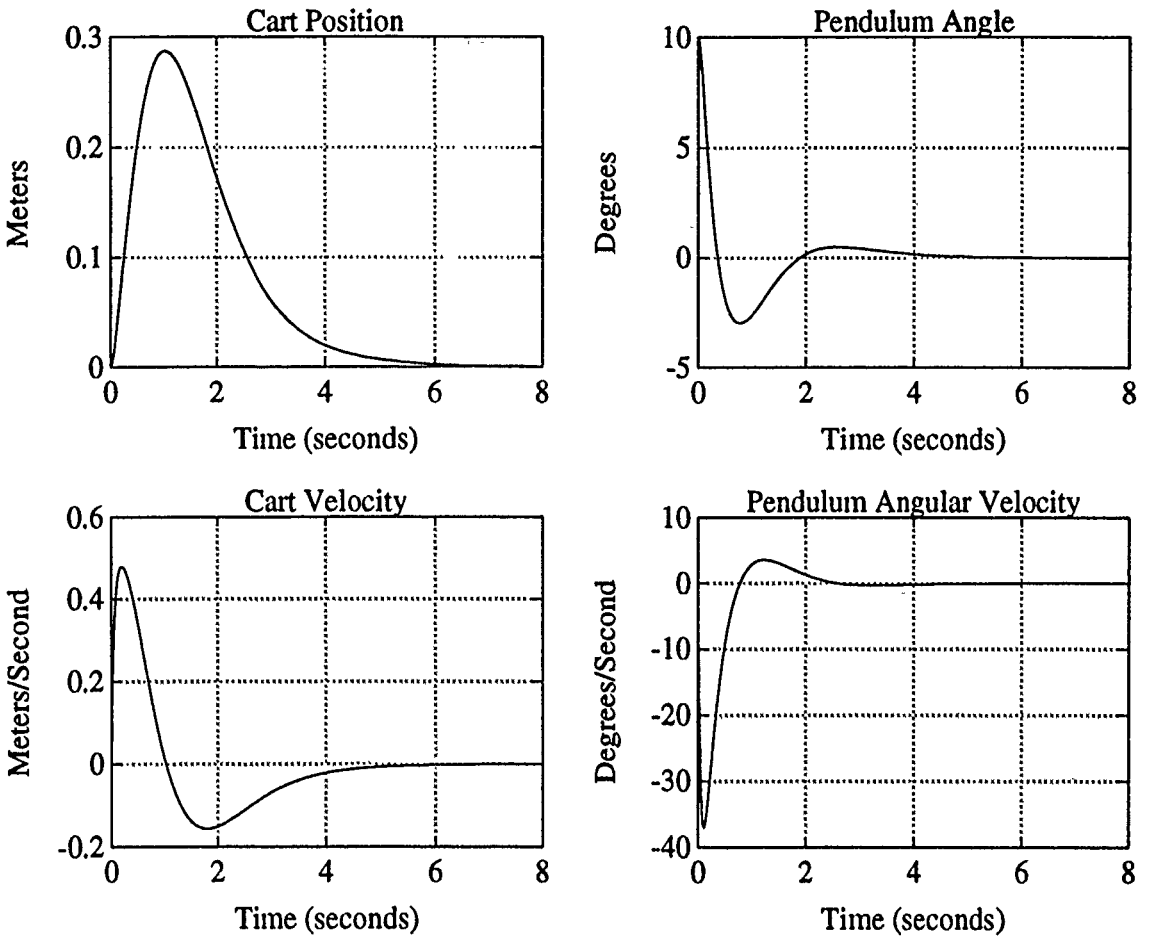

Figure 4.8: State Time Histories for Case 1: LQR Only, No Integrators

recovered:

$$\begin{aligned} Gain\ Margin\ GM &= -11.47\ db \\ Phase\ Margin\ \phi &= -80.14^{\circ} \end{aligned}$$

Figures 4.7 and 4.8 show the time histories of the four states for control systems with and without integrators, respectively. The simulations begin with a non-homogeneous initial condition only on θ of 10°. Clearly, in both instances, the control is very effective in returning both the cart position and the pendulum angle to zero.

Of course, not all states are measurable directly, so incorporation of an estimator is necessary and will undoubtedly degrade this "ideal" performance and robustness.

For the sake of simplicity, we set the noise matrices initially as identity matrices as follows:

$$V = \begin{bmatrix} 1 & 0 & 0 \\ 0 & 1 & 0 \\ 0 & 0 & 1 \end{bmatrix} \qquad W = \begin{bmatrix} 1 \end{bmatrix}$$

and we allow the matrix Γ to assume the values in the matrix B to simulate noise within the actuator input:

$$\Gamma = [.000 \quad .000 \quad .2815 \quad -.6563]^T$$

Solution of the related Ricatti equation as discussed above produces the following optimal estimation Kalman gain matrix:

$$K = \begin{bmatrix} .3081 & -.2708 & .0880 \\ -.2708 & 9.6765 & -1.5053 \\ .0880 & -1.5053 & .2821 \\ -1.3313 & 47.9871 & -7.4821 \end{bmatrix}$$

Closing the loop with the estimator included produces the following robustness properties:

$$\begin{aligned} Gain\ Margins\ GM &= 1.029\ db \\ Phase\ Margins\ \phi &= 5.671^\circ \end{aligned}$$

Clearly, these margins are far below acceptable levels. However, application of the Loop Transfer Recovery techniques mentioned above should help to improve robustness. We hope, of course, that the non-minimum phase characteristics of our system will not hamper our efforts. After some experimentation, multiplying the W matrix by a value of $\rho = 1.0 + e7$ is found to produce acceptable stability margins. Using the new W matrix and resolving the LQE problem, the revised Kalman gain matrix is found to be:

$$K = 1000 \times \begin{bmatrix} .0010 & -.0001 & .0010 \\ -.0001 & .0098 & -.0023 \\ .0010 & -.0023 & .8896 \\ -.0007 & .0509 & -2.0735 \end{bmatrix}$$

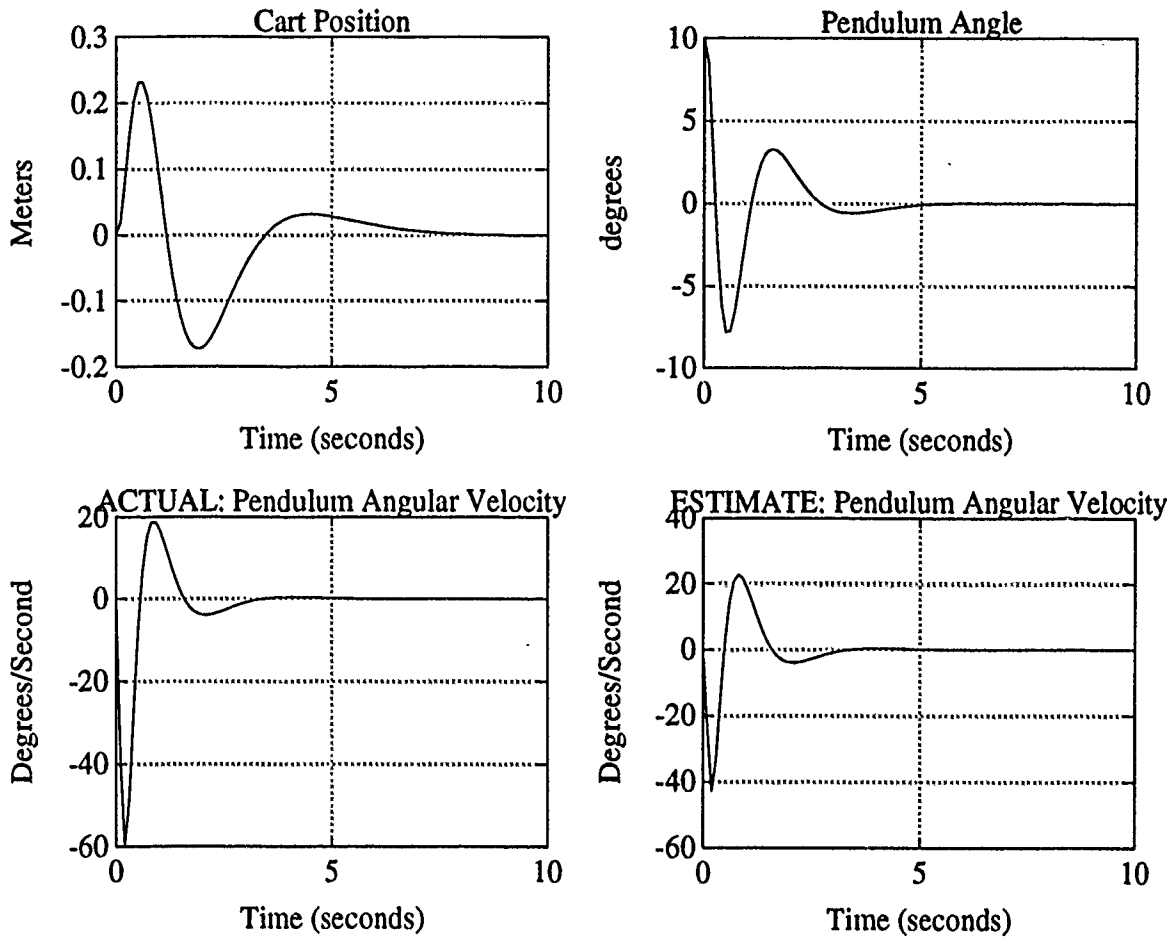

Figure 4.9: State Time Histories for Case 1: LQG with LTR

Now, after Loop Transfer Recovery, our robustness properties are:

$$\begin{aligned} \textit{Gain Margin } GM &= -11.0\, \textit{db} \\ \textit{Phase Margin } \phi &= -77.23^{\circ} \end{aligned}$$

These can be observed directly in Figure 4.10. As we expect, the margins are not as good as those obtained through straightforward LQR analysis, but are reasonably large. Figure 4.9 shows the time histories for three states, s, θ, and $\dot{\theta}$, as well as the estimator estimate for $\dot{\theta}$. A small measure of error is detectable on the plot, but otherwise the estimator performs rather effectively.

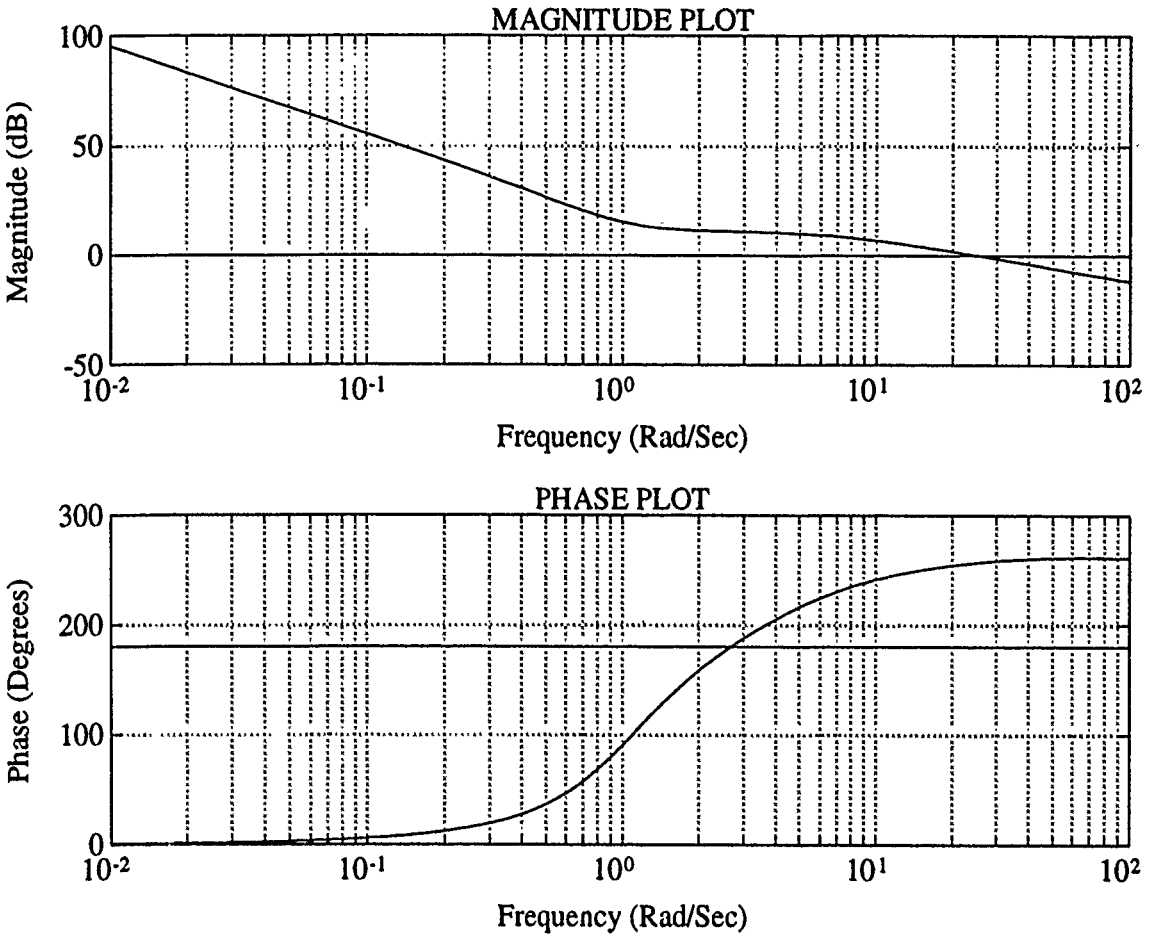

Figure 4.10: Control Loop Bode Plot for Case 1: LQG with LTR

The closed-loop eigenvalues of the final LQR/LQE system are the same closed-loop eigenvalues found under LQR analysis (i.e the poles of (A-BG)), plus the eigenvalues of the estimator (the poles of A-KC), given below:

$$\lambda_7 = -890.28$$
$$\lambda_8 = -6.1005$$
$$\lambda_9 = -3.7219$$
$$\lambda_{10} = -1.0058$$

4.5.2 CASE 2: Addition of Simple First-Order Actuator State

Our second simulation case will include a simple first-order model (without a zero) for the actuator state with the time constant $\tau = 0.10$ as shown:

$$\frac{F_U}{F_{U_{COMMAND}}} = \frac{1}{.1s+1} = \frac{10}{s+10}$$

The effect is to introduce a small lag in the system between the control command u_c and actual control input F_U. Addition of this first-order model to the loop increases the order of the system by one and results in the following state space matrices:

$$A = \begin{bmatrix} -10 & 0 & 0 & 0 & 0 & 0 & 0 \\ 0 & 0 & 0 & 1 & 0 & 0 & 0 \\ 0 & 0 & 0 & 0 & 1 & 0 & 0 \\ 2.8153 & 0 & -0.8946 & -0.7256 & 0.0007 & 0 & 0 \\ -6.5625 & 0 & 24.9454 & 1.6915 & -0.0183 & 0 & 0 \\ 0 & 1 & 0 & 0 & 0 & -.00002 & 0 \\ 0 & 0 & 1 & 0 & 0 & 0 & -.00001 \end{bmatrix}$$

$$B = \begin{bmatrix} 1 & 0 & 0 & 0 & 0 & 0 & 0 \end{bmatrix}^T$$

$$C = \begin{bmatrix} 1 & 0 & 0 & 0 \\ 0 & 1 & 0 & 0 \\ 0 & 0 & 1 & 0 \end{bmatrix} \qquad D = \begin{bmatrix} 0 \\ 0 \\ 0 \end{bmatrix}$$

This configuration gives us an additional open-loop plant pole at:

$$\lambda_7 = -10.0$$

which is reasonably close to the other system poles.

Setting the weight on the actuator state to *zero*, i.e. $\sigma_7 = 0$, and keeping all other weights identical to those in Case 1 (integrators included) produces the following full-state feedback gain matrix G:

$$G = [\ 18.82 \quad -40.87 \quad -351.01 \quad -52.35 \quad -78.11 \quad -15.811 \quad -5.654e-9\ ]$$

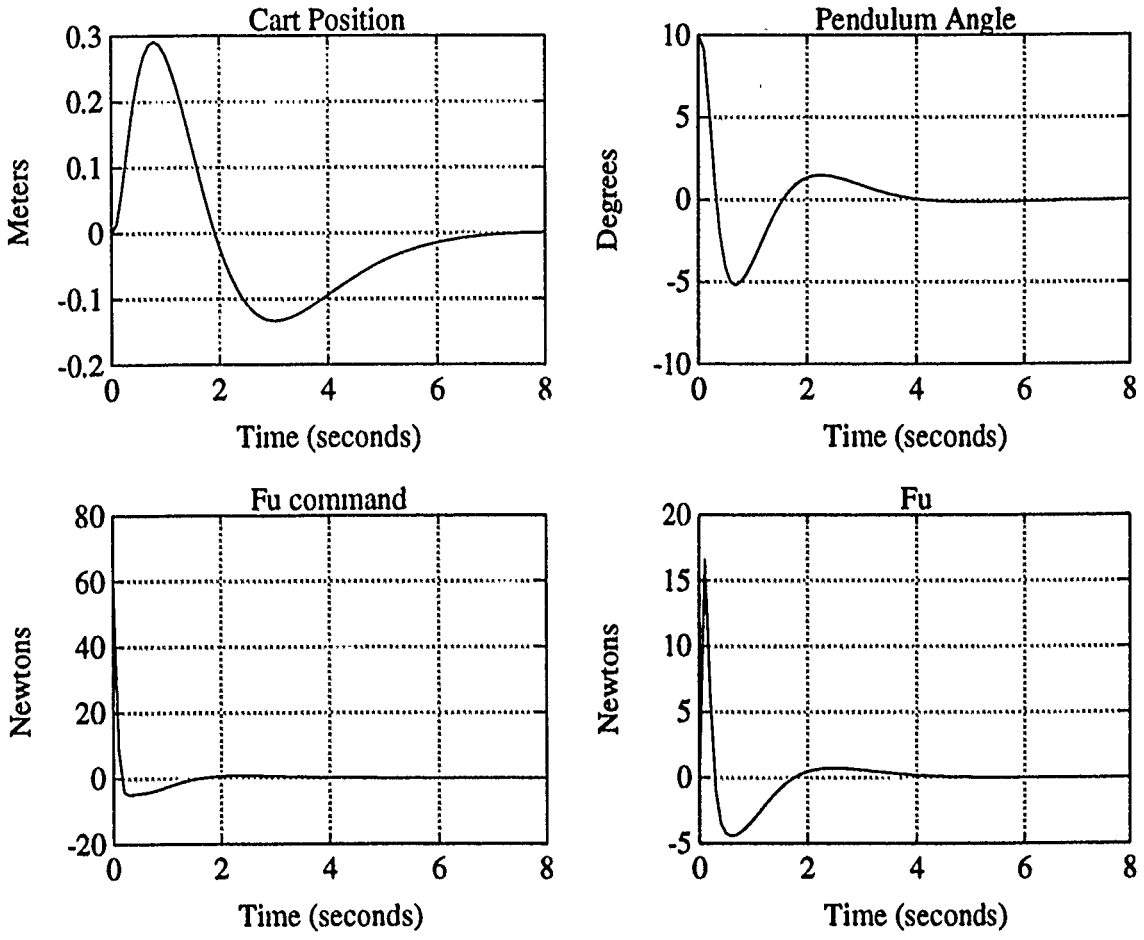

Figure 4.11: State Time Histories for Case 2: LQR only

And the following control loop robustness properties are recovered:

$$\begin{aligned} Gain\ Margin\ GM &= -10.93\ db \\ Phase\ Margin\ \phi &= -66.6^{\circ} \end{aligned}$$

Now the closed loop poles (the eigenvalues of $(A - BG)$) are located at:

$$\begin{aligned} \lambda_1 &= -12.1893 + 8.6795i \\ \lambda_2 &= -12.1893 - 8.6795i \\ \lambda_3 &= -1.7241 + 1.2216i \end{aligned}$$

$$\begin{aligned}\lambda_4 &= -1.7241 - 1.2216i \\ \lambda_5 &= -.8668 + .5162i \\ \lambda_6 &= -.8668 - .5162i \\ \lambda_7 &= -.00001\end{aligned}$$

Figure 4.11 shows the time histories of two states, s and θ, as well as the input command $F_{U_{COMMAND}}$ (the command signal to the actuator) and the actual actuator output F_U. As before, the simulation begins with a non-homogeneous initial condition on θ of 10^o.

Using the same noise weighting matrices, W and V, as before (both identity matrices), we obtain the following Kalman filter gain matrix:

$$K = \begin{bmatrix} .0011 & .00004 & .0128 \\ .3078 & -.2709 & .0579 \\ -.2709 & 9.6705 & -1.5052 \\ .0879 & -1.5052 & .2785 \\ -1.3321 & 47.9864 & -7.4754 \end{bmatrix}$$

The following robustness properties result:

$$\begin{aligned}Gain\ Margins\ GM &= .8027\ db \\ Phase\ Margins\ \phi &= 4.216^o\end{aligned}$$

Again, these margins are far below acceptable values. Employing the same value for ρ used in Case 1 ($\rho = 100$) for Loop Transfer Recovery, we obtain a corrected Kalman gain matrix:

$$K = 1000 \times \begin{bmatrix} .0005 & -.0042 & 2.7225 \\ .0010 & -.0001 & .0010 \\ -.0001 & .0098 & -.0023 \\ .0010 & -.0023 & .1231 \\ -.0007 & .0509 & -.2868 \end{bmatrix}$$

and the following stability margins:

$$\begin{aligned}Gain\ Margins\ GM &= -9.353\ db \\ Phase\ Margins\ \phi &= -52.78^o\end{aligned}$$

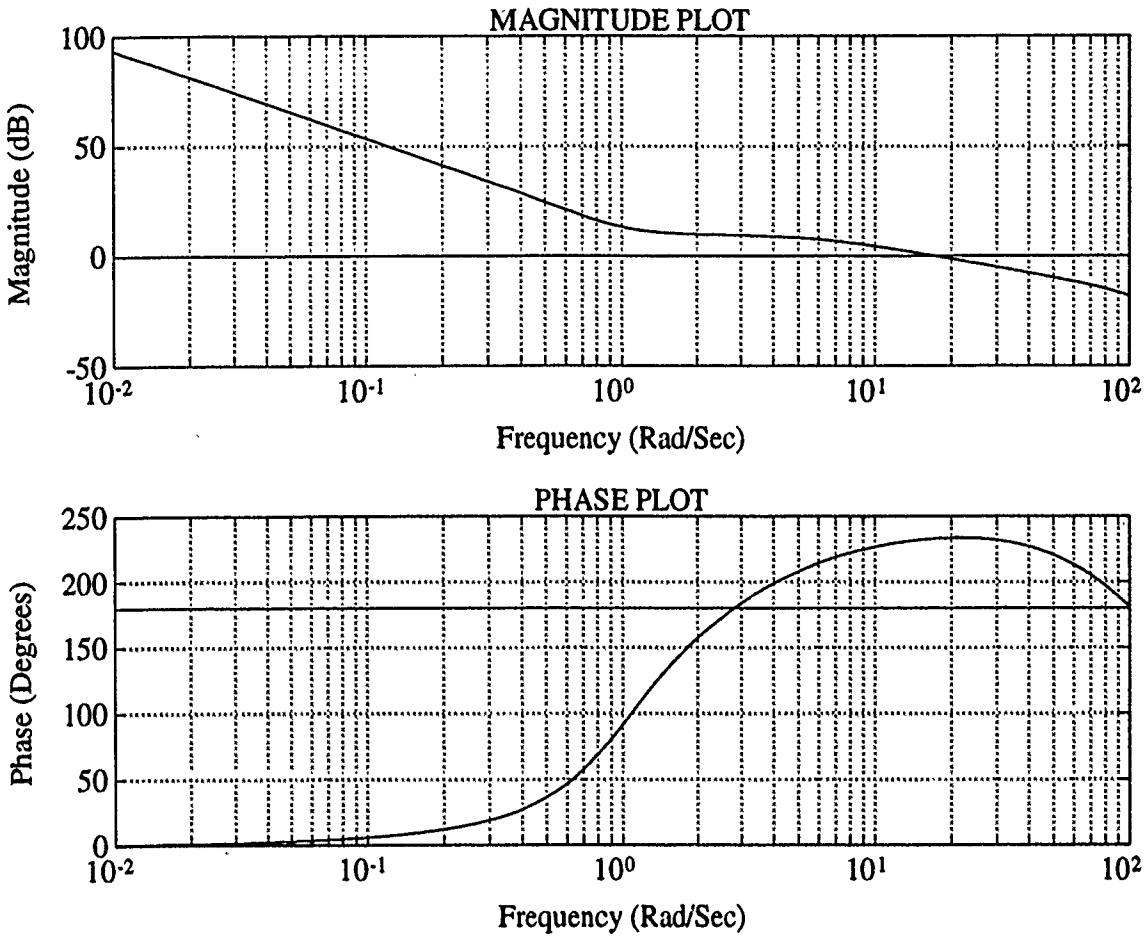

Figure 4.12: Control Loop Bode Plot for Case 2: LQG with LTR

Now the estimator poles (the poles of A-KC) are located at:

$$\begin{aligned}
\lambda_7 &= -66.9027 + 66.5345i \\
\lambda_8 &= -66.9027 - 66.5345i \\
\lambda_9 &= -6.1065 \\
\lambda_{10} &= -3.7219 \\
\lambda_{11} &= -1.0058
\end{aligned}$$

Again, Loop Transfer Recovery recovers most of the original LQR stability margins. These are visible in the control loop Bode plot shown in Figure 4.12. Time

histories of states s and θ as well as $F_{U_{command}}$ and F_U are shown in Figure 4.13. Clearly, the performance is not as good as that for Case 1, where no actuator state was used; however, it is the best performance that can be expected with an actuator that does introduce a lag into the system. The amount of control input indicated relative to the amount of control commanded in Figure 4.13 is evidence of this lag property.

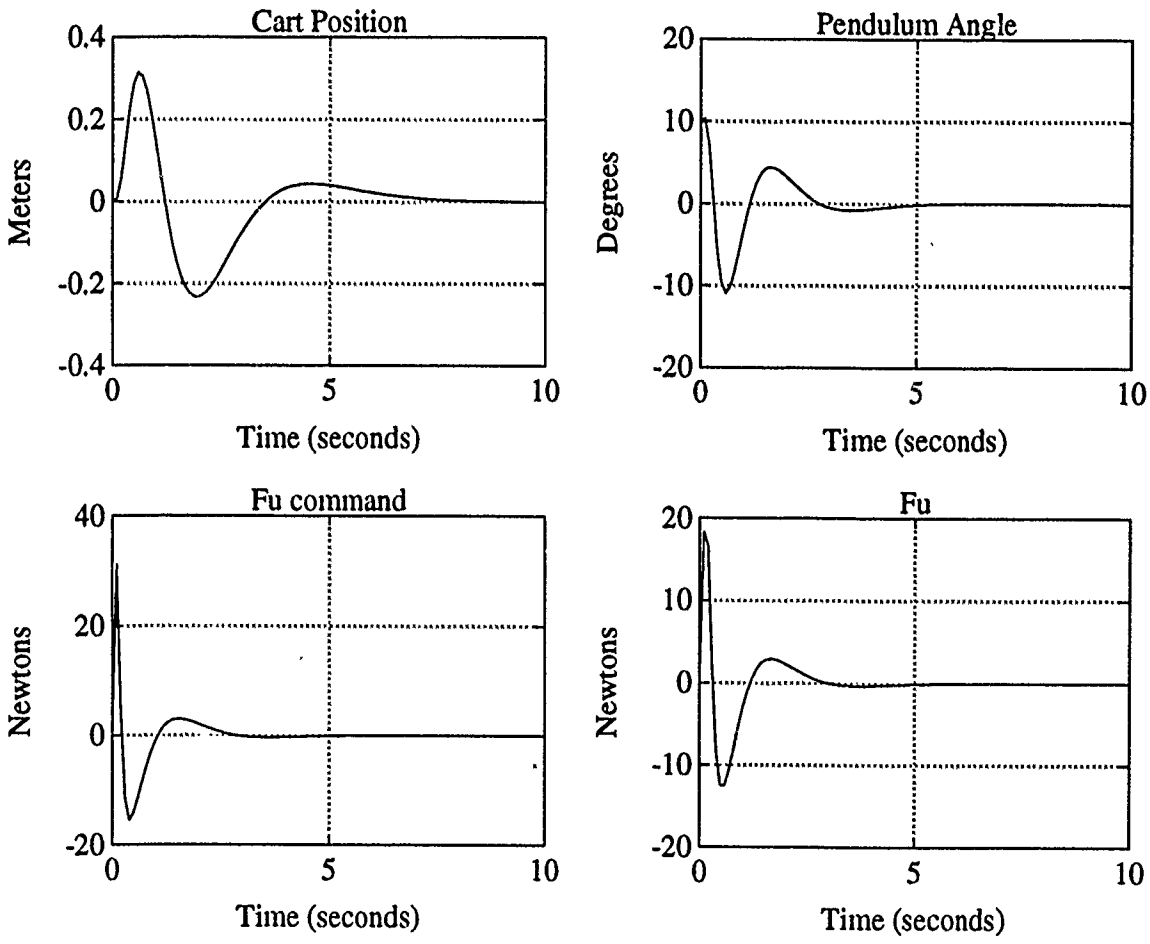

Figure 4.13: State Time Histories for Case 2: LQG with LTR

4.5.3 CASE 3: Addition of Simple First-Order Actuator State

Our third simulation case will include a simple first-order model now including the zero at the origin derived in the motor equations in Chapter 2. The transfer function for the motor-actuator is now:

$$\frac{F_U}{F_{U_{COMMAND}}} = \frac{s}{.1s+1} = \frac{10s}{s+10}$$

This keeps the plant and open loop poles the same as the ones used in Case 2. Keeping the weights on the states the same also produces the following full-state feedback gain matrix G:

$$G = [\ 18.82\ \ -40.87\ \ -351.01\ \ -52.35\ \ -78.11\ \ -15.811\ \ -5.654e-9\ ]$$

And the following control loop robustness properties are recovered:

$$\begin{aligned} Gain\ Margin\ GM &= -15.72\ db \\ Phase\ Margin\ \phi &= \infty^{\circ} \end{aligned}$$

Now the closed loop poles (the eigenvalues of $(A - BG)$) are located at:

$$\begin{aligned} \lambda_1 &= -212.59 \\ \lambda_2 &= -1.7338 + 1.3877i \\ \lambda_3 &= -1.7338 - 1.3877i \\ \lambda_4 &= -.8525 + .4938i \\ \lambda_5 &= -.8525 - .4938i \\ \lambda_6 &= -.00001 \\ \lambda_7 &= 0 \end{aligned}$$

Aplying the LQE/LTR procedure, using $\rho = 1e5$ this time, produces the Kalman gain matrix:

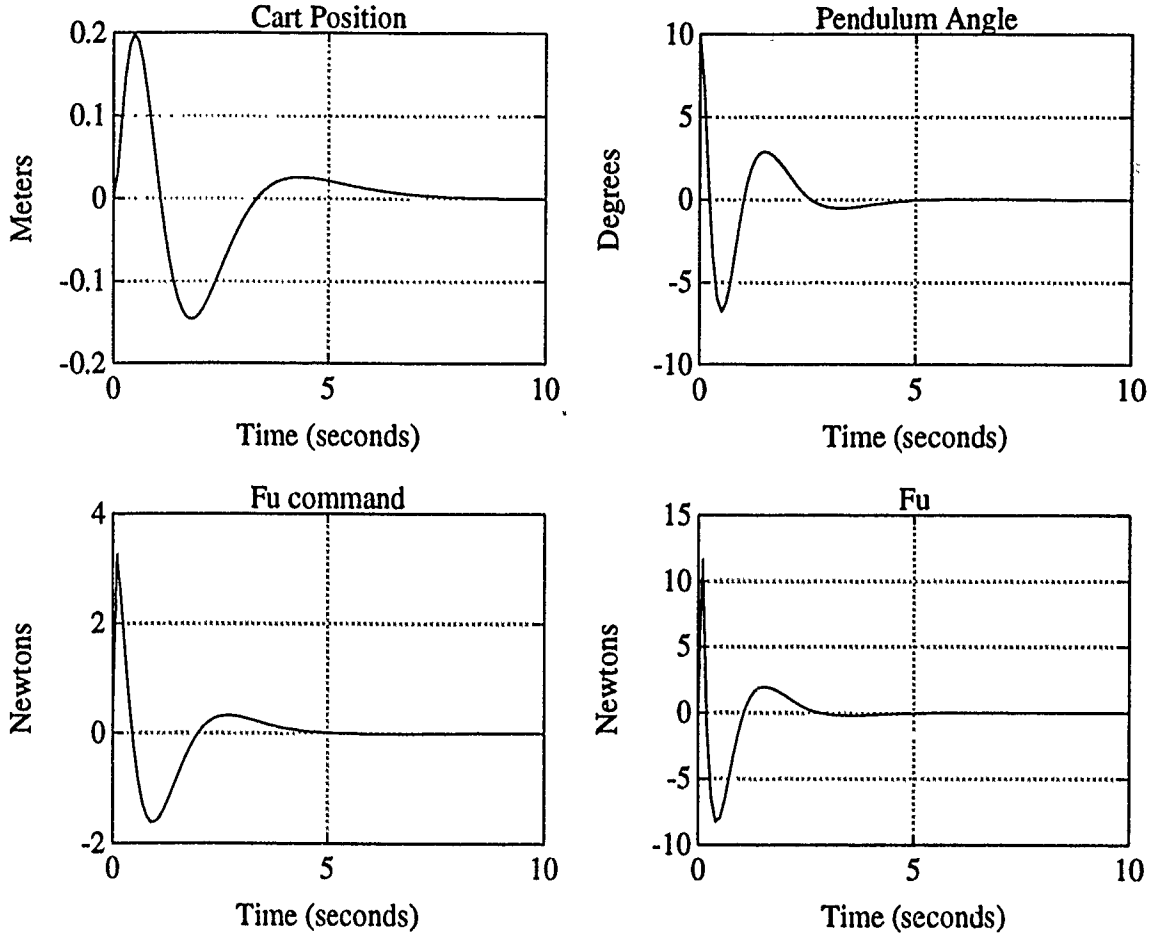

Figure 4.14: State Time Histories for Case 3: LQG with LTR

$$K = \begin{bmatrix} 6.275e-1 & -2.036e-1 & 3.127e+2 \\ 9.944e-1 & -6.921e-2 & 9.811e-1 \\ -6.9201e-2 & 9.819e+0 & -2.304e+0 \\ 9.811e-1 & -2.304e+0 & 8.796e+2 \\ -7.051e-1 & 5.09e+1 & -2.050e+3 \end{bmatrix}$$

and the following stability margins:

$$\begin{aligned} Gain\ Margins\ GM &= -14.72\ db \\ Phase\ Margins\ \phi &= \infty^{o} \end{aligned}$$

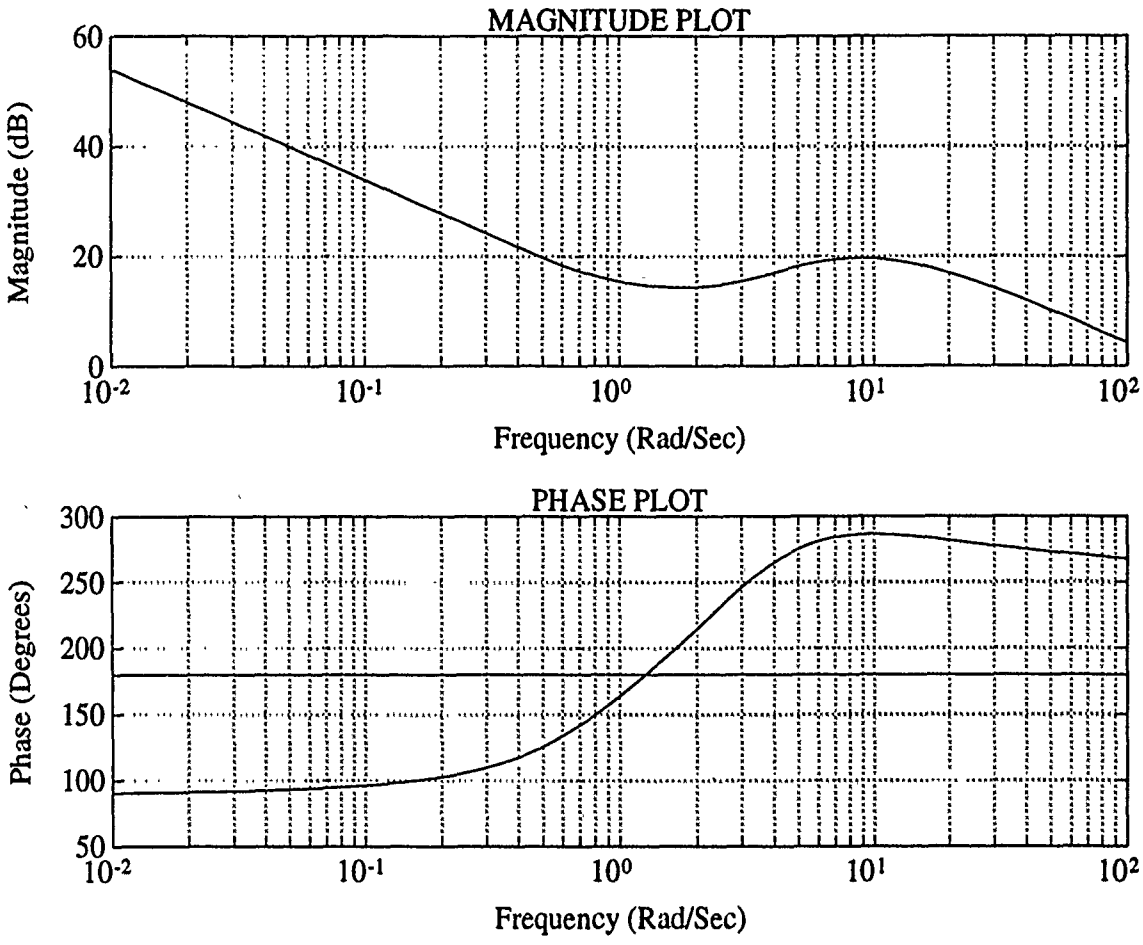

Figure 4.15: Control Loop Bode Plot for Case 3: LQG with LTR

Now the estimator poles (the poles of A-KC) are located at:

$$\begin{aligned} \lambda_7 &= -890.34 \\ \lambda_8 &= -6.1065 \\ \lambda_9 &= -3.7219 \\ \lambda_{10} &= -1.0058 \\ \lambda_{11} &= -6.592e-5 \end{aligned}$$

Figure 4.14 shows the time histories of two states and the control command and input. The amount of control input indicated relative to the amount of control

commanded is evidence of the "lead" property introduced by the zero at the origin.

4.6 Discussion of Expected Results

One of the greatest problems with LQR/LQE methods is the sensitivity of the robustness to plant uncertainties [Maciejowski 231]. Small errors or imperfect models with regard to the plant can make an otherwise robust LQG design have slim stability margins. Tables 4.1 and 4.2 show how the optimal LQR gain matrix G varies with variations in the plant parameters for each of the cases described above. As shown, the gains change very little for 10% variations in each of the individual parameters. The last entry in each table shows the gain matrix required if all parameters are increased by 10%. Again, the changes are not that high, especially compared to the control loop gain margins given for each case. Thus, we might feel confident that the LQG method, including application of LTR principles, has given us a fairly reliable and robust control design.

However, it remains to be seen in actual implementation how effective the system truly is. Unforseen uncertainties or output measurement error could produce problems. LQG design, though complex and powerful, can be sensitive to these unpredictabilities. The best approach is to implement, observe results, and analyze performance to find ways to produce a better overall design.

		GAIN MATRIX G
Nominal		-3.985e+1 -2.494e+2 -4.489e+1 -6.001e+1 -1.581e+1 3.201e-9
b_{VF}	+10%	-3.986e+1 -2.495e+2 -4.519e+1 -6.035e+1 -1.581e+1 -1.746e-9
	-10%	-3.984e+1 -2.493e+2 -4.401e+1 -5.999e+1 -1.581e+1 -4.948e-9
c	+10%	-3.985e+1 -2.494e+2 -4.490e+1 -6.001e+1 -1.581e+1 -9.027e-9
	-10%	-3.985e+1 -2.494e+2 -4.489e+1 -6.001e+1 -1.581e+1 -2.037e-9
ℓ	+10%	-4.003e+1 -2.543e+2 -4.534e+1 -6.315e+1 -1.581e+1 -2.037e-9
	-10%	-3.965e+1 -2.439e+2 -4.440e+1 -5.695e+1 -1.581e+1 -3.492e-9
M	+10%	-3.999e+1 -2.564e+2 -4.527e+1 -6.128e+1 -1.581e+1 -5.675e-9
	-10%	-3.971e+1 -2.425e+2 -4.454e+1 -4.454e+1 -1.581e+1 -2.910e-10
m	+10%	-3.986e+1 -2.498e+2 -4.491e+1 -6.004e+1 -1.581e+1 -8.731e-9
	-10%	-3.985e+1 -2.490e+2 -4.489e+1 -5.999e+1 -1.581e+1 -1.746e-9
All	+10%	-4.021e+1 -2.624e+2 -4.606e+1 -6.458e+1 -1.581e+1 -3.201e-9

Table 4.1: Table of Parameter Variations vs. LQR Gains: Case 1

		GAIN MATRIX G
Nominal		1.881+1 -4.087+1 -3.510+2 -5.235+1 -7.811+1 -1.581+1 -5.654-9
b_{VF}	+10%	1.815+1 -4.087+1 -3.512+2 -5.311+1 -7.814+1 -1.581+1 -5.763-9
	-10%	1.385+1 -4.086+1 -3.509+2 -5.159+1 -7.807+1 -1.581+1 -1.524-9
c	+10%	1.861+1 -4.088+1 -3.512+2 -5.104+1 -7.810+1 -1.581+1 -9.799-10
	-10%	1.862+1 -4.087+1 -3.509+2 -5.509+1 -7.811+1 -1.581+1 -3.765-9
l	+10%	1.795+1 -4.106+1 -3.538+2 -5.267+1 -8.193+1 -1.581+1 -8.618-10
	-10%	1.984+1 -4.066+1 -3.487+2 -5.201+1 -7.431+1 -1.581+1 -4.450-10
M	+10%	1.812+1 -4.108+1 -3.628+2 -5.263+1 -8.042+1 -1.581+1 -6.252-9
	-10%	1.966+1 -4.070+1 -3.393+2 -5.212+1 -7.582+1 -1.581+1 -7.581-9
m	+10%	1.883+1 -4.088+1 -3.521+2 -5.237+1 -7.818+1 -1.581+1 -3.939-10
	-10%	1.880+1 -4.087+1 -3.499+2 -5.234+1 -7.803+1 -1.581+1 -3.541-9
All	+10%	1.723+1 -4.127+1 -3.669+2 -5.372+1 -8.449+1 -1.581+1 -5.413-9

Table 4.2: Table of Parameter Variations vs. LQR Gains: Case 2

Chapter 5

ANALOG IMPLEMENTATION AND EXPERIMENTAL RESULTS

5.1 Introduction

One of the primary objectives for the near-future of the University of Washington Cart-Pendulum is the implementation of a *digital controller* device, i.e. an actual computer, into the control loop. This digital controller will utilize software specifically geared towards the implementation of control designs on physical systems. The broad capabilities of such a controller are discussed in Chapter 6.

Unfortunately, the digital computer controller was not available for the experiments described in this chapter, so use of a less flexible device for a controller was necessary. The tests conducted were limited to implementation of LQR design full-state feedback gains only, with no estimator and a simple differentiator to provide the value for $\dot{\theta}$. Implementation was done without integral states at first, followed by inclusion of $\int\theta$ later.

Before any simulations were attempted on the actual laboratory hardware, extensive testing was performed on the motor itself and on the actuator as a unit to determine dynamic characteristics, as well as appropriate voltage levels and constants. These tests and their results are discussed in Appendix A.

Of particular interest are the circuit proportion constants given in Table A.2. These permit actual physical values of meters, radians, Newtons, etc. to be translated into voltages used within the controller, and vice-versa. In order to implement the gain matrices found under theoretical analysis, the required scaling is as follows:

$$G = K_{sensors} \times G' \times K_U$$

$$K = K_{sensors} \times K'$$

where G and K are the theoretical gain matrices, $K_{sensors}$ and K_U are the constants given in Table A.2, and G' and K' are the gains actually implemented on the system.

The system was wired such that all potentiometer outputs would provide voltages with the same sign conventions (relative to a common ground) as those values they represent. Similarly, the controller output signal u_c was of the same sign as the required system input force, K_U, so all of the circuit proportion constants in Table A.2 are positive.

5.2 *Analog Computer Hookup*

Figure 5.1 shows the basic wiring diagram for the Comdyna GP-6 analog computer used in the conducted experiment. Note that the values for $\dot{\theta}$ and $\int\theta$ are obtained by running the θ signal through a differentiator and integrator, respectively. Each of these devices can be wired easily on a GP-6. The path for the $\int s$ signal is shown as a dotted line, since this integral state was never used in the testing (it is shown merely to demonstrate how it *could* be wired).

Operational amplifiers on the GP-6 automatically *invert* (i.e. change the sign) signals through them, so inverters themselves are necessary in the case of $\dot{\theta}$ and $\int\theta$ (and $\int s$) to "re-invert" to obtain proper sign. These inverters are shown in Figure 5.1 as small triangles.

All signals are multiplied by their respective gains, which are set in potentiometers denoted by circles on the diagram. The signals are then all fed into the summer shown, where they are added to produce the control signal. The output is fed through one more potentiometer, strictly for testing purposes, and then passes out of the GP-6 as the control signal, u_c. Potentiometers in the GP-6 merely multiply a signal by a fraction of unity, so those signals requiring gains greater than unity, namely θ and $\dot{s}$, required additional multiplication at the input of the summer as shown.

5.3 *Implementation and Testing*

To obtain a set of LQR full-state feedback gains without the integral state $\int s$, a new Q matrix was used and a new gain matrix G found. Since no estimator was involved and therefore no estimation of an actuator state was possible, we were forced to assume the proportional gain actuator model (see Case 1, Chapter 4, Section 4.5).

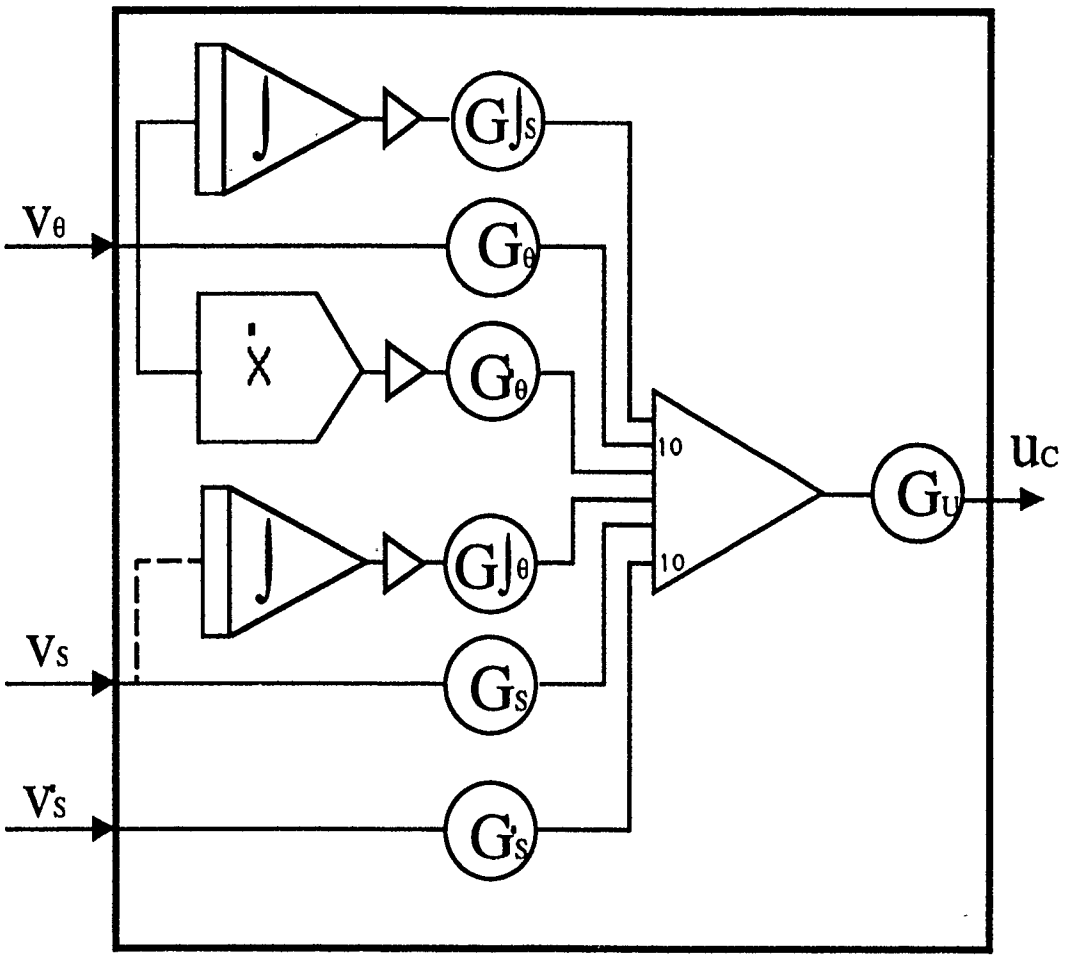

Figure 5.1: GP-6 Wiring Diagram for Test 1

The initial weighting matrices were:

$$Q = \begin{bmatrix} 25.0 & 0 & 0 & 0 & 0 & 0 \\ 0 & 100.0 & 0 & 0 & 0 & 0 \\ 0 & 0 & 0 & 0 & 0 & 0 \\ 0 & 0 & 0 & 25.0 & 0 & 0 \\ 0 & 0 & 0 & 0 & 0 & 0 \\ 0 & 0 & 0 & 0 & 0 & 100.0 \end{bmatrix} \qquad R = \begin{bmatrix} 0.100 \end{bmatrix}$$

Note that the weight on the cart velocity $\dot{s}$, as well as the weight on the integral state $\int s$, was set to zero. Also, the weight on pendulum velocity was reduced, intended to place less emphasis on $G_{\dot{\theta}}$, and therefore less responsibility on the potentially inaccurate differentiator. Solution of the LQR problem using methods described in Chapter 4 produced the following gain matrix G:

$$G = [\ -15.8114\ \ -156.7625\ \ -22.5763\ \ -35.1574\ \ 0.0\ \ -.0000323\ ]$$

The associated stability margins with this particular design were:

$$\begin{aligned} Gain\ Margin\ GM &= -8.371\ db \\ Phase\ Margin\ \phi &= -71.53^{\circ} \end{aligned}$$

The computer simulations produced using this gain arrangement are not too different from those shown in the LQR testcases in Chapter 4.

Implementation of the computed gain matrix G into the analog computer was accomplished in the manner described at the beginning of this chapter. Correcting for the appropriate circuit voltage constants found in Table A.2, the "wired" gains were found as follows:

$$\begin{aligned} G_s = -15.8114 &\longrightarrow G'_s = -.22610302 \\ G_\theta = -156.7625 &\longrightarrow G'_\theta = -2.67233 \\ G_{\dot{s}} = -22.5763 &\longrightarrow G'_{\dot{s}} = -2.71367 \\ G_{\dot{\theta}} = -35.1574 &\longrightarrow G'_{\dot{\theta}} = -.599328 \\ G_{\int\theta} = -.0000323 &\longrightarrow G'_{\int\theta} = -.001000 \end{aligned}$$

Note that the gains G'_θ and $G'_{\dot{s}}$ are both greater than unity, hence the need for the multiplication by 10 at the input to the summer for both of these signals. The potentiometers in the GP-6 were set to the above values (with the potentiometers corresponding to G'_θ and $G'_{\dot{s}}$ being set to -.267233 and -.271367, respectively). The gain $G_{\int\theta}$ was set at -.001, the smallest gain setting possible on the GP-6.

Tests were performed on each state feedback gain independently (i.e. all the rest disconnected) to see if the actuator responded appropriately. The "test" potentiometer, shown in Figure 5.1 as G_U, was varied to provide weak or strong control inputs as desired.

With the gains wired in as described and the pendulum raised to the unstable equilibrium position, the loop was closed and the computer was allowed to assume control. Immediately, the pendulum moved in a $-\theta$ direction, and the cart compensated by moving in the $-s$ direction, but could not right the pendulum and continued until it hit the track limit switches, causing the motor to shut down. This was clearly an unstable condition and an unsatisfactory result.

Subsequent experimentation with the pendulum and monitoring of GP-6 signals revealed a large amount of noise within the differentiator, producing an unpredictable bias in the system even when the pendulum was stationary (the tendency of simple differentiators to produce noise was a drawback mentioned in Chapter 4). With all system states close to their homogeneous conditions, the amount of noise might have been enough to exceed the given gain margin for the control loop.

Further experimentation involved arbitrarily raising the integral gain $G_{\int\theta}$ from its extremely low value to values as high as the gain on the pendulum angle, G_θ. Increasing the integral gain helped the system out considerably, and for a value of $G_{\int\theta} = .800$ the pendulum became reasonably stable for a short period of time. The cart would still travel to the edge of the track and trip the switch, but performed a few oscillations about equilibrium (i.e. the $s = 0$ and $\theta = 0$ points) before doing so.

Finally, the gains on cart position and velocity, G_s and $G_{\dot{s}}$, were reduced to put more emphasis on pendulum stability and less emphasis on cart location. Again, this seemed to help the system. The pendulum angle never exceeded more than two or three degrees, even when provided an "impulse" by a finger. The cart moved slowly and would often remain within the confines of the track for more than a minute before inevitably hitting one of the shutoff switches.

5.4 *Discussion of Results*

Clearly, the actual results were different from the desired results, but important observations and suggestions can be made from the limited tests conducted.

The output potentiometers (and the tachometer) produced signals that were remarkably accurate. Particularly effective was the potentiometer measuring pendulum angle, which was so sensitive the naked eye could barely perceive the angle changes that produced corresponding signal voltage changes. The alignment of zero voltage output with the pendulum vertical was also accurate. Thus, there is probaly little error being produced in the actual outputs of the system.

The aforementioned differentiator noise problem is probably the greatest single source of state error in the system. This factor emphasizes the need for a reliable estimator to produce the needed states. The raising of the integral gain helped to alleviate this problem somewhat, but did not eliminate it. There was no LQR gain schedule G that could be obtained that would not use the state $\dot{\theta}$, so the problem could not be "worked around."

Also, tests on the integrator itself indicated that it tended to "drift" over time, and return or stay at a homogeneous value even when the input (pendulum angle in this case) was homogeneous. This might partially explain, in addition to differentiator noise, the tendency for the cart to wander slowly around at high integral gain. A possible solution to this problem, aside from finding a more reliable "black-box" integrator, is to abolish the black-box altogether and estimate $\int\theta$ within an estimator. Hence another reason to incorporate a reliable estimator.

Another possible source of difficulty lies within the actuator portion of the control loop. The "dead zone" due to friction shown in Appendix A, where a range of small control input voltages around zero produce no motor output, introduces an unmodeled nonlinearity into the system. The effect of this is unpredictable, and may be contributing to some of our problems. Add to this the fact that even a linear model for the actuator is left out of this particular implementation, and the motor-actuator as a source of error becomes even more likely. Once again, use of an estimator to provide an actuator state for full-state feedback would prove useful.

Finally, there may be actual error in the plant model itself. The assumption that all friction forces within the Cart-Pendulum are viscous in nature is certainly not

100% correct, and may be inaccurate enough to cause significant error within the system. Tables 4.1 and 4.2 showed that small changes to the friction parameters (as well as to others) within the plant should not drastically affect the system. However, unmodeled types of friction, to include coulomb, static, etc., might produce greater problems.

Nevertheless, the U.W. Cart-Pendulum control system has reached an operational status, if for not more than a couple minutes or so! The observations gained from these tests should prove useful when additional control designs are ready to be implemented and/or more flexible equipment is available.

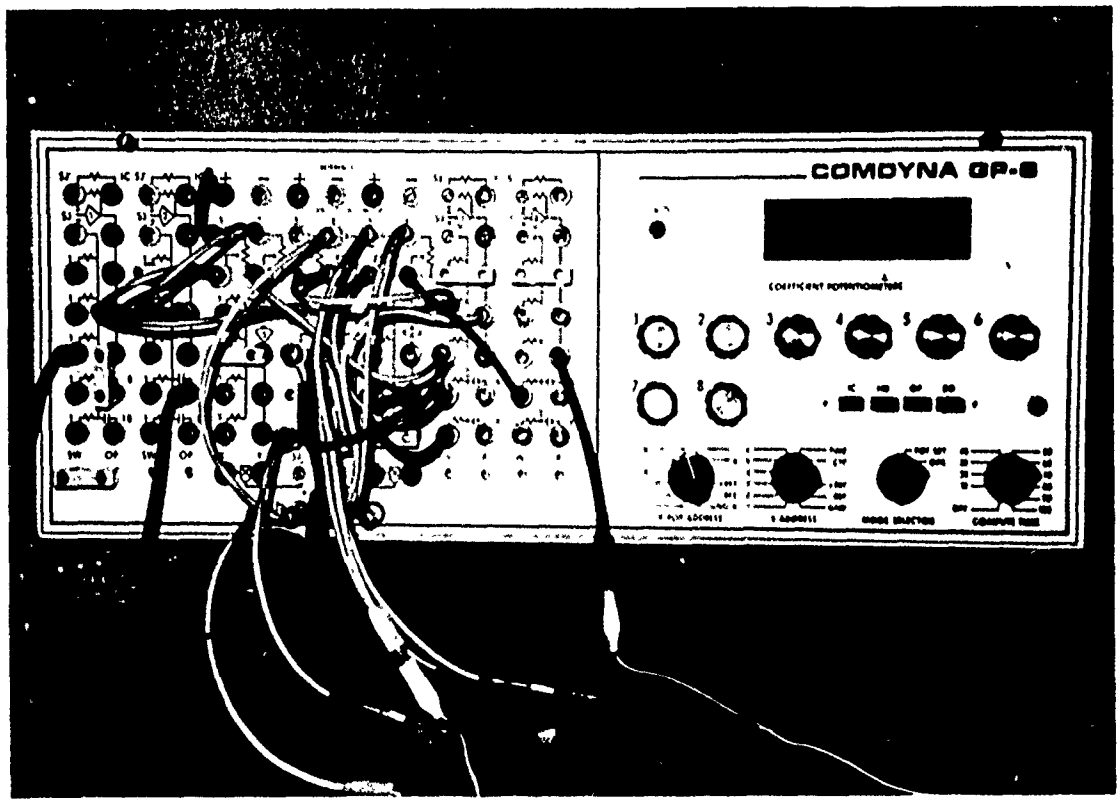

Figure 5.2: GP-6 in Operation in Lab

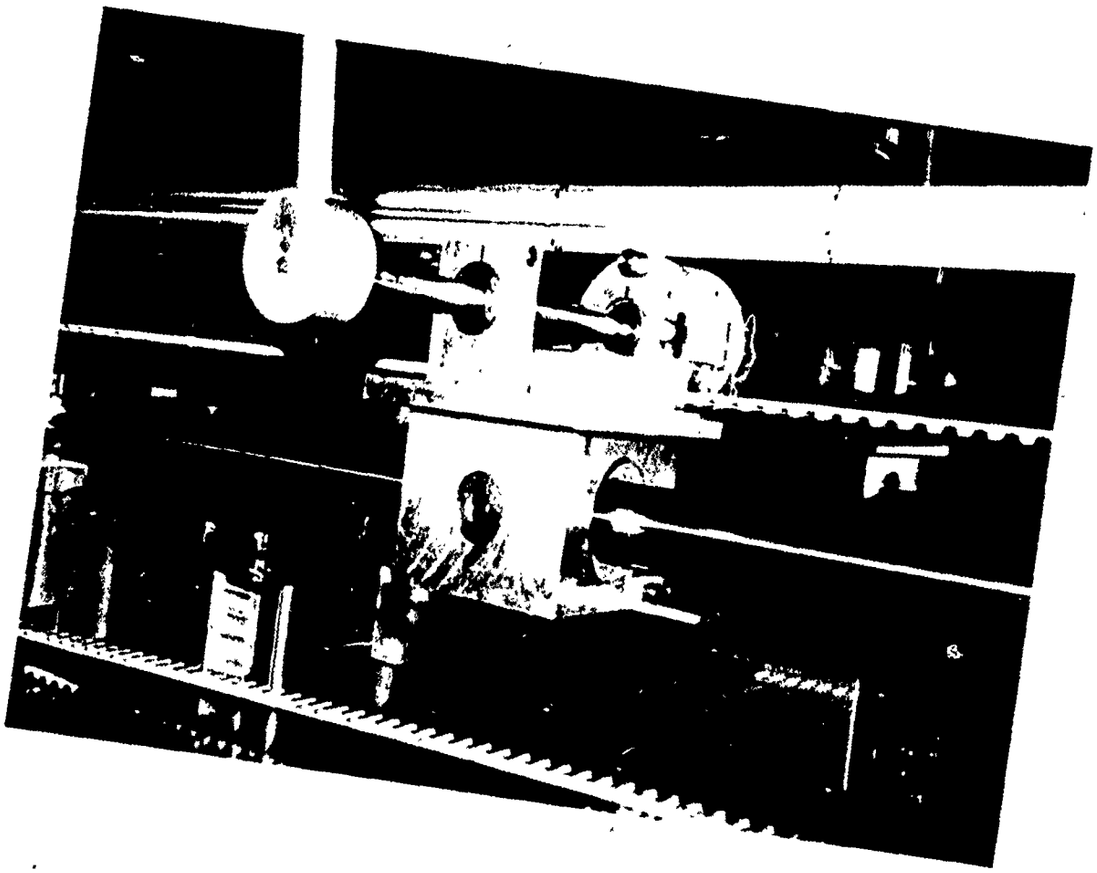

Figure 5.3: Cart in Motion During Testing

Chapter 6

CONCLUSIONS AND RECOMMENDATIONS FOR FURTHER STUDY

6.1 Conclusions

The purpose of this paper has been to provide a baseline for control system design and implementation on the new inverted Cart-Pendulum apparatus at the University of Washington, Department of Aeronautics and Astronautics. The nonlinear equations of motion and linear equations about equilibrium have been developed, and their characteristics have been described. As shown, the nonlinear equations are necessary when addressing the pump-up problem, and have been expressed in state form to provide easy application to computer algorithms and routines. The characteristics of the fourth-order linear system, one which is unstable and non-minimum phase, have also been described.

Analysis to find actual values for system parameters has been carried out, and fairly reliable values have been obtained. Extensive tests on the motor-actuator have produced good approximations for motor parameters and a working transfer function to use as a linear model.

The minimum-time pump-up problem has been addressed through application of optimization principles, and a practical solution in the form of bang-bang control has been suggested. This solution could be applied though an open-loop control law or through closed loop supervisory control logic.

The LQR/LQE approach to control system design has been applied to the particular hardware system at hand, and a good feeling for the quality of performance and robustness has been obtained. LTR procedure during LQE design has thus far shown no ill effects with regard to the non-minimum phase nature of the system, and has permitted recovery of almost all of the robustness properties guaranteed in the LQR portion of design. The variation of the LQG solution with incorporation of different actuator models has been explored.

Finally, a working control loop consisting of the Cart-Pendulum itself with measured outputs, a controlling mechanism, a servo-amplifier, power supply, and motor/actuator has been constructed. Initial implementation of full-state feedback methods on the actual hardware has been made, employing an analog computer as a controller. Although not all control scenarios were tested, the results of experiments thus far should serve as a useful guide for further control design and experimentation on the Cart-Pendulum.

6.2 Recommendations

Clearly, one of the first steps to take towards perfecting control of the Cart-Pendulum should be the implementation of the proposed digital controller mechanism, which would introduce an actual computer into the control loop. Analog computers can be useful for low order controller designs, but the more complex controllers resulting from full-state feedback gains, optimal estimators, and integral state addition can make analog devices difficult to implement and even harder to monitor. A digital controller of the type in question would allow continuous monitoring of plant outputs and control inputs, produce essentially "noiseless" (with respect to plant outputs) integral states and state estimates, and even record system data so that comprehensive post-test analysis can be conducted.

The digital controller will be a necessity if the pump-up control strategy is to be used in any way. The open-loop method could be employed by inserting the bang-bang control schedule into an actual program that would produce the appropriate control signals at the proper times. Supervisory control logic for pump-up should be relatively easy to program into the digital controller as well.

The bare essentials of the minimum-time pump-up problem have been developed here, but solution of the complete two-point boundary problem remains. Subjecting the optimization problem to added constraints, to include hard limits on cart position and velocity, may produce an even more complex problem. Mori et al found the solution of this boundary problem to be extremely complex; they attempted to solve the problem using "a convergence procedure utilizing the gradient method," but were not able to obtain a rigorous solution, stating the "feasible orbits are very 'twisted' and cannot be obtained without special care or a powerful algorithm" [Mori 686].

Nevertheless, it may be possible to construct a strong enough algorithm that can produce a useful solution.

With regard to linear control, it is clear from experimental data that the actuator plays a rather significant role in the dynamics of the system, and probably should not be ignored. A proper step would be to implement a LQG controller employing the zero-pole transfer function derived for the actuator in Chapter 2 and Appendix A. If the actuator continues to cause problems, then a greater understanding of the actuator dynamics, especially of the effects of friction, is needed. It is possible that a second order model may be required to more accurately model the actuator. It is also quite possible that frictional effects are so significant that *no* linear model can accurately describe the actuator dynamics. One other possible conclusion is that the motor at hand (the French-built RX-330-A) may be inadequate in terms of time constant and torque/force available. A more powerful device may diminish the actuator difficulties encountered.

If implementation difficulties with both the controller and the actuator can be minimized, all that remains is to perfect and expand various control designs for different control scenarios. First, the LQG scenarios described in this paper should be tested and the weights in the four LQG weighting matrices Q, R, W, and V varied as necessary to produce the best results. Variations in the design procedure itself might include (1) eliminating the "black box" integrators and producing the integral states through the estimator, and/or (2) experimenting with reduced-order estimator designs that will produce essentially the same outputs as a full-order estimator. Also, a deeper analysis of the response of this non-minimum phase system to LTR procedure might reveal a better way to obtain optimal estimation of the states

Once the LQG control designs have been successfully inplemented, more advanced control concepts could be examined. H-infinity optimal control and parameter optimization techniques might produce control designs far more flexible, effective, and robust than the LQG designs featured here.

Finally, it may prove useful to expand the Cart-Pendulum control system design problem to a more flexible hardware arrangement. Furuta et al have introduced a *turntable* Cart-Pendulum array, where the pendulum is mounted to the outer edge of a rotating disk rather than a cart. This clever arrangement eliminates the track edge constraints imposed by the linear Cart-Pendulum, and instead provides an essentially

infinite, rotating path [Furuta 191]. Also, implementation of the actuator into the loop is far more direct, diminishing the actuator modeling difficulties experienced with the conventional "belt-and-pulley" arrangement. While the elimination of such practical application obstacles may be frowned upon by some educators, such a system would allow for more freedom of design and measurement of system response.

BIBLIOGRAPHY

[Bryson] A.E. Bryson and Y. Ho. *Applied Optimal Control.* Hemisphere Publishing Corporation, 1975.

[D'Souza] A.F. D'Souza and V.K. Garg. *Advanced Dynamics: Modeling and Analysis.* Prentice-Hall, Inc., Englewood Cliffs, New Jersey, 1984.

[Eshbach] O.W. Eshbach and M. Souders. *Handbook of Engineering Fundamentals.* John Wiley and Sons, New York, 1975.

[Franklin] G.F. Franklin, J.D. Powell, and A. Emami-Naeini. *Feedback Control of Dynamic Systems.* Addison-Wesley Publishing Company, 1988.

[Furuta] K. Furuta, M. Yamakita, S Kobayashi, and M. Nishimura. A New Inverted Pendulum Apparatus for Education. *International Federation of Automatic Control: Advances in Control Education*, Preprints for IFAC Conference on Advances in Control Education, Boston, June 24-25, 1991.

[Maciejowski] J.M. Maciejowski. *Multivariable Feedback Design.* Addison-Wesley Publishing Co., 1989.

[Mori] S. Mori, H Nishihara, and F. Furuta. Control of Unstable Mechanical System, Control of Pendulum. *International Journal of Control*, vol.23, no.5, p. 673-692, 1976.

[Oakley] C.M. Oakley. *Experiments in Modelling and End-Point Control of Two-Link Flexible Manipulators.* Ph.D. Dissertation, Mechanical Engineering Dept., Stanford University, April 1991.

[Reekers] E. Reekers. Entwurf und Realisierung eines Zustandsreglers für ein invertiertes Pendel. Universität-GH-Duisburg, August 1983.

Appendix A

MOTOR ANALYSIS AND CONTROLLER/ACTUATOR GAINS

A.1 Motor Analysis

The motor used in actual experimentation was a pulse-modulated Alsthom-Parvex RX-330-A, made in France. A number of tests were performed on the motor before any experiments were conducted. All tests were done with the motor hooked up to the pulleys and belt of the hardware (the cart-pendulum is considered to be a separate system and was not attached).

Many of the parameters given in the motor specifications had to be recalculated, since attachment of the pulleys and belt would have changed their values. Some of those given specifications are:

$$\begin{aligned} R_a &= 0.30\Omega \\ L_a &= 3.30mH \\ J_{motor} &= 0.00072kgm^2 \end{aligned}$$

R_a and L_a remain fixed, while the total inertia J will be higher than just J_{motor} alone.

A.1.1 TEST 1: Computation of K_{tach}

To compute K_{tach}, the motor was run up clockwise (viewing the motor from the front) to various speeds, each of which were measured using a strobescope. The respective tachometer voltage outputs were then recorded. Then the motor was run counter-clockwise, and the same test performed. Plots showing the results are shown in Figure A.1. As shown, the value for K_{tach} was slightly different for clockwise and counter-clockwise rotations of the motor. Reasons for this difference are not known. For the remainder of the tests, whenever K_{tach} was required, the motor was rotated

counter-clockwise. The computed values for K_{tach}:

$$K_{tach_{CCW}} = .0047061\frac{volt}{rpm} = .044940\frac{volt}{rad/sec}$$
$$K_{tach_{CW}} = .0052449\frac{volt}{rpm} = .050085\frac{volt}{rad/sec}$$

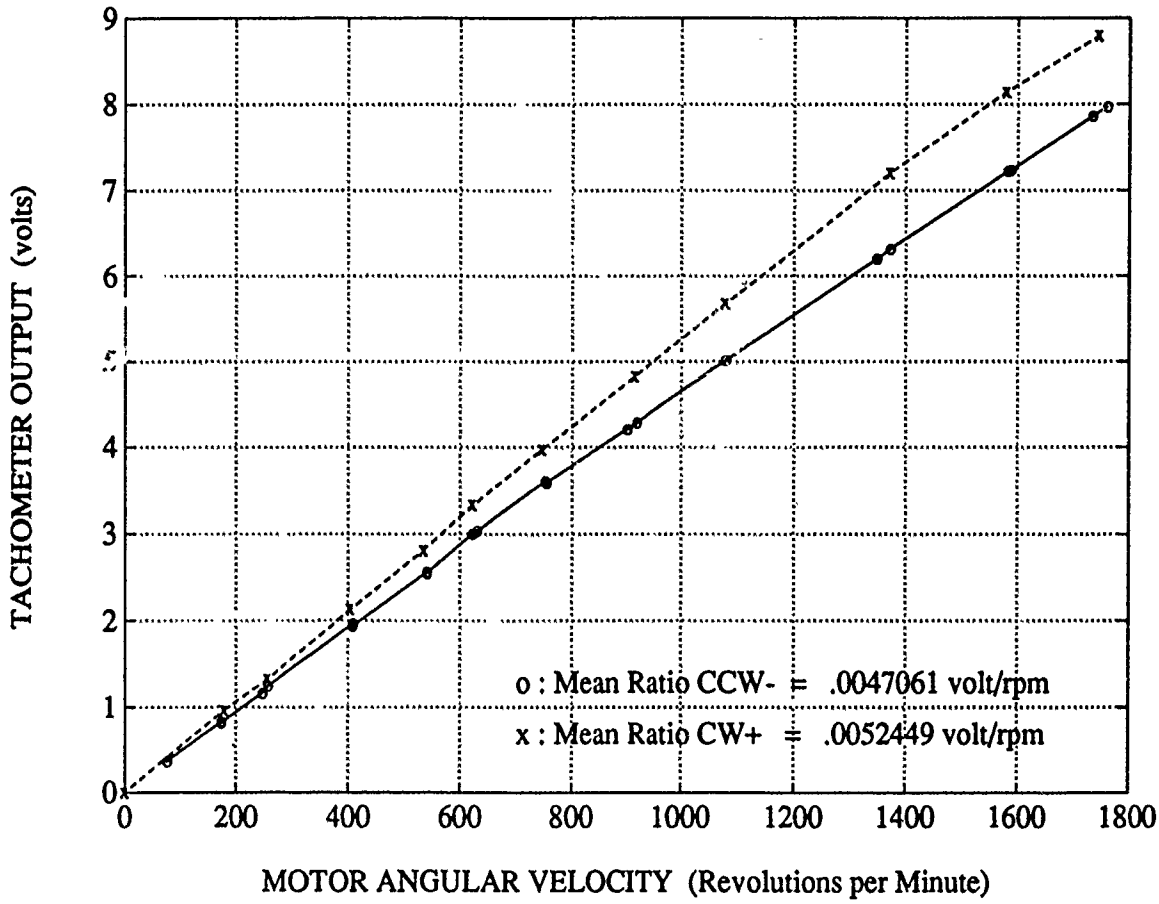

Figure A.1: TEST 1: Plots of Data to Obtain K_{tach}

A.1.2 TEST 2: Computation of Motor Constant K

To obtain the motor constant K, the power supply was disconnected and the motor was rotated by hand to produce the tachometer and motor terminal voltage outputs shown in Figure A.3. K is computed by calculating the ratio between the motor voltage v_a and tachometer voltage v_{tach}, then multiplying by K_{tach}. The actual value for K is shown as follows:

$$\begin{aligned} K &= \frac{v_a}{v_{tach}} \times K_{tach} \\ &= 1.90 \times .044940 \frac{volt}{rad/sec} \\ &= .085386 \frac{volt}{rad/sec} \end{aligned}$$

A.1.3 TEST 3: Zero-Current Test

The zero-current test was performed by simply running up the motor to approximately 1000 rpm, and then shutting off the power supply. The result was a zero-current situation, in which the only forces acting against the motor are mechanical damping forces within the actuator. This is expressed by:

$$J\dot{\omega} = -D\omega - F_f \tag{A.1}$$

The effects of mechanical damping are clearly visible in Figure A.4, and appear almost perfectly linear in nature. The results of this test allow us to make the reasonable assumption that mechanical damping is dominated by the friction force, F_f, which is close to being a constant force. D is clearly very small compared to F_f.

A.1.4 TEST 4: Zero-Voltage Test

To perform the zero voltage test, the motor was first run up to approximately 1000 rpm using an external power supply. Then the power was cut to the motor while a simultaneous short was introduced across the motor. The result was a zero-voltage situation which comanded the motor to zero rpm, which can be expressed by:

$$J\dot{\omega} = -(D + \frac{K^2}{R})\omega - F_f \tag{A.2}$$

The effects of total damping, as shown in Figure A.5, assume the shape of a typical first-order decay, which indicates that the total damping is dominated by the viscous term, $D + \frac{K^2}{R}$. This supports the assumption made back in Chapter 2 that friction forces F_f could be assumed negligible. Since we have already shown that D is small compared to F_f, the $\frac{K^2}{R}$ term clearly dominates total friction. Recall the transfer function calculated in Chapter 2 relating motor speed ω to voltage v_a:

$$\frac{\omega(s)}{v_a(s)} = \frac{\frac{K}{K^2+DR}}{(\frac{J}{D+K^2/R})s+1} \tag{A.3}$$

If we assume the plot shown in Figure A.5 provides a reasonably good approximation of the response of the transfer function $\frac{\omega(s)}{v_a(s)}$ to a step command, fitting an appropriate first-order decay to it should determine the value of the time constant τ. Figure A.6 shows how a first-order decay with $\tau = .2$ produces roughly the same rate of decay as the results of the test in Figure A.5. Thus, the following is true:

$$\tau_{\frac{\omega}{v}} = \frac{J}{D + K^2/R}$$

Since K and R are known and $D \approx 0$, we can obtain a value for J:

$$\begin{aligned} J &= \tau\frac{K^2}{R} \\ &= (.2\,sec)\frac{(.085386\,volts/rad/sec)^2}{0.3\,\Omega} \\ &= .00486\,kg\,m^2 \end{aligned}$$

Note that this number compares favorably with the original specification given on the inertia of the motor alone: $J_{motor} = .00072\,kgm^2$. We would expect the increase shown to accommodate the added inertias of the pulleys and belt. We now have estimates for all of the important parameters for the motor. The final step is to find a numerical expression for the transfer function $\frac{F_U(s)}{v_a(s)}$. Recall from Chapter 2 this transfer function is given by:

$$\frac{F_U(s)}{v_a(s)} = \frac{\frac{JK}{\tau(K^2+DR)}s}{(\frac{J}{D+K^2/R})s+1} \tag{A.4}$$

The radius of the pulley is measured to be: $r = .080573$ *meters* (this is shown in Appendix B). Substituting in the values now known for our motor, we obtain:

$$\begin{aligned}\frac{F_U(s)}{v_a(s)} &= \frac{\frac{JK}{r(K^2+DR)}s}{(\frac{J}{D+K^2/R})s+1} \\ &= \frac{\frac{(.00486)(.085386)}{.08((.085386)^2+0)}s}{(\frac{(.00486)}{0+(.0486)^2/(0.3)})s+1} \\ &= \frac{.7064s}{.2s+1}\end{aligned}$$

Recall from Figure 2.2 that the amplification of the controller signal, u_c, to the servo-amp voltage e_a is given by:

$$e_a = K_a u_c$$

Assuming the voltage drop across the servo-amp resistor R_0 is small, we can use:

$$v_a = K_a u_c$$

Therefore, the final transfer function, in the form shown in Chapter 2, is:

$$\frac{F_U(s)}{v_a(s)} = \frac{.7064\,K_a\,s}{.2s+1} = \frac{K_U\,s}{.2s+1} \tag{A.5}$$

The results of a related test are shown in Figure A.7. Here, the bang-bang capability of the motor is shown. The motor was first run up to approximately 1000 rpm, then the voltage applied to the motor was immediately reversed, effectively commanding the motor to run up to -1000 rpm. After the motor settled at this value, the voltage was reversed again, causing the motor to reverse back to 1000 rpm. We would expect to transition from 1000 rpm to -1000 rpm (and the reverse) to exhibit the same first-order step response shown in Figure A.5. However, as Figure A.7 shows, the decay or rise to the commanded value is noticeably slowed as the motor speed passes through zero. This would appear to indicate the presence of significant friction effects at low speeds; again, something that cannot be ignored during performance analysis.

A.1.5 TEST 5: Computation of K_U

An approximation for the constant K_U was obtained by introducing measured positive and negative voltage inputs to the actuator, u_c, and measuring as accurately as possible the resulting steady-state forces applied to the cart, F_U. Figure A.8 shows the plots of data for positive and negative voltage inputs. A linear proportion can be extracted from them to produce an estimate for K_U. Note the "dead zone" that appears between voltages of approximately 0.20 and -.20 volts. At these inputs, no output force was detectable. It should be noted that the observed forces would have already included the constant (nonlinear) friction forces described in Equation 2.39. The effect of the constant friction force is evidenced on explains the observation of the dead zone found during the test.

The approximate value for K_U was computed to be:

$$K_U = 14.010 \frac{Newtons}{volt}$$

The magnitude of this constant friction force could be approximated by the width of the dead zone on either side of the origin multiplied by K_U:

$$.20\ volts \times K_U = 2.80\ Newtons$$

This assumes, of course, that the friction force F_f is a constant, and that the relationship between F_U and u_c is linear near the origin, and that K_U is also a valid constant of proportion for the relationship.

A.2 System Gain Computation

The potentiometers attached to the Cart-Pendulum and the tachometer attached to the motor produce outputs in the form of volts, although they essentially measure quantities in other units; i.e. meters, radians, etc. Also, as already established, the motor-actuator assembly, at a minimum, has a proportional gain which allows us to translate the command voltage u (from the controller) into a force on the cart. Thus, an experimenatally determined set of gains is required to make the proper transformation in order for the controller's theoretical gain matrices to have any meaning. Most of these were obtained by simply measuring physical quantities in the

system and recording the corresponding voltage. As stated in Chapter 5, the system was wired such that all potentiometer outputs (and the controller signal u_c) would provide voltages with the same sign conventions (relative to a common ground) as those values they represent, so all of the circuit proportion constants are positive. The constant K_U was determined from motor tests, as described in the previous section. Figure A.2 shows the location of the gain constants within the closed system.

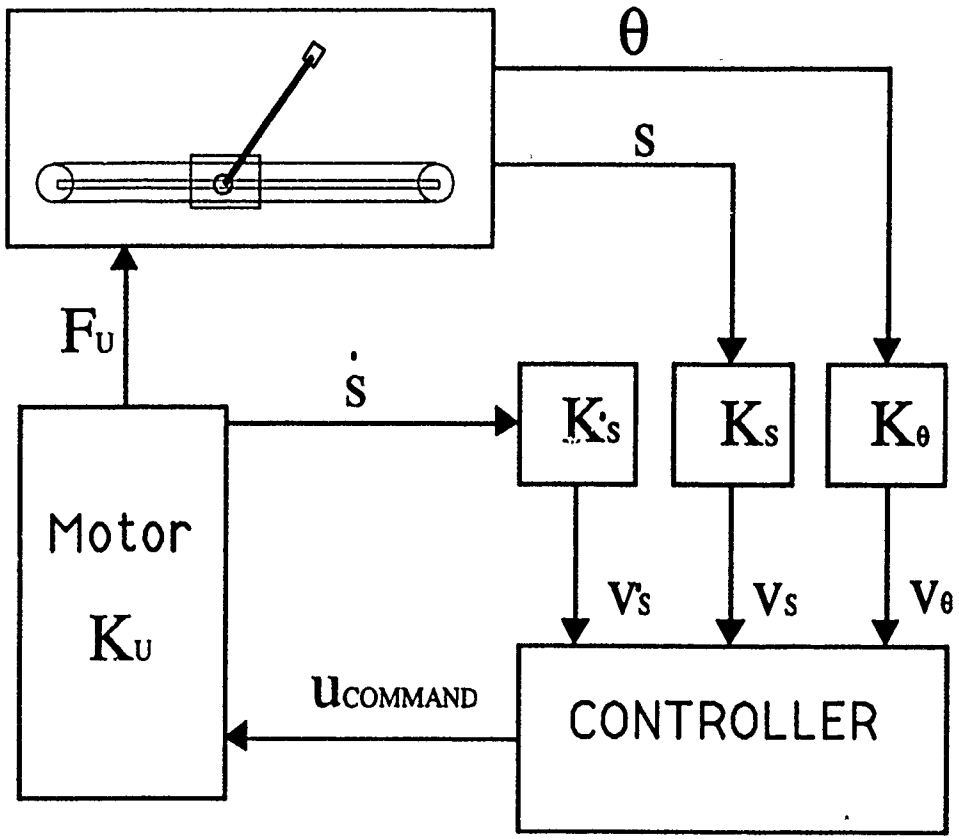

Figure A.2: System with Gain Arrangement

The following values were found for the final system state gain constants:

$$K_s = 5.000 \frac{volts}{meter}$$

$$
\begin{aligned}
K_\theta &= 4.190 \frac{volts}{radian} \\
K_s &= 1.990 \frac{revolutions}{m/sec} \times K_{tach} = 0.5941 \frac{volts}{m/sec} \\
K_{\dot{\theta}} &= 4.190 \frac{volts}{rad/sec} \\
K_U &= 14.010 \frac{Newtons}{volt}
\end{aligned}
$$

These are displayed in Table A.2.

Motor Resistance (given, at $25^{\circ}C$)	R_a	0.30	Ω
Motor Inductance (given)	L_a	3.30	mH
Motor-Actuator Constant	K	.085386	$\frac{volt}{rad/sec}$
Motor-Actuator Inertia	J	.00486	$kg\,m^2$
Tachometer Constant - CW Rotation	$K_{tach_{CW}}$	.050085	$\frac{volt}{rad/sec}$
Tachometer Constant - CCW Rotation	$K_{tach_{CCW}}$	.044940	$\frac{volt}{rad/sec}$

Table A.1: Table of Motor-Actuator Parameters

Cart Position Constant	K_x	5.000	volts/meter
Pendulum Angle Constant	K_θ	4.190	volts/radian
Cart Velocity Constant	$K_{\dot{x}}$	0.5941	volts/m/sec
Pendulum Velocity Constant	$K_{\dot{\theta}}$	4.190	volts/rad/sec
Actuator Command Constant	K_U	14.010	Newtons/volt

Table A.2: Table of Computed System Constants

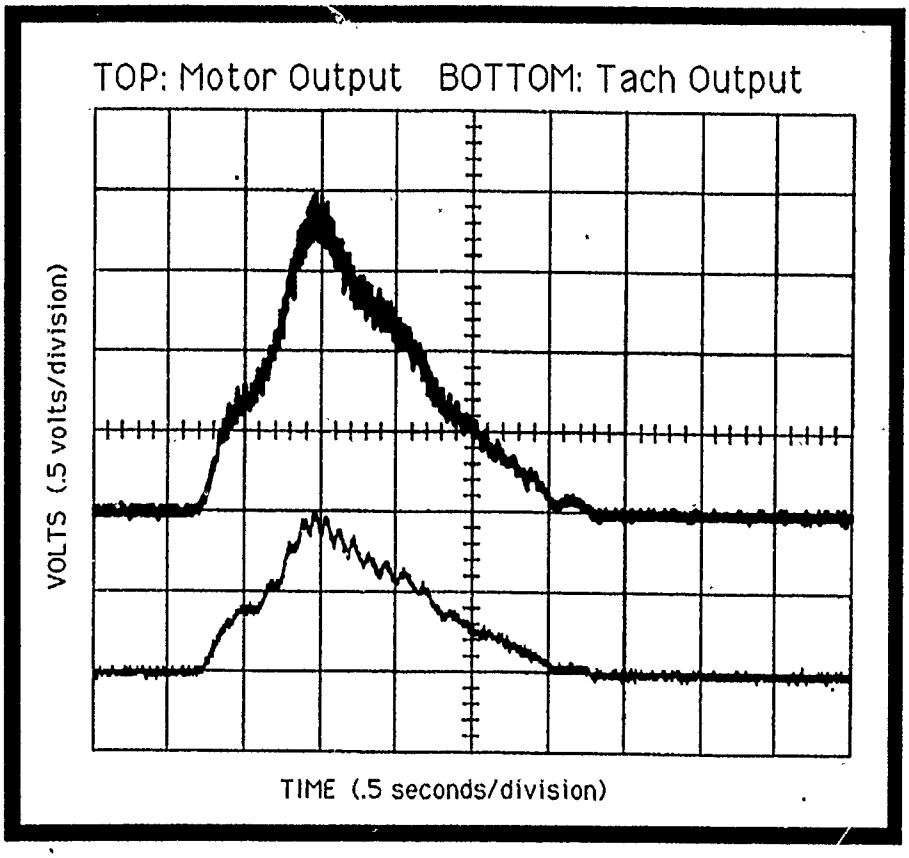

Figure A.3: TEST 2: Data to Obtain Motor Constant K

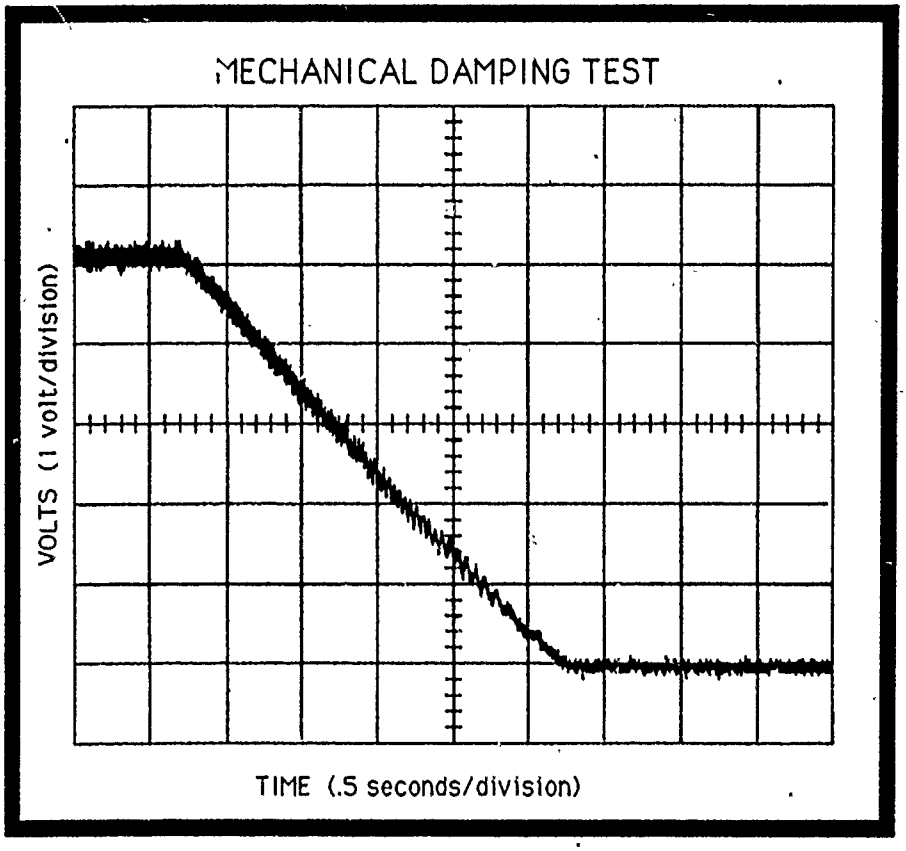

Figure A.4: TEST 3: Zero-Current - Mechanical Damping

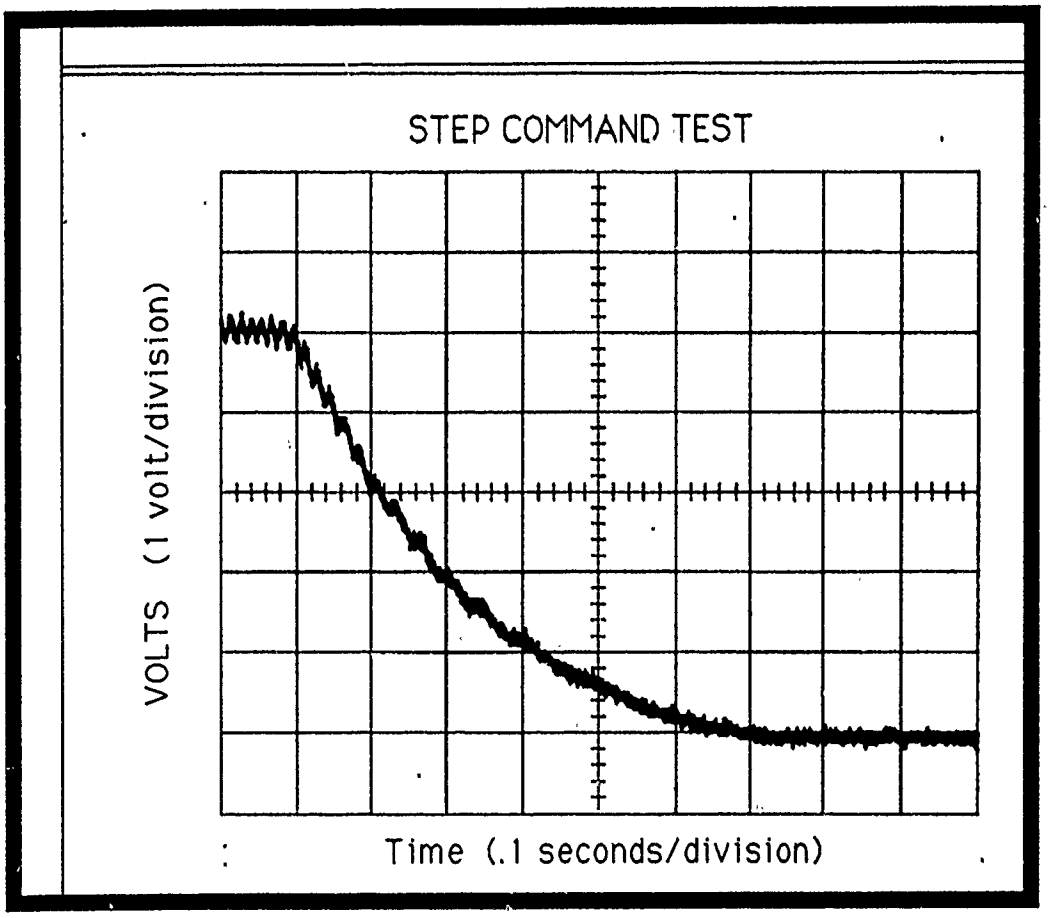

Figure A.5: TEST 4: Zero-Voltage - Total Damping

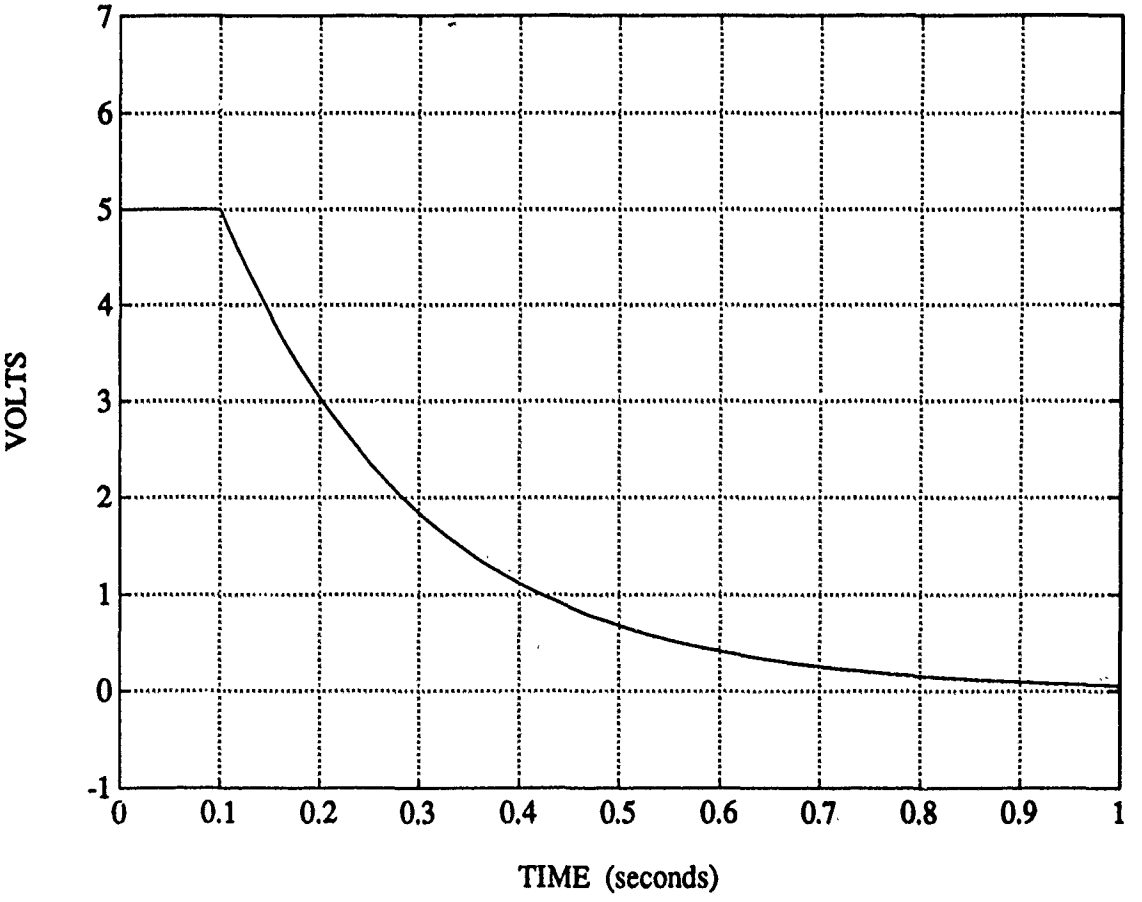

Figure A.6: Comparing Theoretical First-Order with Motor

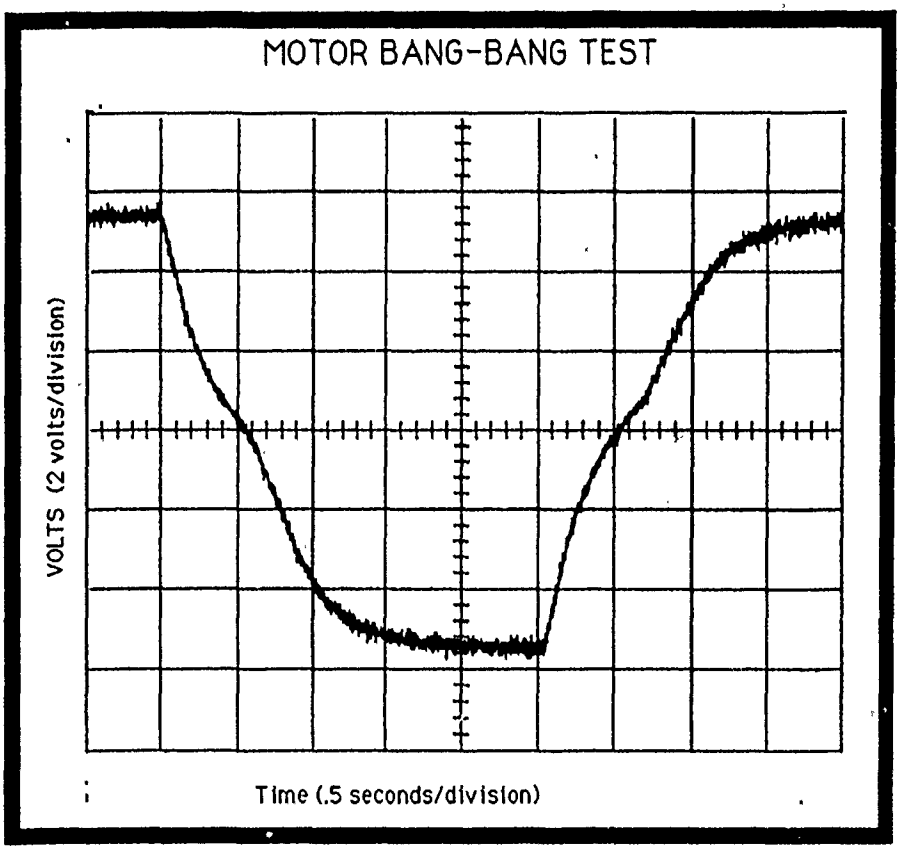

Figure A.7: Actuator Bang-Bang Test

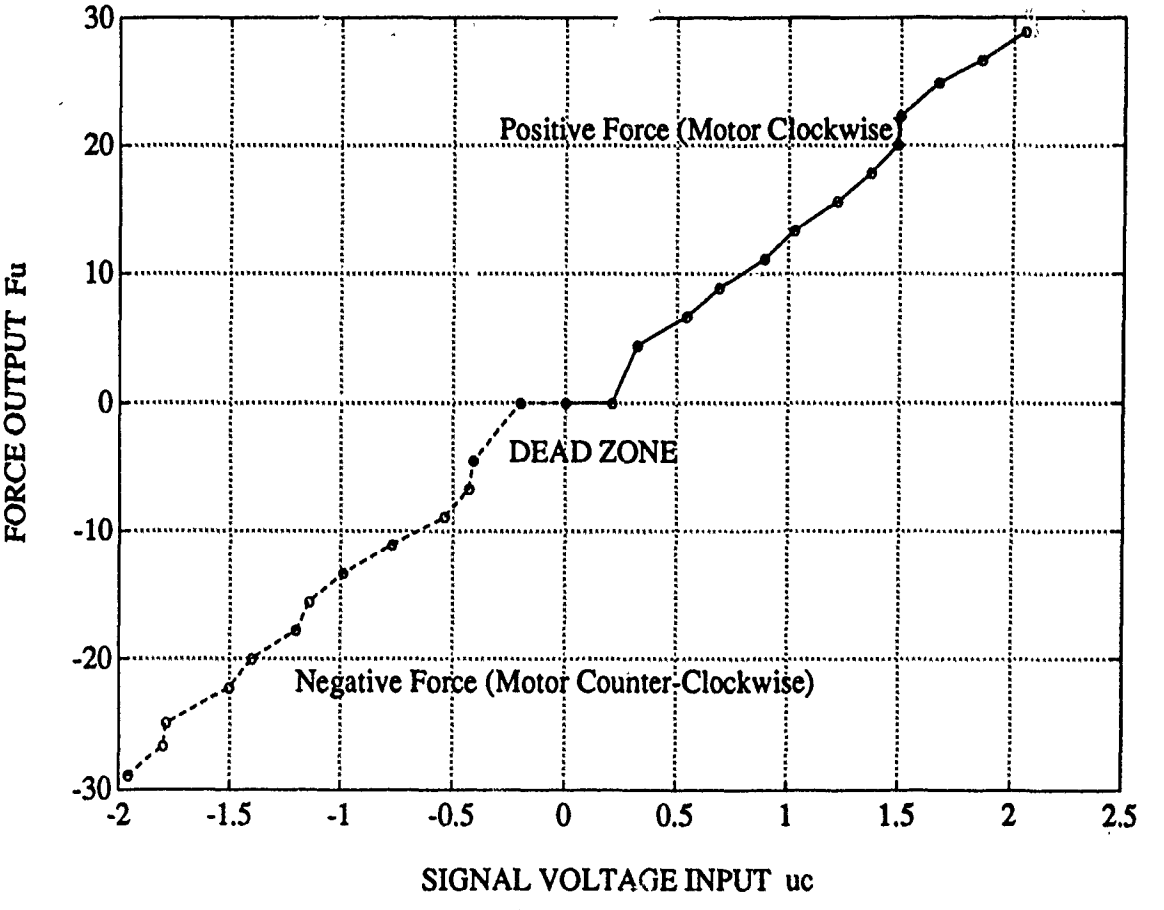

Figure A.8: TEST 5: Plots of Data to Obtain K_U

Appendix B

EXPERIMENTAL DETERMINATION OF SYSTEM PARAMETERS

B.1 Review of System Parameters

Recall from Chapter 2 the parameters used to describe the dynamics of the Cart-Pendulum array:

m : pendulum mass (kg)

M : cart mass (kg)

ℓ : "effective length" of the pendulum (meters)

g : gravitational acceleration (m/s^2)

b_{VF} : viscous friction constant, proportional to cart velocity (kg/m)

c : rotational friction constant, proportional to angular velocity

We add to these two more parameters of interest:

d : cart usable track length (meters)

r : pulley radius

The first four quantities should be relatively trivial to obtain. The mass of the pendulum can be measured using reliable weight-measuring devices. The "effective length" of the pendulum was assumed to be the distance from the point at which the pendulum was attached to the hinge to the center of mass of the pendulum, and is easily determined. The cart on the actual apparatus could not be removed for weighing, since it contained sealed bearings. However, documentation from Duisburg, the source of manufacture, quotes a value for the cart mass which appears to be accurate, based on density and volume estimates for the aluminum cart. The value for gravitational acceleration is widely published; since the actual experimentation was performed at the University of Washington at low elevation, a reliable value for g at sea level was obtained from Eshbach's Handbook for Engineers.

The value for d, the usable track length, was found by simply measuring the distance from one cutoff switch to the other (these switches were described in Chapter 1). The pulley radius r, which serves to convert motor output torque to force applied to the cart, was measured by moving the cart a fixed distance on the rail, observing the precise number of rotations of the pulley, and converting the measured linear distance to pulley radii.

Actual Values obtained for the basic pendulum configuration were:

$m = 0.324\ kg$

$M = 3.552\ kg$

$\ell = 0.429\ m$

$g = 9.807\ m/s^2$

$d = 1.090\ m$

$r = .080573\ m$

B.2 Frictional Terms

The final two parameters to determine are both friction terms. These are characteristically the most difficult to determine, and are most likely to change unpredictably. It may be difficult to consistently lubricate the bar or hinge to the same degree to maintain the same values for sliding and roational friction, and there may be unmeasurable inperfections in the system parts that may introduce unseen resistance forces. Thus, the elements of uncertainty in the system may very well be dominated by imperfectly modeled frictional effects. Nevertheless, a reasonable estimate of the forces opposing motion within the system may be obtained through proper analysis.

B.2.1 Cart Sliding Viscous Friction

As discussed in Chapter 2, the frictional effects resulting from the movement of the cart on the lubricated bar or rail were assumed to be completely viscous in nature. This assumes that that any constant (i.e. coulomb) friction forces are very small and negligible compared to viscous friction forces. This assumption is least accurate, of course, when the cart is stationary; at this instance, the only frictional forces present are coulomb forces. However, observation of the performance of the cart on the well-lubricated bar seems to indicate that general frictional effects seem to be dominated by

those proportional to the cart's own speed: velocity decay appears more exponential (indicative of viscous friction) than linear (a coulomb friction indication).

Thus, assuming that friction on the sliding cart was strictly viscous, the following method was employed to determine the viscous friction constant, b_{VF}. The entire pendulum array was elevated at one end to make the angle of the bar with horizontal equal to an angle ϕ. Then the cart (with pendulum attached but fixed) was allowed to slide from the high end of the bar to the low end, and the time taken to travel this distance was recorded. The motion of the cart can be described by the following equation:

$$(M+m)\ddot{s} + b_{VF}\dot{s} = (M+m)g\sin\phi \qquad \text{(B.1)}$$

This is a second order differential equation, with the quantities $M+m$, g, and ϕ known, and b_{VF} being the parameter we wish to find. A normal second-order differential equation requires two conditions to be completely solved, so we require a third in order to obtain the unknown constant. These three initial and boundary conditions are known from experimentation:

$$\begin{aligned} s(0) &= 0 \\ \dot{s}(0) &= 0 \\ s(t_f) &= d \end{aligned}$$

where d is the total length of the bar and t_f is the time taken for the cart to travel the length of the bar. The final expression is not explicit in terms of b_{VF}, so iteration is necessary to arrive at a final value.

For our particular configuration, the differential equation took the form:

$$\ddot{s} + b\dot{s} = (9.81 m/s^2)\sin 9.5^o \qquad \text{(B.2)}$$

where $b = b_{vf}/(M+m)$. Solving this equation and applying the boundary conditions mentioned above, with:

$$\begin{aligned} s(0) &= 0 \\ \dot{s}(0) &= 0 \\ s(t_f) &= 132.5cm \\ t_f &= 1.460sec \end{aligned}$$

we obtain an implicit solution for b in the form:

$$1.325b^2 - 2.3886b + e^{1.46b} - 1.636 = 0 \tag{B.3}$$

Iteratively solving for b produces $b = .665$ and, subsequently:

$$b_{VF} = 2.57754 kg/s$$

It should be noted that these tests were performed with the rail and cart freshly lubricated with a common lubricant, WD-40. The same lubrication should be applied before experiments to assure the frictional force is as close to the predicted values of possible. Small changes in the lubrication condition of the apparatus could lead to large differences between expected and actual values for the cart viscous friction.

B.2.2 Pendulum Rotational Viscous Friction

As with the cart viscous friction, we assume the friction opposing rotation of the pendulum about its hinge is solely viscous in nature. This assumption is not a necessity; indeed, it has been shown that good estimates for both viscous and coulomb friction constants can be obtained from thorough experimentation [Oakley 271]. However, as with the cart, observation of the behavior of the swinging pendulum indicates that forces opposing its rotation seem to be dominated by those frictional effects proportional to velocity.

To obtain an estimate for the viscous rotational friction constant, c, the pendulum was allowed to swing freely with the cart fixed on the bar. The motion of the pendulum can be described by the following equation:

$$I\ddot{\theta} + c\theta + m\ell g \sin\theta = 0 \tag{B.4}$$

where I is the moment of inertia of the pendulum about the hinge. If we assume $I = m\ell^2$ (as we have done throughout our dynamic modeling), we obtain:

$$\ddot{\theta} + \frac{c}{m\ell^2}\theta + \frac{g}{\ell}\sin\theta = 0 \tag{B.5}$$

Clearly, if $c = 0$, the pendulum, given an initial angle of elevation, would oscillate in the pattern of a perfect sinusoid forever. Therefore, by observing the decay of

pendulum swing over time, we can estimate the amount of damping that the friction must be injecting into the system.

The method used to determine c involved starting the pendulum at some initial angle ϕ, and then allowing it to swing freely. By observing plots of the pendulum angle vs. time, a first order decaying exponential curve could be obtained that would describe the decay of the oscillating amplitude.

The value obtained for c was checked by simulating the same experiment on a computer, using the obtained value for viscous damping friction. Results similar to those obtained in the laboratory were obtained, verifying our results. Note also that the fact that the friction manifested itself as a first-order exponential decay and not a linear curve verifies that friction is dominated by viscous and not coulomb effects.

The value for c for our basic configuration was found to be approximately:

$$c = 0.001 kgm^2/s$$

Cart Mass	M	3.552	kg
Pendulum Mass	m	0.324	kg
Pendulum Length	ℓ	0.429	m
Gravitational Acceleration	g	9.807	m/s^2
Cart Viscous Friction Constant	b_{VF}	2.5775	kg/s
Pendulum Viscous Friction Constant	c	0.001	kgm^2/s
Usable Track Length	d	1.090	m
Pulley Radius	r	.080573	m

Table B.1: Table of Computed Physical System Parameters